

**Alma Mater Studiorum – Università di Bologna**

**DOTTORATO DI RICERCA IN  
SCIENZE BIOMEDICHE**

**Ciclo XXIX**

**Settore Concorsuale di afferenza: 06/F4**

**Settore Scientifico disciplinare: MED/33**

**Investigation of Different Crosslinking Strategies to Develop  
3D Polymer Scaffolds for Cartilage Tissue Engineering**

**Presentata da: Natalia Ewa Gostynska**

**Coordinatore Dottorato**

**Prof. Lucio Cocco**

**Relatore**

**Prof. Lucio Cocco**

**Correlatore**

**Prof. Maurilio Marcacci**

**Esame finale anno 2017**



# ACKNOWLEDGMENTS

I would like to thank all the people that helped me to achieve this important goal.

I would like to thank Prof. Maurilio Marcacci and Dr Elizaveta Kon for offering me the position as a Marie Curie PhD student at the Rizzoli Orthopaedic Institute. It was a pleasure to be a part of Bio-inspire Consortium (European Union Seventh Framework Programme FP7/2007-2013 under grant agreement n ° 607051), share the ideas, experience, and create friendships with other Marie Curie members. Hence, I wish to record my thanks to Dr Alice Roffi and all NABI Laboratory group at the Rizzoli Orthopaedic Institute for introducing me to the fascinating field of cartilage and bone regeneration.

I express my gratitude to Prof. Lucio Cocco for being tutor and coordinator of my PhD studies. It was an honour to study at the Department of Biomedical and Neuromotor Science at the University of Bologna.

Finally, I declare my profound thanks to my supervisors and colleagues from the Institute of Science and Technology for Ceramics, ISTECCNR in Faenza for their knowledge and experience that they passed me during those 3 years. I would like to thank Dr Anna Tampieri for providing me the opportunity to perform research at her institute and herein, for beginning my interests in the field of tissue engineering. I am truly grateful to Dr Monica Sandri, Dr Silvia Panseri, Dr Monica Montesi and Dr Simone Sprio for their invaluable training, mentoring and continuous support. Silvia and Monica, thank you for passing me your passion for science and unconditional help in time of need. Then, I express my gratitude to Gopal Shankar Krishnakumar for the great cooperation and support in every project that we have performed together. Moreover, I thank to all amazing people I had pleasure to work with, in particular, Tatiana Patricio, Gloria Belen Ramirez Rodriguez, Elisabetta Campodoni and Samuele Dozio. Without your advices and positive energy, the work would not be the same.

At the end, I would like to thank my beloved family and friends for believing in me and especially to my Mom for her immense motivation and contribution at each step of my life. I also thank to my boyfriend Giulio for his patience and big dose of optimism that he was giving me every day. I am lucky to have met wonderful friends, Valentina, Elettra, Ivor, Federico, Simone, Riccardo, who made Italy my new home.

Thank you all!

# CONTENTS

<b>Abstract</b>	<b>1</b>
<b>I. INTRODUCTION</b>	<b>3</b>
1. Cartilage tissue	3
1.1. Composition of articular cartilage	4
1.2. Structure and mechanical characterization of articular cartilage	7
2. Cartilage defects and their regeneration	9
2.1. Articular cartilage defects and diseases	9
2.2. Medical interventions in cartilage repair	10
3. Cartilage tissue engineering	12
3.1. The concept of tissue engineering	12
3.2. Cell sources in tissue engineering	14
4. Scaffolds for tissue engineering	16
4.1. Natural polymers	18
4.1.1. Collagen	18
4.1.2. Gelatin	20
4.2. Crosslinking treatment	21
4.2.1. Physical crosslinking (DHT)	22
4.2.2. Chemical crosslinking	23
4.2.3. Natural crosslinking (genipin)	24
4.2.4. Non-enzymatic crosslinking by glycation	24
<b>References</b>	<b>25</b>
<b>II. ANALYTICAL METHODS</b>	<b>32</b>
1. Freeze-drying process	32
2. Microscopy	33
2.1. Scanning electron microscopy (SEM)	33
2.2. Fluorescence microscopy	34
3. Spectroscopy	37
3.1. Ultraviolet–visible (UV-VIS) spectroscopy	37
3.2. Fourier transform infrared spectroscopy (FTIR)	38
4. Thermo-gravimetric Analysis (TGA)	40
5. Mechanical analysis	40
6. Quantitative real-time polymerase chain reaction (qPCR)	43
<b>References</b>	<b>45</b>
<b>III. EXPERIMENTAL</b>	<b>47</b>
<b>1. Experimental procedures</b>	<b>47</b>
1.1. Scaffolds Morphology Analysis	47
1.2. Measurement of porosity	47
1.3. Fluid uptake	48
1.4. Extent of crosslinking	48
1.5. Degradation assays	49

1.5.1. Weight loss measurements	49
1.5.2. Collagenase digestion test	49
1.6. Fourier Transform Infrared Spectroscopy (FTIR)	49
1.7. Thermal characteristics	50
1.8. Mechanical analysis	50
1.8.1. Static compression	50
1.8.2. Dynamic compression	50
1.8.3. Creep	50
1.9. 3D cell culture	51
1.10. Cell viability assay	52
1.11. Cell proliferation assay	52
1.12. Cell morphology	53
1.12.1. Actin-phalloidin staining	53
1.12.2. SEM analysis	53
1.13. Glycosaminoglycan (GAG) assay	54
1.14. RNA isolation and quantitative real-time polymerase chain reaction (qPCR)	54
1.15. Western Blot analysis	55
1.16. Statistical analysis	55
<b>2. Development of 3D porous gelatin scaffolds by different crosslinking approaches: comparative analysis</b>	<b>56</b>
2.1. Introduction	56
2.2. Preparation of scaffolds	57
2.3. Physicochemical characterization	59
2.4. Mechanical properties	66
2.5. Biological evaluation	68
2.5.1. Preliminary cytotoxicity assessment	68
2.5.2. In vitro tests with human chondrocytes	71
2.6. Conclusions	78
<b>3. Design and fabrication of 3D collagen scaffolds reinforced by glycation</b>	<b>80</b>
3.1. Introduction	80
3.2. Preparation of scaffolds	81
3.3. Scaffolds characterization	83
3.3.1. Optimization of crosslinking conditions	83
3.3.2. Evaluation of final compositions	89
3.4. Biological assessment	94
3.5. Conclusions	98
<b>IV. FINAL CONCLUSIONS AND FUTURE PERSPECTIVE</b>	<b>100</b>
<b>References</b>	<b>103</b>
<b>List of publications</b>	<b>109</b>
<b>Scientific congresses and schools</b>	<b>109</b>

# ABSTRACT

Articular cartilage is a highly specialized tissue which when damaged, represents poor potential of self-regeneration. Very often standard medical interventions are not sufficient to treat cartilage defects hence, tissue engineering techniques have started to play a key role in cartilage restoration. Collagen type I and its denatured form, gelatin are in the centre of the most common biomaterials used in tissue engineering due to their biodegradability, low cytotoxicity and promotion of cell adhesion. However, without suitable stabilization, these natural polymers can degrade quickly in the physiological conditions as well as under mechanical load. In order to enhance chemical stability, structural integrity and stiffness of the biomaterials different crosslinking methods (reinforcement) were applied to produce 3D porous polymer scaffolds, which were deeply investigated physicochemically, mechanically and biologically.

The first study of this PhD thesis tends to investigate the feasibility of developing 3D gelatin scaffolds through stabilization by physical (DHT), chemical (BDDGE) and natural (Genipin) crosslinking approaches. The study aimed at comparatively assessing the porous microstructure and the long-term resistance of the scaffolds upon degradation in wet physiological conditions (37 °C, pH = 7.4). The degree of crosslinking increases as function of incorporation of crosslinkers, which was maximum up to 73% for BDDGE. The infrared spectroscopy and thermal analysis confirmed the gelatin structure was preserved during the crosslinking treatments. Mechanical properties of the scaffolds were analysed by static and dynamic compression test, which showed different viscoelastic behaviour upon various reinforcement strategies with the highest compressive modulus for DHT-crosslinked scaffold. Cytocompatibility, bioactivity and overall cell-scaffold interaction was investigated using human osteoblast-like cells and human chondrocytes showing good cell adhesion, viability and proliferation, as well as extensive 3D scaffold colonization. Additionally, the analysis of gene and protein expression as well as glycosaminoglycans content related to the formation of neo cartilage tissue, reported increasing ability with time in the formation of new extra-cellular matrix. In conclusion, out of three different crosslinking methods, the gelatin scaffolds subjected to dehydrothermal treatment (DHT) represented to be the most favourable 3D scaffold for cartilage regeneration.

In the second study, ribose was proposed as a promising, non-toxic, low-cost crosslinker to improve stability and rigidity of type I collagen matrices. The main objective was to determine optimal conditions of glycation by ribose to fabricate 3D porous collagen scaffolds and to verify their effectiveness for use as scaffolds for cartilage tissue engineering, by physicochemical and biological characterization. Two different crosslinking strategies were investigated including variety in the amount of ribose and the time of reaction: pre-crosslinking (PRE) and post-crosslinking (POST). All ribose-glycated collagen scaffolds demonstrated good swelling properties and interconnected porous microstructure suitable for cell growth and colonization. POST samples showed to be superior than PRE in terms of porosity, crosslinking degree, fluid uptake ability and resistance to enzymatic digestion. Moreover, mechanical properties of the scaffolds were significantly improved upon glycation when compared to non-crosslinked collagen, manifesting the best performance for POST matrices crosslinked for 5 days and in the highest amount of sugar. *In vitro* studies analysing cell-material interactions revealed scaffolds cytocompatibility with higher cell viability and cell proliferation as well as higher glycosaminoglycans secretion for POST scaffolds respect to PRE. This report demonstrated feasibility of developing 3D collagen scaffolds by ribose glycation and highlighted POST-crosslinking strategy as a more favourable than PRE-crosslinking to achieve scaffolds suitable for cartilage regeneration.

# PART I

## INTRODUCTION

---

Tissue engineering (TE) is a multidisciplinary field constantly bringing more and more attention and which can completely change the view of future medicine [1]. Thanks to TE, poorly healing defects like cartilage defects can be potentially treated with combination of 3D scaffolds, cells and bioactive factors in order to regenerate damaged tissue. The ideal perspective in the scientific and medical environment is that, every tissue could be replaced or regenerated by tissue engineering techniques thereby, increasing survival and quality of our lives [2]. Articular cartilage tissue was one of first tissues thought to be profitably engineered however, the only one product approved by Food and Drug Administration so far, reveals a challenging nature of this approach [3]. Indeed, it is extremely difficult to mimic the complex architecture and biomechanics of native tissue. Many attempts have been made to create a functional cartilage engineered construct and only a few studies reached the clinical level. Hence, materials and fabrication technologies are highly important in designing and producing biomimetic three-dimensional (3D) templates (scaffolds) for new tissue formation [4].

The research presented in this work is focused on 3D natural polymer-based scaffolds for cartilage TE and on their deep investigation concerning different crosslinking strategies. Nevertheless, before that it is necessary to well understand articular tissue composition, structure and properties, which were described precisely in the following chapter. Then, in further chapters of part I concept of tissue engineering as well as natural polymer scaffolds and diverse crosslinking methods are briefly discussed.

### **1. Cartilage tissue**

Cartilage is a viscoelastic connective tissue that together with bone tissue serve as support for the skeleton [5]. Formulation of cartilage begins in the embryonic phase of human development and its major part is later replaced by bone formation. Importance of cartilage comes from the fact that this tissue provides an interface between bones minimizing in this way



load bearing and friction of bones. Cartilage by its action allows for bone's rotation and influences all locomotor system. Therefore, cartilage tissue is indispensable for the body motion as well as for the protection of bones at joints [6]. Cartilage can be found in the areas of ears, nose, trachea, intervertebral disks, ribs, joints and in many more parts of the human body. This tissue occurs in three forms [7]:

- a) Fibrocartilage – the strongest cartilage; existing for instance in intervertebral disks and meniscus; presence of large amount of collagen I;
- b) Elastic cartilage – appearing in the ear lobe, trachea and epiglottis; abundance of elastic fibers makes this form of cartilage highly elastic;
- c) Hyaline cartilage – present in hip, elbow, shoulder, and knee joints where is also named articular cartilage; presence of large amount of collagen II [7].

### 1.1. Composition of articular cartilage

Articular cartilage is a thin and connective tissue which covers the surfaces of diarthrodial joints [8]. The tissue is white in colour due to the lack of vascularity and forms a layer around 3 mm thick (Fig. 1.1 A). The main components of articular cartilage are water which is the only component of fluid phase and extra cellular matrix (ECM), belonged to the solid phase (Fig. 1.1 B). The fluid component includes a major part of the tissue because even 80% of the total volume.

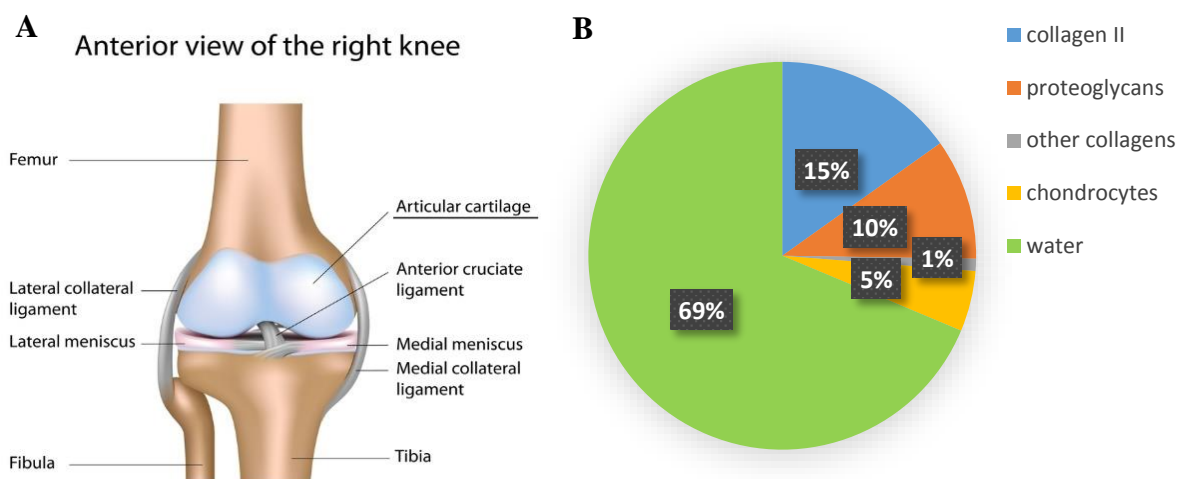


**Fig. 1.1** (A) Design of knee joint with underlined articular cartilage, which covers the end of the bones. White colour of articular cartilage is correlated to lack of vascularization. (Adapted from [www.londonkneeclinic.com](http://www.londonkneeclinic.com)) (B) Diagram presenting approximately amounts (%) of articular cartilage components. Solid phase contains collagen II, proteoglycans, other collagens and very little amount of non-collagenous proteins as glycoproteins, fibronectin etc. (not added on the graph). Liquid phase contains water and electrolytes [9].

The rest is ECM and chondrocytes, the only cell type present in cartilage, which account for approximately (1-5%). Moreover, ECM is composed of mostly type II collagen (15-20%), other types of collagen (2%), proteoglycans (10%) and non-collagenous proteins (Fig. 1.1 B) [8].

Chondrocytes in an adult articular cartilage have very limited proliferative potential and their main role is to preserve the tissue composition by synthesis and production of ECM components [10]. Additionally, chondrocytes can sense and respond to the different mechanical stimuli thus, they contribute indirectly to the biomechanics of cartilage [11].

Chondrocytes are derived from mesenchymal stem cells (MSCs), which in turn originate from mesoderm, one of the three germ layers, developed during embryogenesis [12]. MSCs as multipotent cells can differentiate into various cell types creating at the end different tissues as cartilage, bone or muscle tissue. In order to create cartilage lineage, MSCs have to condensate and then undergo chondrogenesis process in which prechondrogenic cells differentiate through chondroblasts into chondrocytes [12], [13]. Chondrogenesis is a process demanding suitable conditions and several key regulators [14], [15]. Terminal differentiation occurs when mature chondrocytes become hypertrophic and the process of bone formation is started [16]. Articular cartilage is progressively mineralized and blood vessels are promoted. Maturation of articular cartilage in humans takes around 18-21 years and during this time remodelling of cell functionality, phenotype and the EMC deposition occurred. Although, in the early stages of tissue maturation chondrocytes proliferate in a high extent, the mature chondrocytes decreased completely their proliferative and metabolic activity resulting in weak healing capacity upon injuries [8], [11].

Mature chondrocytes have a spherical shape with flattened edges, abundant Golgi apparatus and rough endoplasmic reticulum and noticeable nucleus. The cell-cell interaction among chondrocytes did not exist and the matrix around the cells is termed as pericellular matrix [17]. Phenotype of chondrocytes depends on the architecture and composition of the growing environment, thus chondrocytes cultured in monolayer *in vitro* lose their original phenotype. Some variability in the shape can be a result of slight differences in gene expression, several signalling pathways and differences in synthesis of matrix-specific components [5], [15]. Moreover, single cellular behaviour can be influenced by compressive load applied to the cells, and this phenomenon is called mechano-transduction [18]. Some differences in the chondrocytes phenotype and metabolic activity can be noticed also due to different cell localization inside cartilage tissue [10].

Cells are estimated to occupy only a little part of entire articular cartilage. As has been mentioned above high percentage of total tissue volume belongs to type II collagen (collagen II) and other forms of this protein. Collagen possesses 28 isoforms that have been discovered so far [19]. Collagen is the main structural component of connective tissues; it is the most abundant protein in mammals, making up from 25% to 35% of the whole-body protein content. Chondrocytes produce collagen in the form of soluble procollagen trimers that next undergo enzymatic processes to obtain collagen fibres. Although collagen can emerged in globular form, fibril form is the most numerous group in articular cartilage [20]. More about collagen structure is described in the further chapters.

Collagen II is the main type in hyaline cartilage and it contributes to mechanical tensile properties of tissue. Other collagen isoforms as collagen VI, IX, X and XI are present in cartilage tissue and their amounts change depending on the age. For instance with maturation, proportion of collagen XI respect to other collagens decreases from 10% of fetal cartilage to 3% of adult cartilage. Each type of collagen family can be localized in a different depth of tissue and represent different function [7], [8]. Another very abundant in the human body form of collagen is type I collagen (collagen I) which can be found only on the surface of cartilage, as this protein is a main component of the organic part of bone [8]. In research the ratio between collagen II and collagen I is used as an indicator during differentiation experiments to distinguish hyaline and fibrocartilage as well as verify the state of chondrocytes differentiation [10].

One more important group of ECM components are proteoglycans, special class of glycoproteins that play structural, mechanical and regulation role in articular cartilage. Proteoglycans are consistent of a "core protein" with one or more covalently attached glycosaminoglycan (GAG) chain(s) [20]. GAGs are long, unbranched, polysaccharides consisting of a repeating disaccharide unit. To the most common GAGs belong: chondroitin sulfate, keratin sulfate, dermatan sulfate and hyaluronan, which is the largest one. Hyaluronan binds aggrecan, the main proteoglycan present in cartilage, by a "link protein" creating a strong bound and thereupon, proteoglycan aggregates can be formed. These aggregates possess negative charge that promotes specific osmotic pressure interacting with synovial fluid called as Donnan effect. The osmotic pressure contributes to swelling and manages water amounts within the tissue. Moreover, collagen fibers keep together whole matrix structure with GAG chains and aggrecan supporting cartilage amortization against compression. Therefore, degradation of proteoglycans can be a significant factor in joint disease as osteoarthritis (OA) [21].

The last important component of articular cartilage that I would like to mention is synovial fluid (synovia) [8]. Synovial fluid is a viscous liquid, characterized as non-Newtonian fluid present in the cavities of synovial joints. Synovial fluid contains hyaluronan, protein-rich plasma, electrolytes and superficial zone protein (SZP), also known as PRG4 or lubricin. Thank to this protein, synovial fluid acts as a lubricant protecting articulating joints from frictions. Furthermore, synovia plays role in nutrients transport and waste removal and what is more important, it is responsible for support the load bearing capacity of cartilage. Basically, synovial fluid increase its viscosity when pressure increased which results in joints protection upon loading [7].

## **1.2. Structure and mechanical characterization of articular cartilage**

Architecture of cartilage is a complex form which varies in ECM composition, density, collagen fibers assembling, phenotype and activity of chondrocytes. Four zones can be distinguish within articular cartilage tissue starting from the top layer (Fig. 1.2) [9]:

- a) Superficial zone,
- b) Middle zone (or transitional),
- c) Deep zone (or radial),
- d) Calcified zone.

Each zone has its own particular role that has impact on functionality the whole articular cartilage. In addition, cells from different zones may respond to mechanical forces in different ways and exhibit diverse morphologies [11].

Starting from the top, the superficial zone encompasses only 10–20% of the total tissue thickness, but the amount of collagen in this area is the highest (Fig. 1.2). However, collagen fibers are the thinnest, densely packed and positioned parallel to the surface to form the layer known as *lamina splendens*. Chondrocytes in this zone appear also in high densities with parallel position to the surface and flattened morphology. Less proteoglycans compared to other zones leads to a high fluid permeability. Architecture of this zone is correlated to tensile strength and to decrease of high shear forces [16], [22].

Middle zone, referred also as transitional zone mediates between superficial and deep zone. The amount of collagen decreased compared to superficial zone, the fiber diameter enlarges and they adopt random organization. Chondrocytes changed their morphology for the round shape. Additionally, characteristic feature of the middle zone is a high density of proteoglycans (Fig. 1.2) [1].

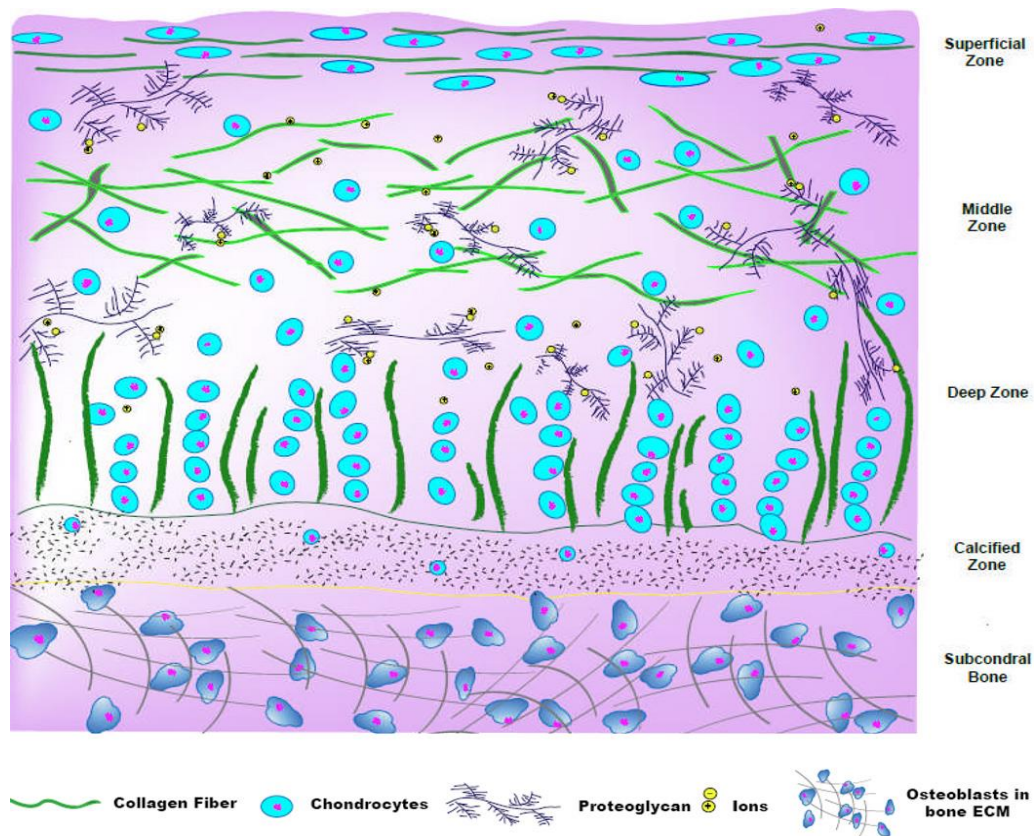


**Fig. 1.2.** Schematic illustration of composition and organization of articular cartilage. Four different zones can be distinguished: Superficial zone, middle zone, deep zone and calcified zone. Subchondral bone aligned under the cartilage is also presented [9].

In the deep zone, collagen fibers are the thickest and oriented perpendicularly to the surface. These collagen fibers are able to create a strong bridge between cartilage and bone. Chondrocytes are arranged in columns along with collagen fiber, also perpendicularly to the articulating surface (Fig. 1.2) [1].

The last one, calcified zone can be found between the deep zone and subchondral bone (Fig. 1.2). Only single chondrocytes are presented here, and production of the collagen II is reduced, in contrast to high production of collagen X which supports mineralization [20].

Articular cartilage is characterized as an anisotropic and viscoelastic tissue thus, it shows non-linear response due to application of mechanical forces [6]. Mechanical behaviors as stress-relaxation or creep are time-dependent and they are strongly related to the permeability of tissue. Cartilage is comparable to the sponge in which fluid can flow through, however with a low rate. At the beginning of deformation, flow rate starts to drop increasing the drag forces. In consequence cartilage increased the hydraulic pressure and mechanical stiffening [6], [11]. As cartilage is composed of two phases: liquid and solid, which interacting with each other to determine viscoelastic properties of tissue, biphasic cartilage model has been proposed [23]. In this model solid component containing collagen, proteoglycans cells and other small proteins

is described as incompressible elastic material and interstitial fluid component is modeled as non-viscous phase. Under compression, friction is generated between liquid and solid phase resulting that fluid flows out from the collagen-proteoglycan solid matrix and this drag compensates the load applied to cartilage tissue. When the load is removed tissue return to its original form, the fluid is restored into the compressed area as well as the elasticity of the solid component is returned [23].

Compressive moduli of the cartilage can vary depends on depth and location. The compressive aggregates modulus of articular joints is ranged from 0.08 MPa in the superficial zone up to 2 MPa in the middle and deep zone [24]. This difference can be related to decrease of fluid flow in the middle and deep zones, which leads to smaller strains in these areas.

Another mechanical properties that can be distinguished regarding cartilage tissue are tensile properties [10]. Tensile properties are influenced by collagen fibrils, and obviously the tensile moduli change among the zones of cartilage since thickness and organization of collagen fibers change as well. Tensile modulus (Young's modulus) can reach between 5 and 25 MPa being the highest in superficial zone, which can be associated to the highest content of collagen in this zone [6].

## **2. Cartilage defects and their regeneration**

### **2.1. Articular cartilage defects and diseases**

Articular cartilage defects can be caused by various factors as unusual loading of the joint, overloading, wear and tear overtime and also traumatic events. Cartilage defects left untreated can lead to degenerative joint disease, osteoarthritis [9]. Independently on the cause of defect, cartilage injuries can be divided into two groups: partial-thickness (chondral) and full-thickness (osteocondral) defects [25]. In chondral defects, damages are made to the cartilage layers without reaching the bone whereas, in osteochondral lesions an injury reaches the subchondral bone. As articular cartilage is a avascular tissue blood or bone cells as well as progenitor cells in bone marrow cannot access to it thus, the healing response is limited [17]. Chondrocytes feature low proliferation and migration rate, which also make complete regeneration of the defect difficult to accomplish. In osteochondral injuries blood cells and mesenchymal progenitor cells have access to the damaged cartilage from subchondral bone and the regeneration process can start [9]. Even if mesenchymal stem cells have capacity to restore the tissue by fast proliferation and differentiation into chondrocytes rather than hyaline cartilage, fibrous cartilage is forming. Fibrous cartilage (fibrocartilage) has weak mechanical properties

and the injury can easily appear again. As can be noticed ability of spontaneous healing the cartilage defects is extremely limited and often results in osteoarthritis (OA) [26].

OA is a serious and wide-spread disease nowadays because it leads to joint pain, movement impairment, inflammation and overall deteriorated quality of life. Hip and knee OA are the 11<sup>th</sup> leading cause of disability as announced World Health Organization (WHO) Global Burden of Disease Study 2010. At the moment Over 70 million Europeans suffer from knee OA [27]. Joints altered by osteoarthritis demonstrate, inter alia, decrease in collagen and proteoglycan content, increase of the water content, fibrillation, inflammation of the synovium and thickening of the subchondral bone. The details of biological changes in OA can be found in a growing number of literature studying this problematic disease [3].

## **2.2. Medical interventions in cartilage repair**

There are three main medical techniques used in clinical practice for treatment of cartilage defects [9], [10]:

- a) Microfracture,
- b) Autologous chondrocyte implantation (ACI),
- c) Auto- and allografts.

Microfracture is a surgical procedure whose goal is to make small holes in the subchondral bone in order to deliver blood with bone marrow mesenchymal stem cells (BMSCs) [10]. BMSCs with their high capacity of self-renewal and differentiation can rebuild the damaged tissue. Very often, similarly as in osteochondral defects instead of hyaline cartilage fibrocartilage is formed which is too mechanically weak to resist load-bearing of the joint and thus, effectiveness of microfracture surgery is limited. Microfracture can be appropriate for treatment of small defects, in relatively young patients who have a faster healing response [25].

Autologous chondrocyte implantation (ACI) was the first method of cell transplantation for cartilage repair and became very common since 1990 [28]. ACI is comprised of two steps: arthroscopy and surgery. At first, a biopsy of healthy cartilage is performed from the low weight-bearing area of the patient's knee and chondrocytes are isolated and expanded *in vitro* for several weeks to significantly amplify the number of cells. At the second step, cells are injected to the lesion and a periosteal patch or synthetic collagen is applied to cover the surface of the drilled area [9]. Although the ACI procedure succeeds in numerous patients, there are some disadvantages, such as long recovery time or many surgeries required to sufficiently harvest cartilage tissue. Furthermore, there are difficulties in optimization of cell number and satisfactory differentiation as well as the possibility to

occur periosteal hypertrophy can be a limitation of this technique [29]. ACI technique was evaluated over years to second-generation ACI where periosteal patch were replaced by collagen membrane and further third-generation known as matrix-assisted ACI (MACI). In MACI procedure autologous chondrocytes are expanded and seeded onto the scaffold which is further implanted into defect [4].

Autografts and allografts are other, very popular options for cartilage regeneration [30]. Briefly, a piece of healthy cartilage belonged to low weight-bearing area is harvested from the patient with a part of subchondral bone (osteochondral autograft) or is taken from cadaveric donor from tissue banks (osteochondral allograft). Then, the healthy piece of tissue is implanted into defect and regeneration process can occur [30]. Autografting technique have showed some satisfactory clinical results however, many limitations to this procedure are present. First of all, insufficient amount or quality of tissue material which is going to be implanted can create problems. Moreover, disadvantage can be a mismatch of the graft and the implant site as the first one can be a part of low weight-bearing and the second one can be a part of high weight-bearing area. Finally, poor stability of the graft and donor site morbidity are the limitation of autografting. Nevertheless, decreasing amount of tissue material that has to be implanted and implanting many small grafts into one defect site can improve the outcome [26], [31].

Allograft used as an alternative to autograft can fill bigger defect size and there are not high limitation to the amount of donor tissue available as well as the donor side morbidity is avoided. However, immuno-rejection and disease transmission can be an issue in case of allografting [30].

All presented above procedure are not sufficient when the defect size is too big or joint injuries are serve or progressive OA is developed [27]. Articular cartilage cannot be restored by any of interventions discussed above and partial or total joint replacements are necessary. In a place where joint has been removed partially or totally artificial implant consisted mainly of metal and small polymer piece is implanted. Although newly produced implants are improved every year, complications as implant loosening, infection, and short life spans of the implants occur very often and second surgery is necessary [30]. As we can see, medical interventions for cartilage regeneration currently available have many limitations and no ideal standard treatment is present. Thereby, searching for alternative solutions in the field of regenerative medicine and the concept of tissue engineering has been raised.



### 3. Cartilage tissue engineering

#### 3.1. The concept of tissue engineering

The first trace of tissue replacement was dated on 1597 when Gasparo Tagliacozzi, Professor of Surgery and Anatomy at the University of Bologna described the nose reconstruction with a forearm flap that he performed [32]. A few centuries after, in 1985, the idea and the term of tissue engineering (TE) has been proposed by Y.C. Fung, a pioneer of the field of biomechanics and of bioengineering, entitled as: “Center for the Engineering of Living Tissues” [33]. The proposal of Fung was not accepted and the definition of TE has been evolving for several years to finally define as: “*Tissue engineering is an interdisciplinary field that applies the principles of engineering and the life sciences toward the development of biological substitutes that restore, maintain, or improve tissue function.*” This interpretation of the TE term was proposed by Robert Langer and Joseph P. Vacanti in the May 14, 1993 issue of Science [34]. By now 82 740 articles can be found on PubMed database using the string “tissue engineering”, indicating on rapidly growing progress and interests in this field.

In fact, TE is area which includes combination of various materials, cells and biologically active molecules to improve or replace biological tissues [35]. The aim of this discipline is to create functional constructs which are able to rebuild and recover damaged tissue or even whole organs. The term of regenerative medicine is often used parallel to TE however, regenerative medicine is focused on incorporation of stem cells to restore tissues or organs. The materials which are fabricated to support tissue regeneration, called also biomaterials or scaffolds due to 3D architecture, have been in the center of attention since decades and can be considered as a separate sub-field of TE [30].

Fig. 1.3 presents simplified scheme of TE approach. Following the illustration firstly piece of tissue is harvested from the patient and autologous cells are expanded *in vitro* in 2D. Afterwards, cells can be combine with the 3D scaffolds or other type of matrices or/and biological molecules (e.g. growth factors) to provide suitable conditions for new tissue organization. Such an engineered tissue-like construct is transplanted into place of damaged tissue in patient’s body and regeneration can occur (Fig. 1.3). Depends on the type of tissue that has to be recreated different types of materials, cells and biological factors need to be applied regarding specific structural and mechanical properties of the tissue [2].

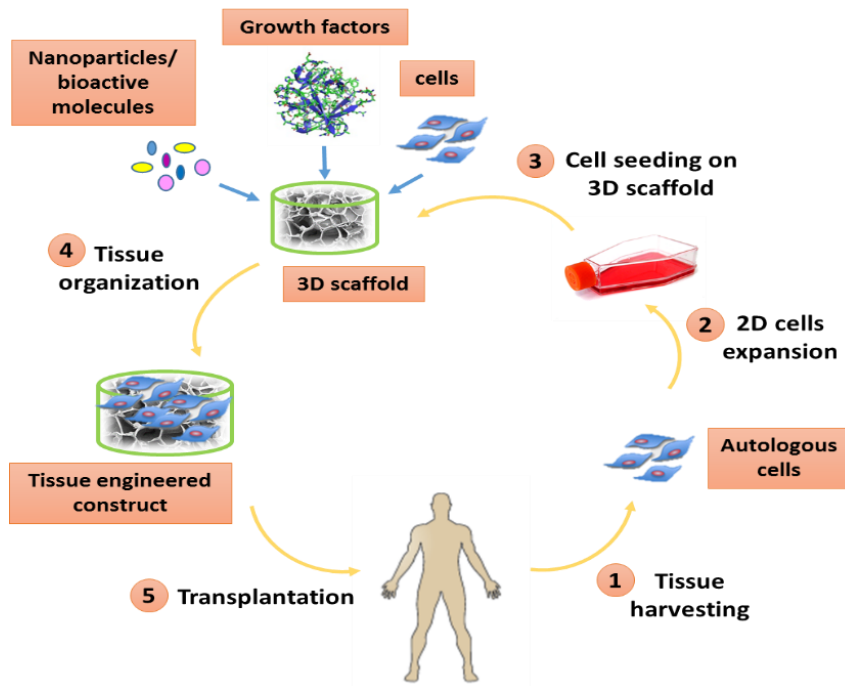


**Fig. 1.3** Schematic illustration of the tissue engineering concept. Five different steps can be distinguished as follows: 1) Tissue harvesting; 2) 2D cell expansion; 3) Cell seeding on 3D scaffold; 4) New tissue organization; 5) Engineered construct transplantation.

Another still less common strategy is to use scaffolds alone, implanted directly to the injured site without cell expansion *in vitro*. In this way scaffold by its own acts as a template for new tissue formation [30]. Currently, by TE is possible to fabricate new tissues starting from scaffolds, cells and biologically active molecules. Nonetheless, to achieve both functional and biomechanical stability as well as vascularization in laboratory-grown tissues destined for transplantation is a huge challenge in the field. Only a few engineered tissues have been approved by the Food and Drug Administration (FDA) and around 600 million dollars are spent every year on new products development. Examples of engineered tissues include artificial skin, cartilage, bone, blood vessels, artificial pancreas and artificial liver [36].

Cartilage tissue engineering focused on developing *in vitro* tissue-materials constructs which can mechanically and biologically mimic cartilage tissue supporting the load applied to the joint. Recent approaches combine scaffolds with microfracture or drilling techniques in order to recruit stem cells from the subchondral bone, which together with scaffold implantation, guide the formation of new tissue. The main challenges in cartilage TE is to reduce the development of mature cartilage which normally in human lasts 18 years to a short time around 1-2 months of culture *in vitro* before implantation [10]. Moreover, to obtain biologically and structurally functional tissue which exhibits mechanical stability as native cartilage is still an issue for scientists nowadays. In the following section tissue engineering

approaches based on different type of cells, will be briefly described and afterwards scaffolds in tissue engineering will be broadly discussed.

### **3.2. Cell sources in tissue engineering**

Currently, cells became the important link of TE to treat cartilage lesions. Cell-scaffold combinations are the most used treatment approach in preclinical and clinical research for cartilage TE. The suitable cell source should have high proliferative potential by its own or should be easily expanded *in vitro* with capacity to produce abundant cartilage ECM components and maintain chondrogenic phenotype without induction of any immunological reaction. Autologous chondrocytes seem to be good choice according to this purpose and in fact there are the most common cell source in clinical studies however, articular chondrocytes have some limitations [37]. As has been mentioned in previous chapters low numbers of these cells obtained when performing the biopsy, requires expansion *in vitro*. Nevertheless, in 2D culture chondrocytes undergo de-differentiation therefore specific culture conditions as for instance, serum-free medium, culture in bioreactors or addition on growth factors are necessary [38]. Despite presented limitations, expanded autologous chondrocytes, existing under the product name of Carticel® are the only one approved by FDA method for cartilage TE in US [10], [30].

Recently, extensive attention has been addressed to mesenchymal stem cells (MSCs), multipotent cells which have high capacity for self-renewal and potential for differentiation into multiple musculoskeletal lineages such as chondrocytes, myocytes, adipocytes, osteoblasts and tenocyte [12]. Figure 1.4 illustrates multipotency of MSCs. MSCs can migrate toward damaged site of the tissue and manifest so called trophic effects which are expressed as synthesis of proliferative, pro-angiogenic and regenerative molecules. In addition, immunomodulatory action of MSCs allows for the allo- and xenotransplantation. MSCs when expanded *in vitro* can proliferate and sustain their multipotency which make them more beneficial than chondrocytes [39]. Very popular in the preclinical and clinical settings are bone marrow mesenchymal stem cells (BMSCs), used also in a form of bone marrow concentrate (BMC) [40]. BMSCs can be relatively easy harvested from the iliac crest and have good chondrogenic potential. Many studies, including randomized controlled trials (RCTs) performed by Vega or Wong showed positive impact of BMSCs on treatment of knee osteoarthritis [41], [42]. Nevertheless, BMSCs have also some disadvantages related to the cell harvest and culture therefore, other sources of MSCs have been investigated as adipose-derived mesenchymal stem cells (ADSCs), stem cells from synovial tissue (SDSCs) or from peripheral blood (PBSCs) [43]. ADSCs showed to have

lower chondrogenic potential than BMSCs however, their abundance and easy way to extract (from adipose tissue by liposuction) make them also an attractive source for cartilage TE [26].

MSCs exhibit excellent candidate for cell therapies however, MSC research has still a lot of drawbacks related to the best source, dosage, form of administration (concentrated or expanded), delivery and so on. Even the characterization of MSCs has not been completed yet due to expression of numerous different markers [44]. Alternative to MSCs can be chondroprogenitor cells which have recently demonstrated their chondrogenic potential even they do not express multipotent character. Use of chondroprogenitor cells can solve the problem of de-differentiation as has been already shown by several studies [45].

Another promising cell source for cartilage TE can be definitely embryonic stem cells (ESCs). ESCs has pluripotent character which means they can differentiate into any cell type and furthermore, ESCs have unlimited proliferation capacity. *In vitro* and *in vivo* studies have proved chondrogenic potential of ESCs by support of growth factors or co-culture with primary chondrocytes [46]. Even though, ESCs seem to be attractive alternative to other cell sources, their mechanism of action and regenerative potential is still not complete understood. Errors in ESCs differentiation could led to teratoma when some other than desired cell types are formed. Besides, allogenic nature can cause immuno-rejection in potential clinical application. Finally, there are serious ethical concerns according to use of ESCs [9].

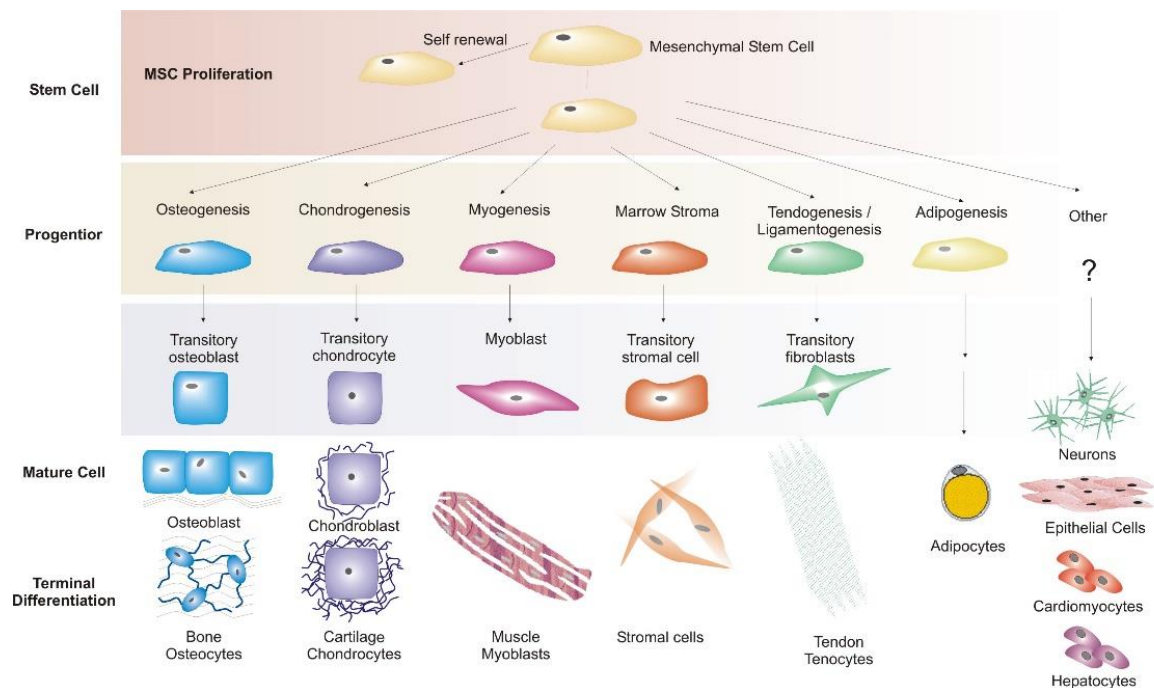


**Fig. 1.4** Multilineage differentiation potential of mesenchymal stem cells. Adapted from [www.mimeresearch.com](http://www.mimeresearch.com).

## 4. Scaffolds for tissue engineering

Biomaterials are the crucial components of tissue engineering and they have been deeply studied for repair cartilage defects. The goal in the TE field is to design and fabricate biomimetic scaffolds [47]. Biomimicry means that scaffold by its chemical composition and 3D architecture can mimic native tissue allowing for tissue regeneration. Such a biomimetic scaffold should possess several essential features:

- a) Should be biocompatible to promote cell attachment, cell growth, tissue integration and minimize immunological response of surrounding tissue;
- b) Should be biodegradable with a suitable degradation rate which matches with the new tissue formation;
- c) Should have porous microstructure with sufficient porosity, pores interconnectivity and pore size suitable for cell migration and transport of nutrients and waste removal;
- d) Should create appropriate mechanical support for neotissue under native mechanical loads [32].

Providing all these features when fabricating scaffolds is extremely difficult. Firstly, the choice of suitable biocompatible material for scaffold preparation, secondly tuning the scaffolds to obtain appropriate degradation rate are essential. Then the 3D architecture with interconnected porous structure which can facilitate cell colonization and further vascularization *in vivo* without hindering mechanical properties are important aspects [48]. Many scaffolds produced have desired architecture however their high porosity refereeing to little amount of material in the scaffold which means low stiffness and weak mechanical stability. Very often scaffolds have potential *in vitro* for good interaction with cells and for promotion ECM but they fail when considering *in vivo* application due to compromised mechanical properties. Especially in cartilage TE scaffolds which will be able to resistant weight-bearing area are of a great importance in the field [4]. Another important factor for scaffold design and fabrication is the cost and accessibility. In order to possess translation from the laboratory to the clinics cost effective production of materials should be able to scale-up according to good manufacturing practice (GMP) [49]. Scaffolds should be also easy to handle by clinicians and reduction of for harvesting autologous tissue resulting in one-step procedure without cell expansion *in vitro* would be an ideal situation.

Among great choice of materials available, scaffolds can be fabricated from natural or synthetic polymers. Natural polymers used in TE include but there are not limited to collagen, gelatin, hyaluronan, agarose, alginate, chitosan and silk. Polymers can have protein as collagen

and gelatin or polysaccharide origin as agarose and hyaluronan [2], [50]. From the protein polymers, collagen and gelatin are very common biomaterials and have shown efficiency as a scaffold for cartilage TE which will be described on the next section in this chapter.

Polysaccharide-based scaffolds demonstrated promotion of chondrogenesis and articular cartilage formation. Scaffold made from hyaluronan named as Hyaff-11 showed good performance in cartilage regeneration *in vivo* when seeded before with autologous chondrocytes as was reported by Grigolo et al [51]. Moreover, agarose and alginate both derived from marine algae were used in many studies regarding cartilage TE showing promising results in cell encapsulation and in support of collagen II and aggrecan production [10]. Nonetheless, alginate and agarose can degrade easily and they have poor mechanical properties. Other polysaccharides as cellulose and chitosan are also used by scientist to produce 3D scaffolds herein, chitosan is usually used as a blend with other polymers [50].

Natural polymers are promising source for 3D scaffolds preparation because of their composition containing specific chemical groups (ligands) which attract cells to attach and spread on their surface. Thus, constructs with natural origin proved to be in general biocompatible and capable to facilitate chondrogenesis. On the other hand, usually weak mechanical properties and fast in particular enzymatic degradation are limitation to their use. Processing these type of scaffolds to desired shape and reproducibility among different batches can also create difficulties [47].

Inversely, synthetic materials are easy to process and tailored to obtain desired structure good mechanical properties and optimal degradation rate. However, their lack of bioactive molecule and hydrophobic character which are unlikely to promote cell adhesion and proliferation are the drawbacks of their use [32]. The most popular synthetic polymers for TE application are poly lactic acid (PLA), poly-glycolic acid (PGA), PGA/PLA copolymers, biodegradable polyurethanes (PUR) and poly ethylene glycol [10]. An example of studies with such materials is chondrocyte/PGA/bioreactor system which showed enhanced chondrogenesis up to 40 days of culture [52]. PLA scaffold also reported satisfactory results concerning complete degradation after suitable time and neo cartilage tissue formation when implanted in mice [53]. Due to some limitations of use synthetic-based scaffolds, the trend is to combine synthetic and natural materials to balance their advantages and disadvantages.

There are a few commercially available scaffolds used for cartilage TE in Europe which have already brought satisfactory results in clinics. The first example is MaioRegen™ (Fincermanica, Italy), a nanostructured scaffold consisting of different ratios of collagen and hydroxyapatite organized in three-layers to mimic native cartilage. Clinical trial with 27

patients and 5 years follow-up proved safety and good clinical outcome with stable results at midterm follow-up [54]. Other examples of 3D materials used for treatment of cartilage defects are Agili-C™ (CartiHeal Ltd, Israel) and TruFit™ (Smith & Nephew, Andover, MA). The first is made of coralline aragonite and the second is a bilayer scaffold made of a semiporous 75:25 PLGA-PGA calcium sulfate biopolymer [55]. TruFit showed some favorable results in clinics, however a number of studies found poor osseous integration coupled with a long time to resorb [56]. Agili-C manifested its potential in a caprine osteochondral defect model and the clinical studies concerning this implant are still ongoing [57], [58].

## **4.1. Natural polymers**

### **4.1.1. Collagen**

Collagen belongs to comprehensive family of structural protein very abundant in animals [59], [60]. Collagen II is a main protein component of articular cartilage as was described earlier [17]. Many advantages of collagen correlated to its natural character make this material broadly used in producing scaffolds for cartilage TE. Due to presence of collagen in native tissue, the surface of collagen scaffolds with biological ligands can be recognized by the cells, facilitating cell adhesion [50], [61], [62]. Indeed, collagen possesses in its structure repeatable motif of the tripeptide Arg-Gly-Asp (RGD) which is responsible for cell attachment but also overall cell behavior as RGD motif is recognized by cell's integrins [63]. Integrins are transmembrane receptors which initiate many cellular processes as cell spreading, motility and differentiation [63], [64]. Additionally low-antigenicity makes collagen an attractive candidate for development 3D porous scaffolds in cartilage regeneration [50]. Apart from biomedical application collagen has been used in cosmetics, nanotechnology, nanobiotechnology, pharmacology, and food industries [65], [66].

Collagen can be processed in the three ways. The first one include the use of collagen-rich tissues which serve as an implant to damaged tissues after special chemical treatment. The second one is based on extraction of collagen from animal (e.g. bovine, porcine and equine) or human sources (cadavers, placenta or amnion) and its subsequent purification and polymerization. In addition, collagen can be also produced by use of recombinant genetic engineering techniques however, they are still limited [65], [66]. This polymeric protein is mainly used in the form of native soluble collagen, enzymatically processed native collagen and soluble collagen of reconstituted fibers [60].

From entire collagen family, type I collagen (collagen I) is the most abundant and thus, it is very common in synthesizing the scaffolds. Collagen I can be extracted from dermis, bone, tendon and ligament [19]. Collagen I, II and XI have capacity to form fibers from a single collagen molecule called tropocollagen. Tropocollagen in collagen I consists of two  $\alpha 1$  and one  $\alpha 2$  peptide chains that together create 300 nm long and 1.5 nm thick triple-helix which is stabilized by many hydrogen bonds [67]. In each of peptide chain repeating sequence of amino acids can be found as follow: Gly-Pro-X or Gly-X-Hyp, where X may be any of various other amino acid residues. Five units of tropocollagen forms supermolecular structure referred as microfibril which possesses so-called D-banding pattern of 67 nm [68]. Around 500 fibrils can aggregate into fibre with a diameter lower than 500 nm and a length lower than 1 cm. Finally, the fibers form fiber bundles with a thickness between 10 and 100 mm [67], [68].

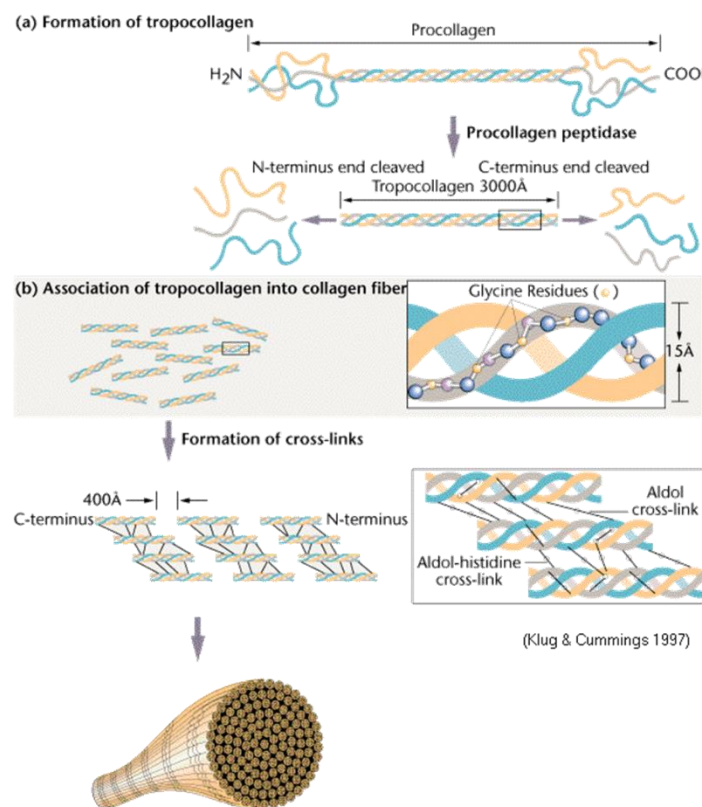


**Fig. 1.5** Collagen assembly *in vivo* and fibers organization. Several different steps are presented: (a) Formation of collagen molecule (tropocollagen) from collagen precursor (procollagen), (b) Association of tropocollagen into collagen fibrils and their aggregation into larger fibers by crosslinking mechanism. At the end, fibers formed fiber bundle of a thickness 10 - 100 mm. The illustration is adapted from [www.mun.ca](http://www.mun.ca).

This well-organized structure can be maintained thanks to crosslinking bonds created among collagen molecules. In physiological conditions cells must first synthesize a precursor of collagen, procollagen which is enzymatically processed giving rise to a tropocollagen molecule



[10]. Collagen self-assembly is a spontaneous and thermally driven reaction which in laboratory conditions can be obtained at pH range from 5.0 to 8.5, ionic strength between 0.1 and 0.8, and temperatures between 15 and 37°C [66].

In literature collagen I based scaffolds demonstrated so far promising results in promotion of large amount of collagen II and GAGs as well as chondrocytes proliferation and cartilage tissue formation [69] [70]. Nevertheless, I cannot omit a few disadvantages in usage of collagen as a biomaterial in TE. First of all, collagen can easily undergoes enzymatic reaction which leads to fast biodegradation *in vivo* [2]. Moreover, low tensile and compressive properties results in poor resistance to mechanical load [50]. To improve structural integrity, biostability and mechanical properties variety number of methods has been applied to reinforce collagen. These methods of reinforcement (crosslinking) are reported in details in the next chapter.

#### **4.1.2. Gelatin**

Another broadly used material in TE is gelatin: thermally denatured form of collagen therefore, gelatin can perfectly serve as a collagen's substitute [70]–[72]. Gelatin derives from animal collagen by acid (gelatin type A) or alkaline (gelatin type B) hydrolysis [72]. Similarly to collagen, gelatin is composed of amino acids, it contains the same amino acid motif, RGD which in gelatin structure may be more exposed than in collagen due to partial denaturation [63]. RGD motif can modulate cell adhesion and overall biological response which contributes to gelatin biocompatibility [64], [73]. Moreover, gelatin is biodegradable, does not exhibit antigenicity in physiological condition and has significant economic value hence is mainly used in food manufacture [74]–[77]. In TE, her low cost, simple preparation and feasible modifying of physicochemical properties can make gelatin even more attractive polymer than collagen to synthesise 3D scaffolds.

During denaturation process, collagen loses its triple-helix structure and takes a form of random coils becoming a gelatin [78]. At temperature of around 40°C gelatin is an aqueous solution in the sol state and when the temperature drops down starts to turn into gel. This sol-gel transformation occurs due to conformational changes of the gelatin chains. Upon this disorder-order transition of gelatin thermo-reversible network is created by associating helices stabilized by hydrogen bonds [74], [79]. The transformation of gelatin from sol to gel makes the fabrication of gelatin scaffolds apparently simple and it provides the opportunity to easily modulate shape of the scaffold.

Although there are numbers of benefits in using gelatin as a biomaterial for TE its fast dissolution in aqueous environment and weak mechanical properties need to be overcome, the same as in producing collagen scaffolds, by crosslinking. In contrast to collagen which as soon as is in fibrous form is resistant to degradation in aqueous solutions, gelatin represents very high solubility in certain temperature [67], [75].

So far, gelatin hydrogels and gelatin porous scaffolds have been deeply studied for different TE approaches. For instance, after 30 days of culture with primary chondrocytes on freeze-dried gelatin scaffolds a tissue with a cell distribution resembling that of the native cartilage was developed [76]. Gelatin hydrogels are also often used in cartilage research as a material for cell encapsulation which can be further implanted to the defects [80], [81].

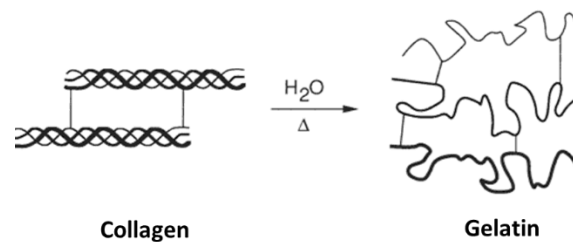


**Fig. 1.6** Process of collagen denaturation into gelatin. Triple-helix structure of collagen under denaturation changes a form to the random coils.

## 4.2. Crosslinking treatment

Crosslinking is a general term to name creation of bonds between two polymer chains. The bonds can be covalent or ionic [82]. Crosslinking is used in both synthetic polymer chemistry and in the biological sciences. Although the term is equal for these two areas, crosslinking agents (crosslinker) as well as the extent, mechanism and final effect of crosslinking can vary [83]. Crosslinking is also a natural process occurs in the body, in which bonds are formed between proteins, i.e., crosslinking of native collagen leads to tissue stiffening and ageing [84]. In tissue engineering crosslinking refers to a method by which biomaterial is reinforced as its physical properties are changed upon crosslinking [47]. The reinforcement can aim at resistance to degradation or/and improvement of mechanical properties. Therefore, the idea of crosslinking is to obtain biologically and mechanically stable biomaterial which can be implanted *in vivo* and fulfill its function in tissue regeneration. The amount of crosslinking agents has to be always well optimize to do not create any toxic effects to the cells [59]. Moreover, crosslinking treatment should be easy accessible to perform, time-consuming and ideally it should have low cost. Apart from reinforcement crosslinking treatment can influence hydrophilicity, microstructure, thermal behavior of the material and also cellular response *in*

*vitro* [50]. Plenty of crosslinking methods have been applied in TE, as ionic, thermal, photo-crosslinking, chemical, natural, enzymatic and non-enzymatic crosslinking [85]. Every of them can be appropriate depending on the type of material and application. The trend in the scientific world goes towards improving the crosslinking processes and finding better functioning, completely anti-toxic and cheap crosslinkers. This chapter focused on a few crosslinking treatments which are described below.

#### **4.2.1. Physical crosslinking (DHT)**

The physical crosslinking is a traditional reinforcement method which includes dehydrothermal (DHT), ultraviolet (UV), and gamma irradiation treatment [85]. DHT is a method which involves subjecting a material to high temperature ( $> 90^{\circ}\text{C}$ ) under the vacuum. This procedure removes water from polymer molecules and intermolecular, covalent bonds are formed through condensation reactions which can be esterification or amide formation [86]. In native conditions two types of crosslinks can be generated in protein polymer as collagen based on the aldehyde groups formed from (hydroxy) lysine residues in the telopeptides. First, is an intramolecular crosslink which occurs within the same protein molecule by an aldol condensation reaction of two aldehyde groups. Second is an intermolecular crosslink where the bond is created between two adjacent molecules. The aldehyde group of one molecule reacts with the amino group of an (hydroxy)lysine residue of an another molecule, yielding an aldimine or a Schiff base [60]. In gelatin chains, upon DHT crosslinking the intermolecular bridges are formed between amine and carboxyl group of two adjacent molecules. It has been reported that DHT treatment can be effective only when amino and carboxyl group are sufficiently close to each other [87].

DHT is common method used in TE approaches as it has no toxic effects and application of high temperature serves also as an sterilization of materials [88]. Using either of too high temperature or too long time of treatment can cause degradation of gelatin molecule. On the other hand, denaturation may reduce the inflammation response *in vivo* and expose specific receptor sites to attract the cells [86], [89]. Complete removing of water from the polymer can result in lower hydrophilicity of scaffold and less surface energy available for crosslinking. In literature different conditions of DHT crosslinking can be found, mostly agreeing that longer treatment and higher temperature (even up to  $180^{\circ}\text{C}$ ) can positively influence mechanical strength and crosslinking extent but also increase denaturation of protein [86], [88], [90].

### 4.2.2. Chemical crosslinking

Variety of chemical crosslinker has been used in stabilization of biomaterials. The most popular groups include: carbodiimide, glutaraldehyde, epoxy compounds and acyl azide [91]–[94]. The mechanism of crosslinking can be different for each compound however, the main principle which is creating intra- and intermolecular bonds within polymer structure is preserved. Chemical crosslinkers are able to crosslink polymers in a higher extent than physical methods that is correlated to capability of reaction with more functional side group.

Glutaraldehyde (GTA) demonstrates the highest crosslinking degree however, the reaction mechanism is very complex due to the fact that aqueous solutions of glutaraldehyde contain a mixture of free aldehyde and mono- and dihydrated glutaraldehyde and monomeric and polymeric hemiacetals [60], [95], [96]. In general, the reaction involves aldehydes which react with the amine groups of (hydroxy)lysine residues of the protein, yielding a Schiff base which can be stabilized by a reduction reaction [60]. The limitation of GTA, as well as other chemical crosslinkers is that the unreacted compounds can lead to cytotoxicity [62], [76].

Carbodiimides are another group of chemical crosslinkers in which the water-soluble carbodiimide 1-ethyl-3-(3-dimethyl aminopropyl)carbodiimide (EDC) is commonly used for stabilization of collagen and gelatin. The crosslinks occur between carboxylic acid and amine groups and EDC by itself is not incorporated [97].

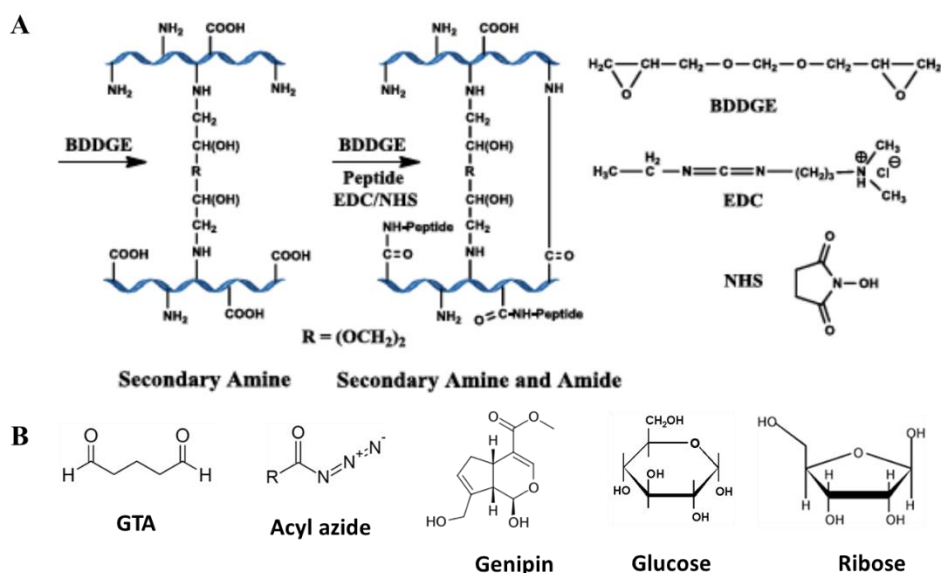


**Fig. 1.7** (A) Scheme of crosslinking mechanism of protein molecule by epoxy compounds: BDDGE and EDC/NHS coupling [98]. (B) Some crosslinking agents represented with their chemical formula. Adapted from [www.wikipedia.org](http://www.wikipedia.org).

Epoxy compounds are of our interest in this work and one of their representative is 1,4-butanediol diglycidyl ether (BDDGE). BDDGE is a bi-functional epoxy compound which is

active to react at basic pH [93], [98]. BDDGE has highly strained three-membered ring, susceptible to a nucleophilic attack. The mechanism of crosslinking encompasses the reaction with the amine groups of (hydroxy)lysine residues and the reaction with the secondary amine groups of histidine. In addition, this chemical can also react with the carboxylic acid groups of aspartic and glutamic acid showing its versatility among crosslinkers [98], [99]. BDDGE has not been yet properly explored in the field of tissue engineering, nonetheless its functionality was reported i.e., to improve the elasticity and tensile strength of the collagen implants [98], to develop poly( $\gamma$ -glutamic) hydrogel [100] or to stabilize hyaluronic acid sponges [99].

#### **4.2.3. Natural crosslinking (genipin)**

Genipin is a naturally existing crosslinking agent derived from geniposide which is extracted from the fruit of *Gardenia jasminoides* [101]. Genipin and its related iridoid glucosides have been broadly used in herbal medicine [102]. In TE genipin became one of the first choice crosslinkers considering its lower cytotoxicity compared to chemical compounds [78]. During crosslinking reaction with proteins genipin releases dark blue pigment used in the fabrication of food dyes. Mechanism of crosslinking based on two reactions with genipin molecule [77]. Firstly, by nucleophilic attack of the genipin on primary amine group and intermediate aldehyde is formed. Then, secondary amine reacts with that aldehyde group which results in generation of heterocyclic compound. At final step, ester group on protein molecule is replaced by a secondary amide bond [77]. Amino acids of protein employed in this reaction are mostly lysine, hydroxyl(lysine) and arginine residues [85]. It has been demonstrated that genipin is even 10000 times less cytotoxic than GTA and by this reason, genipin has been applied to microcapsules for drug delivery [103] or used in nerve guiding conduits [104] and of course to crosslink scaffolds for articular cartilage engineering [76].

#### **4.2.4. Non-enzymatic crosslinking by glycation**

Among large group of chemical crosslinkers and physical methods non-enzymatic crosslinking by glycation is an unconventional method which has not been particularly used in the scaffolds fabrication. The term glycation refers to ability of reducing sugars as monosaccharides (glucose, fructose, galactose, ribose, arabinose) to create covalent bonds of protein or lipid molecules [105]. In physiological conditions, collagen undergoes mainly enzymatic crosslinking by the enzyme lysyl oxidase, yielding intra- and intermolecular links between single molecules. Nonetheless, alternative pathway of collagen crosslinking *in vivo* as

non-enzymatic process also exists [60]. Research towards glycation of collagen has been mostly performed regarding diabetes and aging [84], [106]. Stiffening of proteins by crosslinking is a part of aging process of the ECM components in connective tissues. Moreover, in diabetes high amount of glucose in the blood results in the glycation of long-lived proteins as collagen [106], [107]. Glycation contributes to the formation of heterogeneous complex of fluorophores and chromophores collectively referred to as advanced glycation end products (AGEs) which can cause protein oxidation, impairing their overall function [107]. It has been found that AGEs are associated with delayed wound healing in diabetes and other degenerative diseases such as Alzheimer and cardiovascular disease [107], [108].

The mechanism of glycation begins from so-called Maillard reaction in which the aldehyde group of reducing sugar reacts with amino group of collagen amino acid residue producing a Schiff base [109], [110]. The Schiff base undergoes Amadori rearrangements to form stable Amadori products which, subsequently are converted to AGEs. Consequently, intermolecular crosslink is generated between lysine residue of collagen molecule and an arginine residue of another adjacent collagen molecule [111].

Very little is known about non-enzymatic crosslinking in the field of cartilage or bone tissue engineering. Primarily glycation has been investigated for skin and blood vessel substitutes [112], [113]. Several studies showed positive effect of glycation on decreasing degradation rate of native collagen and also on collagen gels [109], [113], [114]. Additionally, long-lasting efficiency of glycation by ribose used in dermal filler has been confirmed in a rabbit model [105]. Concerning cartilage TE Roy et al. reported improvement in viscoelastic properties and GAG release in glycated collagen compared to untreated sample [115].

## References

- [1] A. M. Bhosale and J. B. Richardson, "Articular cartilage: Structure, injuries and review of management," *Br. Med. Bull.*, vol. 87, no. 1, pp. 77–95, 2008.
- [2] P. X. Ma, "Scaffolds for tissue fabrication," *Mater. Today*, vol. 7, no. 5, pp. 30–40, 2004.
- [3] J. Farr and A. H. Gomoll, "2016 Barriers To Cartilage Restoration," *J. Clin. Orthop. Trauma*, vol. 7, no. 3, pp. 183–186, 2016.
- [4] A. F. C. and B. A. K. Rocky S. Tuan, "Cartilage Regeneration," *J Am Acad Orthop Surg.*, vol. 21, no. 5, pp. 303–311, 2013.
- [5] P. Rebecca, *Supporting Tissue: Cartilage*, AnatomyOne. 2012.
- [6] J. M. Mansour, "Biomechanics of Cartilage," *Kinesiolog. Mech. pathomechanics Hum. Mov.*, pp. 66–79, 2009.
- [7] T. E. Whitesides, *Orthopaedic Basic Science, Biology and Biomechanics of the Musculoskeletal System*, 2nd ed. 2001.
- [8] D. Buckwalter, JA.; Hunziker, EB.; Rosenberg, LC.; Coutts, R.; Adams, M.; Eyre, *Articular cartilage: composition and structure*. 1991.

- [9] A. K. Zhang L, Hu J, “The role of tissue engineering in articular cartilage repair and regeneration,” *Crit Rev Biomed Eng.*, vol. 37, no. 1–2, pp. 1–57, 2009.
- [10] W. C. Camarero-Espinosa S, Rothen-Rutishauser B, Foster EJ, “Articular cartilage: from formation to tissue engineering,” *Biomater Sci.*, vol. 4, no. 5, pp. 734–767, 2016.
- [11] G. Ofek and K. A. Athanasiou, “Micromechanical properties of chondrocytes and chondrons: relevance to articular cartilage tissue engineering,” *J. Mech. Mater. Struct.*, vol. 2, no. 6, pp. 1059–1086, 2007.
- [12] da S. M. L. Beyer Nardi N, “Mesenchymal stem cells: isolation, in vitro expansion and characterization.,” *Handb Exp Pharmacol.*, vol. 174, pp. 249–82, 2006.
- [13] M. F. Pittenger *et al.*, “Multilineage Potential of Adult Human Mesenchymal Stem Cells,” *Science (80-. )*, vol. 284, no. April, pp. 143–147, 1999.
- [14] T. D. Bornes, N. M. Jomha, A. Mulet-Sierra, and A. B. Adesida, “Hypoxic culture of bone marrow-derived mesenchymal stromal stem cells differentially enhances in vitro chondrogenesis within cell-seeded collagen and hyaluronic acid porous scaffolds,” *Stem Cell Res. Ther.*, vol. 6, no. 1, p. 84, 2015.
- [15] T. Bornes, N. Jomha, A. Mulet-Sierra, and A. Adesida, “Optimal Seeding Densities for In Vitro Chondrogenesis of Two and Three Dimensional-Isolated and Expanded Bone Marrow-Derived Mesenchymal Stromal Stem Cells within a Porous Collagen Scaffold.,” *Tissue Eng. Part C. Methods*, vol. 3, no. 7, pp. 111–23, 2016.
- [16] S. A. R. A.D. Pearle, R.F. Warren, “Basic science of articular cartilage andosteoarthritis,” *Clin. Sport. Med.*, vol. 24, pp. 1–12, 2005.
- [17] D. Correa and S. A. Lietman, “Articular cartilage repair: Current needs, methods and research directions,” *Semin. Cell Dev. Biol.*, 2016.
- [18] D. E. Discher, “Tissue Cells Feel and Respon to the Stiffness of Their Substrate,” *Science (80-. )*, vol. 310, no. 5751, pp. 1139–1143, 2005.
- [19] C. R. Patino MG, Neiders ME, Andreana S, Noble B, “Collagen: an overview.,” *Implant Dent*, vol. 11, no. 3, pp. 280–5, 2002.
- [20] A. J. Sophia Fox, A. Bedi, and S. A. Rodeo, “The basic science of articular cartilage: structure, composition, and function,” *Sports Health*, vol. 1, no. 6, pp. 461–8, 2009.
- [21] C. Kiani, L. Chen, Y. J. Wu, A. J. Yee, and B. B. Yang, “Structure and function of aggrecan,” *Cell Res.*, vol. 12, pp. 19–32, 2002.
- [22] L. J. Schwartz MH, Leo PH, “A microstructural model for the elastic response of articular cartilage,” *J Biomech.*, vol. 27, no. 7, pp. 865–73, 1994.
- [23] A. C. Mow VC, Kuei SC, Lai WM, “Biphasic creep and stress relaxation of articular cartilage in compression. Theory and experiments.,” *J Biomech Eng.*, vol. 102, no. 1, pp. 73–84, 1980.
- [24] K. A. Athanasiou, M. P. Rosenwasser, J. A. Buckwalter, T. I. Malinin, and V. C. Mow, “Interspecies Comparisons of Insitu Intrinsic Mechanical-Properties of Distal Femoral Cartilage,” *J. Orthop. Res.*, vol. 9, no. 3, pp. 330–340, 1991.
- [25] C. J. J. Laurencin CT, Ambrosio AM, Borden MD, “Tissue engineering: orthopedic applications.,” *Annu Rev Biomed Eng.*, vol. 1, pp. 19–46, 1999.
- [26] F. Perdisa, N. Gostynska, A. Roffi, G. Filardo, M. Marcacci, and E. Kon, “Adipose-Derived Mesenchymal Stem Cells for the Treatment of Articular Cartilage :A Systematic Review on Preclinical and Clinical Evidence,” *Stem Cells Int.*, vol. 2015, p. Article ID 597652, 2015.
- [27] M. Cucchiarini *et al.*, “Basic science of osteoarthritis,” *J. Exp. Orthop.*, vol. 3, no. 1, p. 22, 2016.
- [28] P. L. Brittberg M, Lindahl A, Nilsson A, Ohlsson C, Isaksson O, “Treatment of deep cartilage defects in the knee with autologous chondrocyte transplantation.,” *N. Engl. J. Med.*, vol. 331, no. 14, pp. 889–95, 1994.

- [29] L. F. M. Ambra, A. Phan, M. Mastrocola, and A. H. Gomoll, "Cell-seeded Autologous Chondrocyte Implantation (cs-ACI) - A Simplified Implantation Technique with Maintained Clinical Outcomes," *Orthop. J. Sport. Med.*, vol. 4, no. 7 Suppl, pp. 3–4, 2016.
- [30] M. K. and M. V. Robi Kelc, Jakob Naranda, *Novel Therapies for the Management of Sports Injuries*. 2013.
- [31] M. Marcacci *et al.*, "Stem cells associated with macroporous bioceramics for long bone repair: 6- to 7-year outcome of a pilot clinical study.," *Tissue Eng.*, vol. 13, no. 5, pp. 947–55, 2007.
- [32] F. J. O'Brien, "Biomaterials & scaffolds for tissue engineering," *Mater. Today*, vol. 14, no. 3, pp. 88–95, 2011.
- [33] Y. C. Fung, "3 . 0 Emergence and Evolution of a Shared Concept," *J. Biomech. Eng.*, pp. 18–24, 2001.
- [34] V. J. Langer R, "Tissue engineering," *Science (80- )*, vol. 260, no. 5110, pp. 920–6, 1993.
- [35] A. J. Ryan and F. J. O'Brien, "Insoluble elastin reduces collagen scaffold stiffness, improves viscoelastic properties, and induces a contractile phenotype in smooth muscle cells," *Biomaterials*, vol. 73, pp. 296–307, 2015.
- [36] "Tissue engineering," *Wikipedia*. .
- [37] A. R. Phull, S. H. Eo, Q. Abbas, M. Ahmed, and S. J. Kim, "Applications of Chondrocyte-Based Cartilage Engineering: An Overview," *Biomed Res. Int.*, vol. 2016, 2016.
- [38] A. K. Darling EM, "Rapid phenotypic changes in passaged articular chondrocyte subpopulations.," *J Orthop Res.*, vol. 23, no. 2, p. 425–32., 2005.
- [39] G. Filardo, H. Madry, M. Jelic, A. Roffi, M. Cucchiari, and E. Kon, "Mesenchymal stem cells for the treatment of cartilage lesions: From preclinical findings to clinical application in orthopaedics," *Knee Surgery, Sport. Traumatol. Arthrosc.*, vol. 21, no. 8, pp. 1717–1729, 2013.
- [40] J. C. Vinatier C, Bouffi C, Merceron C, Gordeladze J, Brondello JM and N. D. Weiss P, Guicheux J, "Cartilage tissue engineering: towards a biomaterial-assisted mesenchymal stem cell therapy.," *Curr Stem Cell Res Ther.*, vol. 4, no. 4, pp. 318–29, 2009.
- [41] O. Vega A, Martín-Ferrero MA, Del Canto F, Alberca M, García V, Munar A and G.-S. J. L, Soler R, Fuertes JJ, Huguet M, Sánchez A, "Treatment of Knee Osteoarthritis With Allogeneic Bone Marrow Mesenchymal Stem Cells: A Randomized Controlled Trial.," *Transplantation.*, vol. 99, no. 8, pp. 1681–90, 2015.
- [42] H. J. Wong KL, Lee KB, Tai BC, Law P, Lee EH, "Injectable cultured bone marrow-derived mesenchymal stem cells in varus knees with cartilage defects undergoing high tibial osteotomy: a prospective, randomized controlled clinical trial with 2 years' follow-up.," *Arthroscopy*, vol. 29, no. 12, pp. 2020–8, 2013.
- [43] H. Saeed *et al.*, "Mesenchymal stem cells (MSCs) as skeletal therapeutics-an update.," *J. Biomed. Sci.*, vol. 23, no. 1, p. 41, 2016.
- [44] G. Filardo, F. Perdisa, A. Roffi, M. Marcacci, and E. Kon, "Stem cells in articular cartilage regeneration.," *J. Orthop. Surg. Res.*, vol. 11, p. 42, 2016.
- [45] O. K. Russell KC, Phinney DG, Lacey MR, Barrilleaux BL, Meyertholen KE, "In vitro high-capacity assay to quantify the clonal heterogeneity in trilineage potential of mesenchymal stem cells reveals a complex hierarchy of lineage commitment.," *Stem Cells.*, vol. 28, no. 4, pp. 788–98, 2010.
- [46] J. Kramer, C. Hegert, K. Guan, a M. Wobus, P. K. Müller, and J. Rohwedel, "Embryonic stem cell-derived chondrogenic differentiation in vitro: activation by BMP-2 and BMP-4.," *Mech. Dev.*, vol. 92, no. 2, pp. 193–205, 2000.



- [47] T. Lu, Y. Li, and T. Chen, "Techniques for fabrication and construction of three-dimensional scaffolds for tissue engineering," *Int. J. Nanomedicine*, vol. 8, pp. 337–350, 2013.
- [48] J. C. C Liu, Z Xia, "Design and development of three-dimensional scaffolds for tissue engineering," *Chem. Eng. Res. Des.*, vol. 85, no. 7, pp. 1051–1064, 2007.
- [49] V. Marx, "Tissue engineering: Organs from the lab," *Nature*, vol. 522, no. 7556, pp. 373–377, 2015.
- [50] A. H. Doulabi, K. Mequanint, and H. Mohammadi, "Blends and nanocomposite biomaterials for articular cartilage tissue engineering," *Materials (Basel)*, vol. 7, no. 7, pp. 5327–5355, 2014.
- [51] G. R. Grigolo B, Roseti L, Fiorini M, Fini M, Giavaresi G, Aldini NN and F. A., "Transplantation of chondrocytes seeded on a hyaluronan derivative (hyaff-11) into cartilage defects in rabbits," *Biomaterials*, vol. 22, no. 17, pp. 2417–24, 2001.
- [52] V.-N. G. Freed LE, Hollander AP, Martin I, Barry JR, Langer R, "Chondrogenesis in a cell-polymer-bioreactor system," *Exp Cell Res.*, vol. 240, no. 1, pp. 58–65, 1998.
- [53] Y. Gong, Q. Zhou, C. Gao, and J. Shen, "In vitro and in vivo degradability and cytocompatibility of poly(l-lactic acid) scaffold fabricated by a gelatin particle leaching method," *Acta Biomater.*, vol. 3, no. 4, pp. 531–540, 2007.
- [54] M. M. Kon E, Filardo G, Di Martino A, Busacca M, Moio A, Perdisa F, "Clinical results and MRI evolution of a nano-composite multilayered biomaterial for osteochondral regeneration at 5 years," *Am J Sport. Med.*, vol. 42, no. 1, pp. 158–65, 2014.
- [55] E. Kon, G. Filardo, F. Perdisa, G. Venieri, and M. Marcacci, "Clinical results of multilayered biomaterials for osteochondral regeneration," *J. Exp. Orthop.*, vol. 1, no. 1, p. 10, 2014.
- [56] E. D. Dhollander AA, Liekens K, Almqvist KF, Verdonk R, Lambrecht S and V. P. Verbruggen G, "A pilot study of the use of an osteochondral scaffold plug for cartilage repair in the knee and how to deal with early clinical failures," *Arthroscopy*, vol. 28, no. 2, pp. 225–33, 2012.
- [57] R. D. Kon E, Drobnic M, Davidson PA, Levy A, Zaslav KR, "Chronic posttraumatic cartilage lesion of the knee treated with an acellular osteochondral-regenerating implant: case history with rehabilitation guidelines," *J Sport Rehabil*, vol. 23, no. 3, pp. 270–5, 2014.
- [58] R. Kon E, Filardo G, Shani J, Altschuler N, Levy A, Zaslav K, Eisman JE and D., "Osteochondral regeneration with a novel aragonite-hyaluronate biphasic scaffold: up to 12-month follow-up study in a goat model," *J Orthop Surg Res.*, 2015.
- [59] C. Liu, Z. Xia, and J. T. Czernuszka, "Design and Development of Three-Dimensional Scaffolds for Tissue Engineering," *Chem. Eng. Res. Des.*, vol. 85, no. 7, pp. 1051–1064, 2007.
- [60] R. Zeeman *et al.*, "Crosslinking and modification of dermal sheep collagen using 1,4-butanediol diglycidyl ether," *J. Biomed. Mater. Res.*, vol. 46, no. 3, pp. 424–433, 1999.
- [61] L. P. Yan, J. M. Oliveira, A. L. Oliveira, S. G. Caridade, J. F. Mano, and R. L. Reis, "Macro/microporous silk fibroin scaffolds with potential for articular cartilage and meniscus tissue engineering applications," *Acta Biomater.*, vol. 8, no. 1, pp. 289–301, 2012.
- [62] L. Ma, C. Gao, Z. Mao, J. Zhou, and J. Shen, "Enhanced biological stability of collagen porous scaffolds by using amino acids as novel crosslinking bridges," *Biomaterials*, vol. 25, no. 15, pp. 2997–3004, 2004.
- [63] A. V. Taubenberger, M. A. Woodruff, H. Bai, D. J. Muller, and D. W. Hutmacher, "The effect of unlocking RGD-motifs in collagen I on pre-osteoblast adhesion and differentiation," *Biomaterials*, vol. 31, no. 10, pp. 2827–2835, 2010.

- [64] G. E. Davis, K. J. Bayless, M. J. Davis, and G. a Meininger, "Regulation of tissue injury responses by the exposure of matricryptic sites within extracellular matrix molecules.," *Am. J. Pathol.*, vol. 156, no. 5, pp. 1489–1498, 2000.
- [65] Y. Y. Peng, L. Howell, V. Stoichevska, J. A. Werkmeister, G. J. Dumsday, and J. A. M. Ramshaw, "Towards scalable production of a collagen-like protein from *Streptococcus pyogenes* for biomedical applications.," *Microb. Cell Fact.*, vol. 11, no. 1, p. 146, 2012.
- [66] G. B. Ramírez-Rodríguez, M. Iafisco, A. Tampieri, J. Gómez-Morales, and J. M. Delgado-López, "pH-responsive collagen fibrillogenesis in confined droplets induced by vapour diffusion," *J. Mater. Sci. Mater. Med.*, vol. 25, no. 10, pp. 2305–2312, 2014.
- [67] M. D. Shoulders and R. T. Raines, "Collagen Structure and Stability," *Annu Rev Biochem*, vol. 78, pp. 929–958, 2010.
- [68] J. P. R. O. Orgel, A. Miller, T. C. Irving, R. F. Fischetti, A. P. Hammersley, and T. J. Wess, "The in situ supermolecular structure of type I collagen," *Structure*, vol. 9, no. 11, pp. 1061–1069, 2001.
- [69] and F. M.-G. Stéphanie Claus, Nathalie Mayer, Elisabeth Aubert-Foucher, Hanane Chajra, Emeline Perrier-Groult, Jérôme Lafont, Muriel Piperno, Odile Damour, "Cartilage-Characteristic Matrix Reconstruction by Sequential Addition of Soluble Factors During Expansion of Human Articular Chondrocytes and Their Cultivation in Collagen Sponges," *Tissue Eng. Part C Methods.*, vol. 18, no. 2, pp. 104–112, 2012.
- [70] C. N. Grover, R. E. Cameron, and S. M. Best, "Investigating the morphological, mechanical and degradation properties of scaffolds comprising collagen, gelatin and elastin for use in soft tissue engineering," *J. Mech. Behav. Biomed. Mater.*, vol. 10, pp. 62–74, 2012.
- [71] T. Mazaki *et al.*, "A novel, visible light-induced, rapidly cross-linkable gelatin scaffold for osteochondral tissue engineering.," *Sci. Rep.*, vol. 4, p. 4457, 2014.
- [72] M. E. Hoque, T. Nuge, T. K. Yeow, N. Nordin, and R. G. S. V Prasad, "Gelatin Based Scaffolds for Tissue Engineering – a Review," *Polym. Res. J.*, vol. 9, no. 1, 2014.
- [73] K. D. Mauney JR, Volloch V, "Matrix-mediated retention of adipogenic differentiation potential by human adult bone marrow-derived mesenchymal stem cells during ex vivo expansion.," *Biomaterials*, vol. 26(31), pp. 6167–75, 2005.
- [74] GIMA, "Gelatin handbook," *Gelatin Manuf. Inst. Am.*, p. 25, 2012.
- [75] K. G. Shankar *et al.*, "Investigation of different crosslinking approaches on 3D gelatin scaffolds for tissue engineering application: A comparative analysis," *Int. J. Biol. Macromol.*, 2016.
- [76] S. M. Lien, W. Te Li, and T. J. Huang, "Genipin-crosslinked gelatin scaffolds for articular cartilage tissue engineering with a novel crosslinking method," *Mater. Sci. Eng. C*, vol. 28, no. 1, pp. 36–43, 2008.
- [77] C. Tonda-turo, P. Gentile, S. Saracino, V. Chiono, V. K. Nandagiri, and G. Muzio, "Comparative analysis of gelatin scaffolds crosslinked by genipin and silane coupling agent," *Int. J. Biol. Macromol.*, vol. 49, no. 4, pp. 700–706, 2011.
- [78] A. Bigi, G. Cojazzi, S. Panzavolta, N. Roveri, and K. Rubini, "Stabilization of gelatin films by crosslinking with genipin," *Biomaterials*, vol. 23, no. 24, pp. 4827–4832, 2002.
- [79] G. F. Djabourov M, Lechaire JP, "Structure and rheology of gelatin and collagen gels.," *Biorheology*, vol. 30, no. 3–4, pp. 191–205, 1993.
- [80] G. D. Nicodemus and S. J. Bryant, "Cell {Encapsulation} in {Biodegradable} {Hydrogels} for {Tissue} {Engineering} {Applications}," *Tissue Eng. Part B. Rev.*, vol. 14, no. 2, pp. 149–165, 2008.
- [81] H. Lin, A. W. Cheng, P. G. Alexander, A. M. Beck, and R. S. Tuan, "Cartilage Tissue Engineering Application of Injectable Gelatin Hydrogel with In Situ Visible-Light-Activated Gelation Capability in both Air and Aqueous Solution.," *Tissue Eng. Part A*,

- vol. 20, no. 17–18, pp. 2402–2411, 2014.
- [82] “Cross-link,” *Wikipedia*. .
- [83] A. D. Jenkins / P. Kratochvíl / R. F. T. Stepto / U. W. Suter, “Glossary of basic terms in polymer science (IUPAC Recommendations 1996),” *Pure Appl. Chem.*, vol. 68, no. 12, pp. 2287–2311, 2009.
- [84] R. D. Semba, E. J. Nicklett, and L. Ferrucci, “Does accumulation of advanced glycation end products contribute to the aging phenotype?,” *Journals Gerontol. - Ser. A Biol. Sci. Med. Sci.*, vol. 65 A, no. 9, pp. 963–975, 2010.
- [85] K. Hunger, N. Schmeling, H. B. T. Jeazet, C. Janiak, C. Staudt, and K. Kleinermanns, “Investigation of cross-linked and additive containing polymer materials for membranes with improved performance in pervaporation and gas separation,” *Membranes (Basel)*, vol. 2, no. 4, pp. 727–763, 2012.
- [86] M. G. Haugh, M. J. Jaasma, and F. J. O’Brien, “The effect of dehydrothermal treatment on the mechanical and structural properties of collagen-GAG scaffolds,” *J. Biomed. Mater. Res. - Part A*, vol. 89, no. 2, pp. 363–369, 2009.
- [87] C. S. W. c I. Prasertsung , R. Mongkolnavin, S. Damrongsakkul, “Surface modification of dehydrothermal crosslinked gelatin film using a 50 Hz oxygen glow discharge,” *Surf. Coatings Technol.*, vol. 205, no. SUPPL. 2, pp. 133–138, 2011.
- [88] D. Nadeem, M. Kiamehr, X. Yang, and B. Su, “Fabrication and in vitro evaluation of a sponge-like bioactive-glass/gelatin composite scaffold for bone tissue engineering,” *Mater. Sci. Eng. C. Mater. Biol. Appl.*, vol. 33, no. 5, pp. 2669–78, 2013.
- [89] S. R. Gomes, G. Rodrigues, G. G. Martins, C. M. R. Henriques, and J. C. Silva, “In vitro evaluation of crosslinked electrospun fish gelatin scaffolds,” *Mater. Sci. Eng. C*, vol. 33, no. 3, pp. 1219–1227, 2013.
- [90] K. S. Weadock, E. J. Miller, E. L. Keuffel, and M. G. Dunn, “Effect of physical crosslinking methods on collagen-fiber durability in proteolytic solutions,” *J. Biomed. Mater. Res.*, vol. 32, no. 2, pp. 221–226, 1996.
- [91] N. Davidenko *et al.*, “Control of crosslinking for tailoring collagen-based scaffolds stability and mechanics,” *Acta Biomater.*, vol. 25, pp. 131–142, 2015.
- [92] H. C. Ma L, Gao C, Mao Z, Shen J, Hu X, “Thermal dehydration treatment and glutaraldehyde crosslinking to increase the biostability of collagen-chitosan porous scaffolds used as dermal equivalent,” *J Biomater Sci Polym Ed.*, vol. 14, no. 8, pp. 861–874, 2003.
- [93] A. Nicoletti, M. Fiorini, J. Paolillo, L. Dolcini, M. Sandri, and D. Pressato, “Effects of different crosslinking conditions on the chemical-physical properties of a novel bio-inspired composite scaffold stabilised with 1,4-butanediol diglycidyl ether (BDDGE),” *J. Mater. Sci. Mater. Med.*, vol. 24, no. 1, pp. 17–35, 2013.
- [94] H. D. Petite H, Rault I, Huc A, Menasche P, “Use of the acyl azide method for crosslinking collagen-rich tissues such as pericardium,” *J Biomed Mater Res.*, vol. 24, no. 2, pp. 179–87, 1990.
- [95] D. Cigognini *et al.*, “Engineering in vitro microenvironments for cell based therapies and drug discovery,” *Drug Discov. Today*, vol. 18, no. 21–22, pp. 1099–1108, 2013.
- [96] L. H. H. Olde Damink, P. J. Dijkstra, M. J. A. Van Luyn, P. B. Van Wachem, P. Nieuwenhuis, and J. Feijen, “Glutaraldehyde as a crosslinking agent for collagen-based biomaterials,” *J. Mater. Sci. Mater. Med.*, vol. 6, no. 8, pp. 460–472, 1995.
- [97] M. J. O. and J. M. L. Sergio Torres-Giner†, Jose V. Gimeno-Alcañiz‡, “Comparative Performance of Electrospun Collagen Nanofibers Cross-linked by Means of Different Methods,” *ACS Appl. Mater. Interfaces*, vol. 1, no. 1, pp. 218–223, 2009.
- [98] L. B. Koh *et al.*, “Epoxy cross-linked collagen and collagen-laminin peptide hydrogels as corneal substitutes,” *J. Funct. Biomater.*, vol. 4, no. 3, pp. 162–177, 2013.

- [99] A. La Gatta *et al.*, “Hyaluronan scaffolds via diglycidyl ether crosslinking: Toward improvements in composition and performance,” *Carbohydr. Polym.*, vol. 96, no. 2, pp. 536–544, 2013.
- [100] B. Y. Ao, C. Y. Ang, K. Z. Hang, H. S. Ong, and M. C. Hen, “Syntheses and characterization of pH-sensitive hydrogel from poly (  $\gamma$ -glutamic ) acid,” vol. 27, no. 1, 2009.
- [101] Damian Martin Kirchmajer, Clare A Watson, Marie Ranson, and Marc in het Panhuis, “Gelapin, a degradable genipin cross-linked gelatin hydrogel,” *RSC Adv.*, vol. 3, no. 4, pp. 1073–1081, 2012.
- [102] C. H. Yao, B. S. Liu, C. J. Chang, S. H. Hsu, and Y. S. Chen, “Preparation of networks of gelatin and genipin as degradable biomaterials,” *Mater. Chem. Phys.*, vol. 83, no. 2–3, pp. 204–208, 2004.
- [103] L. B. Nath SD, Abueva C, Kim B, “Chitosan-hyaluronic acid polyelectrolyte complex scaffold crosslinked with genipin for immobilization and controlled release of BMP-2.,” *Carbohydr Polym.*, vol. 22, no. 115, pp. 160–9, 2015.
- [104] C. CJ., “Effects of nerve growth factor from genipin-crosslinked gelatin in polycaprolactone conduit on peripheral nerve regeneration--in vitro and in vivo.,” *J Biomed Mater Res A.*, vol. 91, no. 2, pp. 586–96, 2009.
- [105] S. Pitaru *et al.*, “Long-term efficacy of a novel ribose-cross-linked collagen dermal filler: A histologic and histomorphometric study in an animal model,” *Dermatologic Surg.*, vol. 33, no. 9, pp. 1045–1053, 2007.
- [106] B. Boonkaew, K. Tompkins, J. Manokawinchoke, P. Pavasant, and P. Supaphol, “Characterization and cytological effects of a novel glycated gelatine substrate,” *Biomed Mater*, vol. 9, no. 2, p. 25001, 2014.
- [107] F. EA., “Advanced glycosylated end products and hyperglycemia in the pathogenesis of diabetic complications.,” *Diabetes Care.*, vol. 22, pp. 65–71, 1999.
- [108] M. G. Srikanth V, Maczurek A, Phan T, Steele M, Westcott B, Juskiw D, “Advanced glycation endproducts and their receptor RAGE in Alzheimer’s disease.,” *Neurobiol Aging.*, vol. 32, no. 5, pp. 763–77, 2011.
- [109] S. Tanaka, G. Avigad, E. F. Eikenberry, and B. Brodsky, “Isolation and partial characterization of collagen chains dimerized by sugar-derived cross-links.,” *J. Biol. Chem.*, vol. 263, no. 33, pp. 17650–17657, 1988.
- [110] R. Roy, A. Boskey, and L. J. Bonassar, “Processing of type I collagen gels using nonenzymatic glycation,” *J. Biomed. Mater. Res. - Part A*, vol. 93, no. 3, pp. 843–851, 2010.
- [111] H. Chiue, T. Yamazoye, and S. Matsumura, “Localization of the dominant non-enzymatic intermolecular crosslinking sites on fibrous collagen,” *Biochem. Biophys. Res. Commun.*, vol. 461, no. 3, pp. 445–449, 2015.
- [112] T. R. Girton TS, Oegema TR, Grassl ED, Isenberg BC, “Mechanisms of stiffening and strengthening in media-equivalents fabricated using glycation.,” *J Biomech Eng.*, vol. 22, no. 3, pp. 216–223, 2000.
- [113] T. R. Girton TS, Oegema TR, “Exploiting glycation to stiffen and strengthen tissue equivalents for tissue engineering.,” *J Biomed Mater Res.*, vol. 46, no. 1, pp. 87–92, 1999.
- [114] M. E. Francis-Sedlak, S. Uriel, J. C. Larson, H. P. Greisler, D. C. Venerus, and E. M. Brey, “Characterization of type I collagen gels modified by glycation,” *Biomaterials*, vol. 30, no. 9, pp. 1851–1856, 2009.
- [115] B. L. Roy R, Boskey AL, “Non-enzymatic glycation of chondrocyte-seeded Engineering., collagen gels for cartilage tissue,” *J Orthop Res.*, vol. 26, no. 11, pp. 1434–9, 2008.

# PART II

## ANALYTICAL METHODS

---

### 1. Freeze-drying process

Variety of techniques have been applied to fabricate scaffolds from synthetic and natural biomaterials which include conventional methods as solvent-casting and particulate leaching, gas foaming, phase separation, melt molding, and freeze drying. There are also other more advanced techniques as electrospinning and rapid prototyping which includes stereolithography (SLA), selective laser sintering (SLS), fused deposition modeling (FDM), three dimensional (3D) printing, and 3D plotting [1], [2].

In the research of this PhD thesis freeze-drying (FD), i.e., lyophilisation method was used to produce 3D porous scaffolds from the natural polymers. FD process is consistent of three main steps: 1) Freezing at low temperature (usually in the range from  $-40\text{ }^{\circ}\text{C}$  to  $-80\text{ }^{\circ}\text{C}$ ) where the polymer solution is completely frozen and the solvent forms ice crystals, forcing the polymer molecules to aggregate into the interstitial spaces; 2) Primary drying, where the solvent is removed by direct sublimation thanks to applying very low pressure through a partial vacuum; 3) Secondary drying, where the unfrozen water molecules are removed by desorption and the final product in a form of dry polymer scaffold is obtained. Whereas, porosity of the scaffold depends on the concentration of the polymer solution, pore size distribution can be controlled by the freezing temperatures [3], [4]. The main advantage of FD method is the exclusion of many washing steps because water as well as polymer solvent can be removed directly [2]. Moreover, special organic and sometimes toxic solvents are not necessary which makes scaffolds more suitable for biomedical application. Finally, this technique can be also applied to dry biological samples without destroying their bioactivity. Nonetheless, there are difficulties to achieve scaffold homogeneity or scaffolds with hierarchical structures, e.g., vascularized systems, by FD [3].

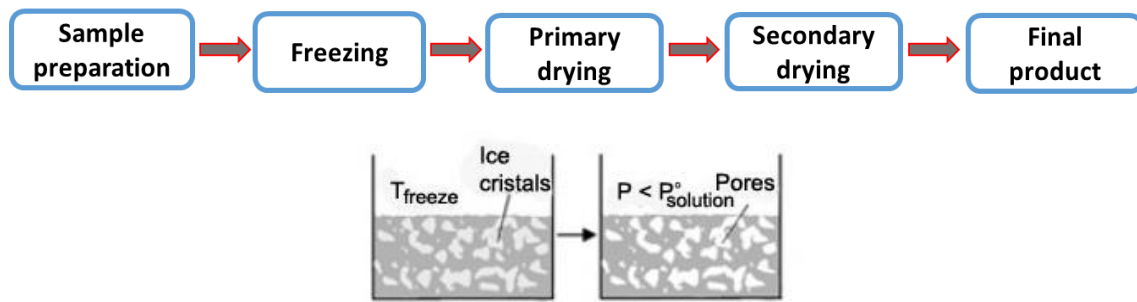


**Fig. 2.1** Steps of the freeze-drying process and its principle; a polymer solution is cooled down, forming solvent ice crystals. Then the solvent is removed by using a pressure lower than the equilibrium vapor pressure of the solvent ( $P^\circ$  solution), giving a porous structure [1].

## 2. Microscopy

### 2.1. Scanning electron microscopy (SEM)

The principle of scanning electron microscopy (SEM) is to use a focused beam of high-energy electrons to generate a variety of signals at the surface of solid specimens resulting in capture of various images. The interaction between electrons and the sample deliver information about the sample including external morphology (texture), chemical composition, and crystalline structure. SEM allows to capture high-resolution images of a sample surface, with the area ranging from approximately 1 cm to 5 microns in width (magnification ranging from 20X to approximately 30,000X, spatial resolution of 50 to 100 nm) [5].

The signals result from interactions of the electron beam with atoms at various depths within the sample include secondary electrons (that produce SEM images), back-scattered electrons (BSE), diffracted back-scattered electrons (EBSD that are used to determine crystal structures and orientations of minerals), photons (characteristic X-rays that are used for elemental analysis and continuum X-rays), visible light (cathodoluminescence–CL), and heat. Both secondary electrons and back-scattered electrons are the most common in samples imaging. Secondary electrons play important role in illustrating morphology and topography of samples and back-scattered electrons can provide information about the distribution of different elements in the sample. Characteristic X-rays are emitted when the electron beam removes an inner shell electron from the sample, causing a higher-energy electron to fill the shell and release energy. These characteristic X-rays are used to identify the composition and measure the abundance of elements in the sample [6], [7].

In a typical SEM, an electron beam is thermionically emitted from an electron gun fitted with a tungsten filament cathode. Electron gun guides the accelerated electron beam of energy ranging from 0.2 keV to 40 keV toward anode. Then, the beam passes through pairs of scanning coils or pairs of deflector plates in the electron column and the beam is inverted horizontally

and vertically and it is able to scan over a rectangular area of the sample surface. During the interaction of primary electrons with the sample, the electrons lose energy by repeated random scattering and absorption within so-called interaction volume of the specimen (dimension of teardrop) which extends from less than 100 nm to approximately 5  $\mu\text{m}$  into the surface. This energy exchange between the electron beam and the sample results in the reflection of high-energy electrons, emission of secondary electrons and the emission of electromagnetic radiation by different scatterings, each of which can be detected by specialized detectors. The final image can be generated due to the fact that each pixel of computer video memory is synchronized with the position of the beam on the specimen in the microscope, and the concluding image is therefore a distribution map of the intensity of the signal being emitted from the scanned area of the specimen [6], [8].

To prepare the sample for the SEM examination, a specimen has to be electrically conducting to obtain a sharp picture. Conductivity can be achieved by sample's coating in gold in sputter coater under a vacuum [5], [8]. The microscope employed in this study was a high resolution SEM FEI Quanta 200, UK.

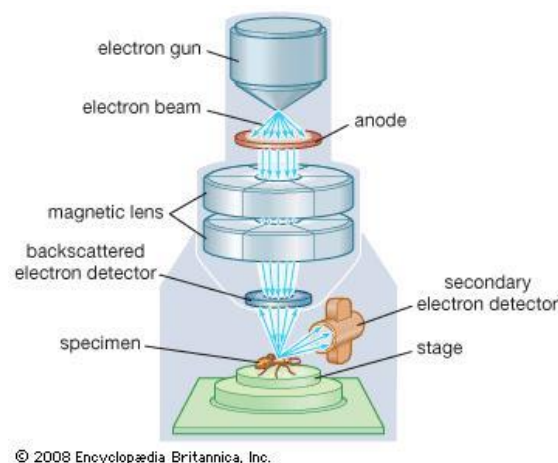


**Fig. 2.2** Scheme of Scanning Electron Microscope.

## 2.2. Fluorescence microscopy

Fluorescence microscopy is an indispensable tool in biomedical research nowadays which revolutionized optical microscopy and expanded possibilities in science. The principles of fluorescence microscopy are derived from fluorescence and phosphorescence which are both types of luminescence [9]. Molecules with fluorescent properties, means those which possess fluorophores or exhibit autofluorescence, absorb the light with short wavelength (for example UV light) invisible to the human eye and then they emit the light in the visible region, with long wavelength and low energy. These two processes are called excitation and emission and are

strictly related to the energy levels of the electrons in the atomic structure of fluorescent specimen. A range of wavelengths of light can excite the electrons of a fluorophore resulting in the emission spectrum shifted to longer wavelengths which is known as Stokes' shift (Fig. 2.3) [9], [10]. As Stokes' shift values increase, it becomes easier to separate excitation from emission light through the use of fluorescence filter combinations. In immunofluorescence a single wavelength can be used to excite several fluorophores with different Stokes shifts and thereby produce a variety of fluorescence colours [11].

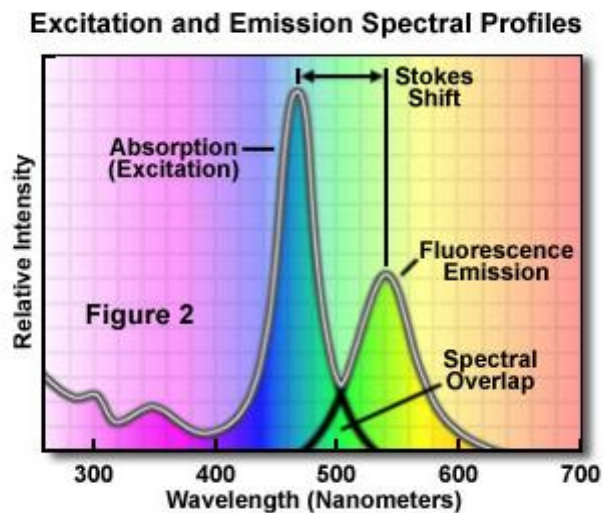


**Fig. 2.3.** Schematic example of excitation and emission spectrum with well notable Stokes shift of a fluorescent specimen. Adapted from [www.physicsforums.com](http://www.physicsforums.com)

In the fluorescence the essential role play already mentioned chemical compounds with fluorescence properties so-called fluorophores or fluorochromes. The application of fluorochromes allows to identify cells and sub-microscopic cellular components with a high degree of specificity among non-fluorescing material [12]. Fluorochromes are stains that attach themselves to visible or sub-visible structures, are often highly specific in their attachment targeting, and have a significant quantum yield (the ratio of photon absorption to emission). In immunofluorescence fluorochromes can be attached to antibodies which will then bind to specific chemical structures on or inside cells. The widespread growth in the utilization of fluorescence microscopy is closely linked to the development of new synthetic and naturally occurring fluorophores with known intensity profiles of excitation and emission, along with well-understood biological targets. The examples of fluorophores widely used in research are Hoechst 33342 or DAPI which bind to DNA, fluorescein isothiocyanate (FITC) and tetramethylrhodamine (TRITC) which can be conjugated with antibodies or other compounds [12].



The majority of fluorescence microscopes, especially those used in the life sciences, are of the epifluorescence design where excitation of the fluorophore and detection of the fluorescence are done through the same light path, i.e. through the objective (Fig. 2.4). Typical components of a fluorescence microscope are a light source, the excitation filter, the dichroic mirror (or dichroic beamsplitter), and the emission filter [13]. The filters and the dichroic mirror are chosen to match the spectral excitation and emission characteristics of the fluorophore used to label the specimen. In this manner, the distribution of a single fluorophore (color) is imaged at a time. In epifluorescence microscope light of the excitation wavelength is focused on the specimen through the objective lens. The fluorescence emitted by the specimen is focused to the detector by the same objective that is used for the excitation which for greater resolution will need objective lens with higher numerical aperture. Since most of the excitation light is transmitted through the specimen, only reflected excitatory light reaches the objective together with the emitted light and the epifluorescence method therefore gives a high signal-to-noise ratio. An additional wavelength specific filter between the objective and the detector can filter out the remaining excitation light from fluorescent light. Fluorescence microscopy requires intense, near-monochromatic, illumination which some widespread light sources, like halogen lamps cannot provide. Four main types of light source are used, including xenon arc lamps or mercury-vapor lamps with an excitation filter, lasers, supercontinuum sources, and high-power LEDs [9], [13].

The microscope used in this project was Eclipse Ti-U (NIKON).

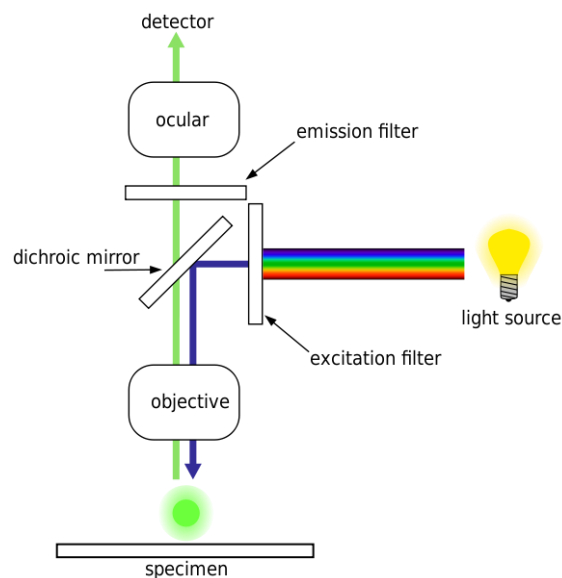


**Fig. 2.4.** Scheme of fluorescent microscope. Adapted from wikipedia.org.

### 3. Spectroscopy

#### 3.1. Ultraviolet–visible (UV-VIS) spectroscopy

Ultraviolet and visible spectrometers have been in general use for the last 35 years and over this period have become the most important analytical instrument in the modern day laboratory. UV-VIS spectroscopy attributes absorption and uses light in the visible and adjacent, near-UV and near-infrared ranges. The human eye is only sensitive to a tiny proportion of the total electromagnetic spectrum between approximately 380 and 780 nm and within this area the absorption directly affects the perceived color of the chemicals involved (Table 2.1) [14]. According to electronic transitions which undergo atoms and molecules in the electromagnetic spectrum, absorption in contrast to fluorescence, measures transitions from the ground state to the excited state. Molecules containing  $\pi$ -electrons or non-bonding electrons (n-electrons) can absorb the energy in the form of ultraviolet or visible light to excite these electrons to higher anti-bonding molecular orbitals. The more easily excited the electrons, the longer the wavelength of light it can absorb [15].

Color absorbed	Color observed	Absorbed radiation (nm)
Violet	Yellow-green	400-435
Blue	Yellow	435-480
Green-blue	Orange	480-490
Blue-green	Red	490-500
Green	Purple	500-560
Yellow-green	Violet	560-580
Yellow	Blue	580-595
Orange	Green-blue	595-605
Red	Blue-green	605-750

**Table 2.1.** Relationship between light absorption and color [14].

UV-VIS spectroscopy is commonly used in analytical chemistry for the quantitation of different substances, such as metal ions, conjugated organic compounds and biological macromolecules. The quantification of a material (absorber) in the solution can be obtained based on Beer-Lambert law which claims that the absorbance of a solution is directly proportional to the concentration of the absorbing species in the solution and the path length. To access the absorbance changes with concentration, it is necessary to prepare first the calibration curve by measuring the spectrum of a standard with a known concentration. The principle of UV-VIS spectrophotometer is to measure the intensity of light passing through a sample ( $I$ ) and compare it to the intensity of light before it passes through the sample ( $I_0$ ).

The ratio ( $I/I_0$ ) is called the transmittance, and is usually expressed as a percentage (%T). Then the absorbance A can be expressed as:  $A = -\log (\%T/100\%)$  [14], [15].

The basic parts of a spectrophotometer are a light source, a holder for the sample, a diffraction grating in a monochromator or a prism to separate the different wavelengths of light, and a detector. The radiation source is often a Tungsten filament (300-2500 nm), a deuterium arc lamp, which is continuous over the ultraviolet region (190-400 nm), Xenon arc lamp, which is continuous from 160-2,000 nm; or more recently, light emitting diodes (LED) for the visible wavelengths. Liquid samples in standard UV-VIS spectrophotometer are measured in 1 cm transparent cuvettes for allow the radiation to pass over the spectral region of interest. Usually, cuvettes are made of high quality fused silica or quartz glass (UV radiation). Normal glass and plastic cuvettes are also common, however glass and most plastics absorb in the UV, which limits their accuracy to visible wavelengths [15]. Current technology allows also for measurement of samples with small volumes (microplates) and moreover, absorption of many samples can be read at once.

The instruments used in this study are: UV-Visible spectrophotometer (7315 Jenway, UK) and Multiskan FC Microplate photometer (Thermo Scientific, USA).

### **3.2. Fourier transform infrared spectroscopy (FTIR)**

In Fourier transform infrared spectroscopy (FTIR) an infrared spectrum (IR) of absorption or emission of different substances like solid, liquid or gas can be accomplished. FTIR spectrometer is able to simultaneously collect high spectral resolution data over a wide spectral range resulting in generation of spectra with patterns representing molecular structure of the sample. Each molecule possesses different functional groups therefore, by FTIR spectra an unknown sample can be identified as well as, specific impurities of the materials can be detected [16].

Three different regions of infrared portion of the electromagnetic spectrum can be distinguished depending on their relation to the visible spectrum as follows: i) the far-IR of approximately  $400-10\text{ cm}^{-1}$  ( $1000-30\ \mu\text{m}$ ) which is positioned adjacent to the microwave region, has low energy and may be used for rotational spectroscopy; ii) the mid-IR, approximately  $4000-400\text{ cm}^{-1}$  ( $30-1.4\ \mu\text{m}$ ) may be used to study the fundamental vibrations and associated rotational-vibrational structure and iii) the higher energy near-IR, approximately  $14000-4000\text{ cm}^{-1}$  ( $1.4-0.8\ \mu\text{m}$ ) can excite overtone or harmonic vibrations [16], [17].

IR spectroscopy takes advantage of the fact that each molecule has its specific frequency at which it rotates or vibrates corresponding to discrete energy levels (Fig.2.5). The specific,

resonant frequencies are determined by the shape of the molecular potential energy surfaces, the masses of the atoms and, by the coupling of vibrational and electronic interactions in the molecule. Therefore, the resonant frequencies can be correlated to a particular bond type and can be used for the characterization of very complex mixtures [18].

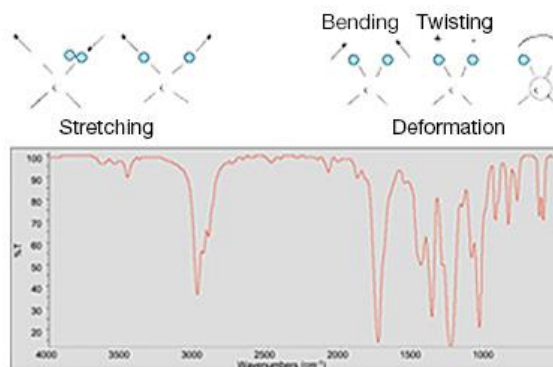


**Fig. 2.5** Possible vibrations detected by infrared spectroscopy (top of the illustration) and example of the corresponding FTIR spectrum [18].

In the FTIR instrument a beam of infrared light goes through an interferometer and onto the sample absorbing all the different wavelengths characteristic of its spectrum at once. Instead, in standard IR spectrometer with a monochromator the source radiation is separated into its different wavelengths limiting the amount of signal which can be obtained at a particular resolution. Thanks to the beamsplitter which send the light through moving and stationary mirrors the beam passing through the sample is recombined and the detector reports variation in energy versus time for all wavelengths simultaneously (Fig. 2.6) [17].

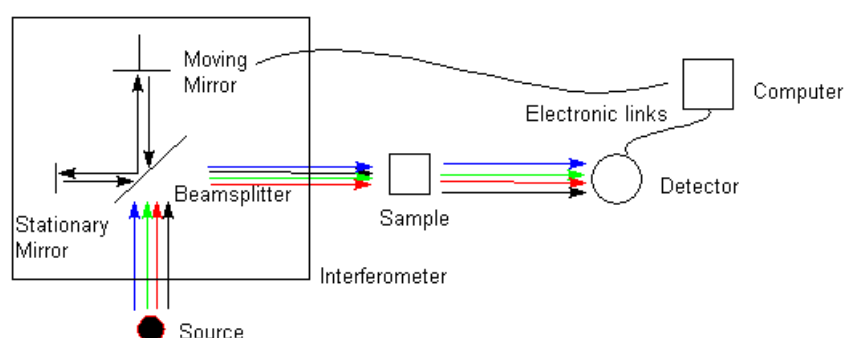


**Fig. 2.6** Scheme of FTIR spectrometer. Adapted from [www.chemistry.oregonstate.edu](http://www.chemistry.oregonstate.edu) [17].

In order to prepare sample for FTIR analysis, necessary is to grind a quantity of the sample with potassium bromide finely (to remove scattering effects from large crystals), which is used also as a reference. This powder mixture is then crushed in a mechanical die press to form a translucent pellet through which the beam of the spectrometer can pass. The use of reference is important because it can prevent fluctuations in the output of the source affecting the data and

also it allows the effects of the solvent to be cancelled out (the reference is usually pure solvent) [16].

The equipment employed in the present work was a Thermo Nicolet-Avatar 320 FT-IR.

#### **4. Thermo-gravimetric Analysis (TGA)**

Thermogravimetric Analysis (TGA) is a type of testing used to determine changes in weight depending on changes in temperature of tested samples. In TGA analysis three crucial parameters have to be measured accurately, which are: weight, temperature, and temperature change. Due to the fact that many weight loss curves look similar, the weight loss curve requires transformation before results may be interpreted. A derivative weight loss curve can be used to tell the point at which weight loss is most apparent.

The TGA analyzer usually consists of a high-precision balance with a pan loaded with the sample. The sample is placed in a small electrically heated oven with a thermocouple to precisely measure the temperature. The atmosphere may be purged with an inert gas to prevent oxidation or other undesired reactions and a computer is used to control the instrument. Analysis is carried out by raising the temperature gradually and plotting weight against temperature. After the data is obtained, curve smoothing and other operations may be done such as to find the exact points of inflection [19].

A Q600 instrument was used in this study (TA instruments).

#### **5. Mechanical analysis**

Mechanical testing is a powerful analytical tool which can provide information about mechanical properties of the materials. Among variety of tests, mechanical analysis can be simply divided into two categories: static and dynamic mechanical analysis.

*Static mechanical test* is an evaluation in which static loading (force/stress) is applied to the sample in order to obtain values of Young's modulus (elastic modulus), compressive or tensile strength, stiffness etc. [20]. The static test can be performed in the compressive or tensile mode, in compression or tensile clamp respectively. The choice of the clamp depends on the searched information and also on the type of material testing. Gels and elastomers are suitable for the compression clamp while films and fibers can be measured in the tension clamp. Under compression a material undergoes deformation and shortening as its molecules are forced together. Compression or compressive strength is the capacity of a material to withstand axial

loads tending to reduce size, in contrast to tensile strength, which withstands loads tending to elongate. Suitable compressive strength is a key value for scaffolds design [20], [21].

From the basic uniaxial mechanical test we can plot so-called stress-strain curve and based on this curve calculate Young's modulus. The stress-strain curve is obtained by recording the amount of deformation (strain) at distinct intervals of tensile or compressive loading (stress) and it differs for various types of materials (Fig. 2.7). In the stress-strain curve different regions can be distinguished and the most important is the initial linear part where the material follows Hooke's Law. This linear portion of stress-strain curve is an elastic range attributing to elastic modulus (Young's modulus) which refers to the measurement of the material's stiffness, or its resistance to deformation. Young's modulus ( $E$ ) is the ratio of stress ( $\sigma$ ) to strain ( $\epsilon$ ) and can be calculated as follows [22]:

$$E = \frac{\Delta\sigma}{\Delta\epsilon} \text{ where, } l_f = \frac{F}{A_0} \text{ and } \epsilon = \frac{L - L_0}{L_0}$$

$F$  - is the force exerted on an object under tension,  
 $A_0$  - the actual cross-sectional area through which the force is applied,  
 $L_0$  - original length of the sample,  
 $L$  - current length of the sample.

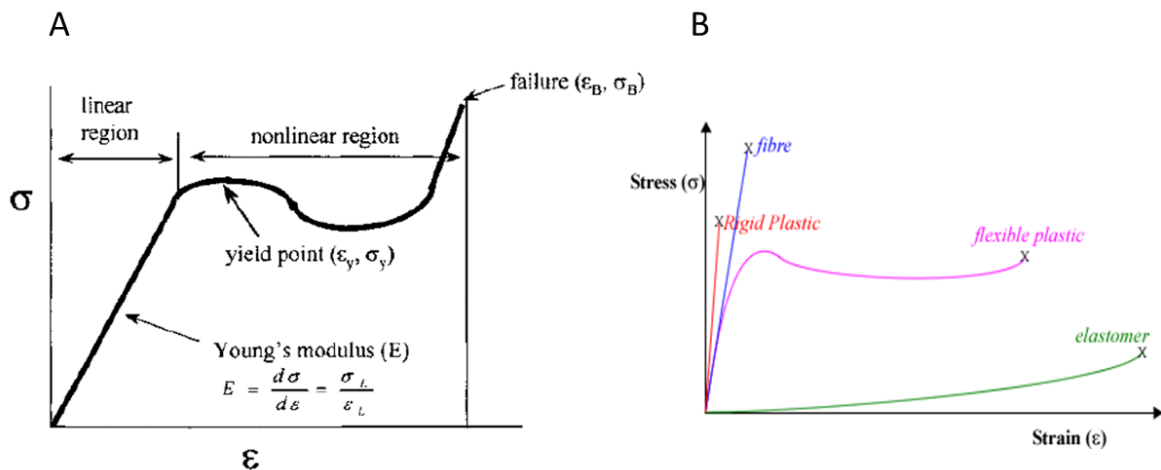


**Fig. 2.7** (A) Example of stress-strain curve and analysis of its different parts as linear and nonlinear region [20]. (B) Diverse stress-strain curves corresponded to different materials; adapted from [www.che.hw.ac.uk](http://www.che.hw.ac.uk)

The linear region terminates at what is known as the yield point. Above this point the material behaves plastically and will not return to its original length once the load is removed. At some load the material will fail (break), and this is known as the ultimate strength, in compression as the compressive strength (Fig. 2.7 A). It should be noted that this failure at the ultimate strength

follows massive deformation of the sample. The area under the curve is proportional to the energy needed to break the sample. The shape of the stress-strain curve and its area tells us about whether the material is tough or brittle or weak or strong. Depends on the type of material tested: plastic, fibre, glass or elastic polymer different Young's modulus and different failure point can be observed (Fig. 2.7 B) [20].

**Dynamic mechanical analysis (DMA)** or dynamic mechanical thermal analysis (DMTA) refer to mechanical tests in which oscillating force is applying to a sample and material's response is analysed to characterize its viscoelastic behaviour [23]. From this, one calculates properties like the tendency to flow (called viscosity) from the phase lag and the stiffness (modulus) from the sample recovery. These properties are often described as the ability to lose energy as heat (damping) and the ability to recover from deformation (elasticity).

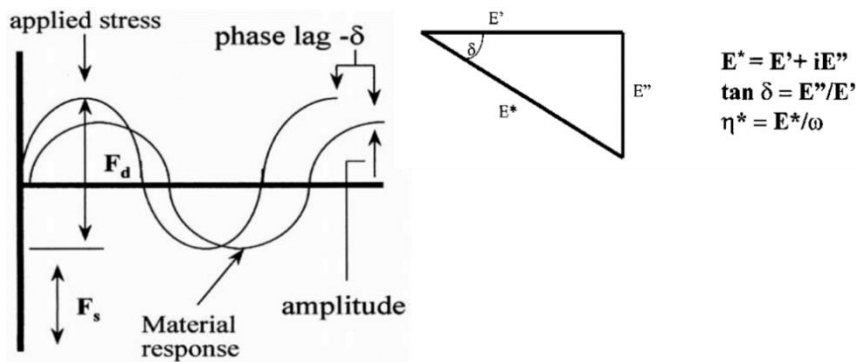


**Fig. 2.8** DMA analysis: The relationship of the applied sinusoidal stress to strain with the resultant phase lag and deformation.  $F_d$  is the dynamic or oscillatory force while  $F_s$  is the static or clamping force. On the right corner: mathematical relation among complex modulus ( $E^*$ ), storage modulus ( $E'$ ), loss modulus ( $E''$ ) and tan delta ( $\delta$ ) [20].

In DMA test a set of multiple or single frequencies can be applied to the sample as well as different temperature range (DMTA). The DMA supplies an oscillatory force, causing a sinusoidal stress to be applied to the sample, which generates a sinusoidal strain. By measuring both the amplitude of the deformation at the peak of the sine wave and the lag between the stress and strain sine waves, quantities like the modulus, the viscosity, and the damping can be calculated (Fig. 2.8) [20], [23]. Dynamic stress,  $\sigma$ , and strain,  $\epsilon$ , are given as:

$$\sigma(t) = \sigma_0 \sin(\omega t + \delta)$$

$$\epsilon(t) = \epsilon_0 \sin(\omega t)$$

where  $\omega$  is the angular frequency.

The modulus measured in DMA is a complex modulus ( $E^*$ ), calculated from the material response to the sine wave and composed of elastic (storage) modulus ( $E'$ ) and imaginary (loss)

modulus ( $E''$ ) [20]. The storage modulus is an in-phase component describing the ability of the material to return or store energy.  $E'$  refers to the elastic response of the material but it is not exactly the same as the Young's modulus. Loss modulus is an out of phase component describing the loss of energy by a material and it is a measure of its viscous response. The ratio of storage to loss modulus is called tan delta ( $\delta$ ) or loss factor and it refers to damping, the measure of energy dissipation of a material [21]. The complex ( $E^*$ ), storage ( $E'$ ) and loss ( $E''$ ) modulus as well as  $\tan \delta$  can be given in mathematical equations as follow:

$$E^* = E' + iE''$$

$$E' = \frac{If_0}{\varepsilon_0} \cos(\delta) \quad \text{and} \quad E'' = \frac{If_0}{\varepsilon_0} \sin(\delta) \quad \tan\delta = \frac{E''}{E'}$$

DMA analyzers allow for performing variety of tests: dynamic oscillatory tests as frequency sweep or stress/strain sweep and also transient tests as creep and stress relaxation. Creep testing is a basic probe of polymer relaxations and a fundamental form of polymer behavior. Creep test involves loading a sample with a set weight and watching the strain change over time. Recovery tests look at how the material relaxes once the load is removed [20].

The instrumentation of a DMA consists of a displacement sensor such as a linear variable differential transformer, which measures a change in voltage as a result of the instrument probe moving through a magnetic core, a temperature control system or furnace, a drive motor (a linear motor for probe loading which provides load for the applied force), a drive shaft support and guidance system to act as a guide for the force from the motor to the sample, and sample clamps in order to hold the sample being tested [24]. Geometry and dimensions of the sample are of the great importance when performing mechanical tests. Soft materials which were tested in this PhD work are suitable for use in the compressive mode as they often possess irregular shape and surfaces which make them more difficult to mount. Additionally, the thickness of the sample should be preferably higher or equal to its width.

DMA Q800 dynamic mechanical analyzer (TA instruments, IT) was the instrument employed in this study.

## 6. Quantitative real-time polymerase chain reaction (qPCR)

A real-time polymerase chain reaction (qPCR) is a laboratory technique in molecular biology which allows to detect and quantify RNA. Similar to traditional PCR (end-point detection), the idea of qPCR is to amplify a piece of DNA across several orders of magnitude, generating thousands to millions of copies of a particular DNA sequence. Nevertheless, unlike conventional PCR, real-time PCR allows monitoring of the desired product at any time in the



amplification process. For traditional PCR data is collected at the end-point (plateau), while real-time PCR collects data in the exponential growth phase. By using real-time PCR post PCR detection methods like electrophoresis in agarose, which are not precise and time consuming, can be avoided [25].

Another variant of PCR is a reverse transcription PCR (RT-PCR), which can be combined with real-time PCR (RT-qPCR) and such a combined technique was used in this study. In RT-PCR, RNA is used as a template to synthesize complementary DNA (cDNA) by enzyme called reverse transcriptase, which further serves as the template in the real-time PCR. To obtain cDNA in RT reaction a few components are needed: purified extracted RNA of interest, deoxyribonucleotides (dNTPs) as building blocks of cDNA, reverse transcriptase, non-specific primers and RNase inhibitor [26].

Two common methods for the detection of PCR products in real-time PCR are: (1) non-specific fluorescent dyes that intercalate with any double-stranded DNA, and (2) sequence-specific DNA probes consisting of oligonucleotides that are labelled with a fluorescent reporter which permits detection only after hybridization of the probe with its complementary sequence [27]. In the first option, commonly used fluorescent dye is a SYBR Green and in the second method, applied in the study of this thesis, is a technique with usage of TaqMan Probes. TaqMan probes are oligonucleotides having a fluorescent probe (reporter) attached to the 5' end and a quencher to the 3' end. During PCR amplification, these probes anneal to the target sequences of cDNA between the forward and reverse primers and as polymerase replicates the template with TaqMan bound, it also cleaves the fluorescent probe due to polymerase 5'-nuclease activity. Thereby, the distance between the reporter and the quencher increases causing the transfer of energy; the fluorescent emissions of the reporter increase captured by the Sequence Detection instrument and displayed by the software [25].

The PCR process normally is composed of approximately 25-50 cycles and contains a few main steps: the first (denaturation), at around 95 °C, allows to disrupt DNA template into single-stranded DNA molecules; the second (annealing), at a temperature of around 50-60 °C, allows the binding of the primers with the DNA template; the third (extension/elongation), at between 68 - 72 °C, facilitates the polymerization carried out by the DNA polymerase [26].

In this work, gene expression analysis has been performed by firstly reverse transcription carried out at different temperature as follow:

- 1) 25 °C for 10 min;
- 2) 37 °C for 2 h;
- 3) 85 °C for 5 min;

4) 4°C for ∞.

Then, qPCR (Taqman assay) could be performed using two pre-steps (1 and 2) and proper qPCR reaction composed of 40 cycles (Step 3 and 4):

1) 50 °C for 2 min; }     Activation of Taq  
2) 95 °C for 10 min; }     polymerase enzyme

3) Denaturation at 95 °C for 15 s;

4) Annealing/Extension at 60 °C for 1 min [25].

The machine for both RT and qPCR was supplied by Applied Biosystems, USA. After the reactions, gene expression can be analysed by absolute or relative quantitation. Absolute quantification relates the PCR signal to input copy number using a calibration curve, while relative quantification measures the relative change in mRNA expression levels correlated to mRNA expression of endogenous control (reference gene). Housekeeping genes e.g. glyceraldehyde 3-phosphate dehydrogenase or β-actin can be used as a reference gene [27].

## References

- [1] Ning Zhu and Xiongbiao Chen, “Biofabrication of Tissue Scaffolds,” in *Advances in Biomaterials Science and Biomedical Applications*, 2013, pp. 316–328.
- [2] Q. L. Loh and C. Choong, “Three-dimensional scaffolds for tissue engineering applications: role of porosity and pore size.,” *Tissue Eng. Part B. Rev.*, vol. 19, no. 6, pp. 485–502, 2013.
- [3] T. Lu, Y. Li, and T. Chen, “Techniques for fabrication and construction of three-dimensional scaffolds for tissue engineering,” *Int. J. Nanomedicine*, vol. 8, pp. 337–350, 2013.
- [4] B. R. Liapis AI, “A theory for the primary and secondary drying stages of the freeze-drying of pharmaceutical crystalline and amorphous solutes - comparison between experimental - data and theory.,” *Sep. Technol.*, vol. 4, no. 3, pp. 144–155, 1994.
- [5] “Scanning Electron Microscopy (SEM).” [Online]. Available: [http://serc.carleton.edu/research\\_education/geochemsheets/techniques/SEM.html](http://serc.carleton.edu/research_education/geochemsheets/techniques/SEM.html).
- [6] D. C. Joy, “Scanning Electron Microscopy,” in *Materials Science and Technology*, 2006.
- [7] A. Argast and C. F. Tennis Iii, “A Web Resource for the Study of Alkali Feldspars and Perthitic Textures Using Light Microscopy , Scanning Electron Microscopy and Energy Dispersive X-ray Spectroscopy,” *J. Geosci. Educ.*, vol. 53, no. 3, pp. 213–217, 2004.
- [8] “Scanning electron microscope,” *Wikipedia*. [Online]. Available: [https://en.wikipedia.org/wiki/Scanning\\_electron\\_microscope](https://en.wikipedia.org/wiki/Scanning_electron_microscope).
- [9] J. Lichtman, JW Conchello, “Fluorescence microscopy,” *Nat Methods.*, vol. 2, no. 12, pp. 910–9, 2005.
- [10] P. Kurzynowski, “Mikroskopia fluorescencyjna.”
- [11] T. Boenisch, “Antibodies,” *Immunohistochem. Stain. Methods*, p. 172, 2009.
- [12] Spring and Davidson, “Introduction to Fluorescence Microscopy.” [Online]. Available: <https://www.microscopyu.com/techniques/fluorescence/introduction-to-fluorescence-microscopy>.
- [13] “Fluorescence microscope,” *Wikipedia*. .

- [14] Thermo Spectronic, "Basic UV-Vis Theory , Concepts and Applications Basic," *ThermoSpectronic*, pp. 1–28, 2013.
- [15] "Ultraviolet–visible spectroscopy," *Wikipedia*. .
- [16] "Fourier transform infrared spectroscopy," *Wikipedia*. .
- [17] K. Gable, "FTIR Spectroscopy." [Online]. Available: <https://chemistry.oregonstate.edu/courses/ch361-464/ch362/irinstrs.htm>.
- [18] "FTIR Spectroscopy Academy." [Online]. Available: [www.thermofisher.com](http://www.thermofisher.com).
- [19] D'Alessandro Teresa, "DEVELOPMENT OF NEWLY CONCEIVED BIOMIMETIC NANO-STRUCTURED BIOMATERIALS AS SCAFFOLDS FOR BONE AND OSTEOCHONDRAL REGENERATION," University of Bologna, 2013.
- [20] K. P. Menard, *DYNAMIC MECHANICAL ANALYSIS A Practical Introduction*. 1999.
- [21] PerkinElmer Inc, "Dynamic Mechanical Analysis (DMA) - A Beginner's Guide," *Introd. to DMA*, pp. 1–23, 2008.
- [22] "Young's modulus," *Wikipedia*. .
- [23] K. S. Kwan Jr, "The Role of Penetrant Structure on the Transport and Mechanical Properties of a Thermoset Adhesive," 1998.
- [24] "Dynamic mechanical analysis," *Wikipedia*. .
- [25] A. Biosystems, "Guide to Performing Relative Quantitation of Gene Expression Using Real-Time Quantitative PCR," *Gene Expr.*, vol. 2009, pp. 1–60, 2008.
- [26] "Real-time polymerase chain reaction," *Wikipedia*. .
- [27] H. Lodish, "Molecular Cell Biology," *Perspective*, vol. 29, p. 973, 2003.

# PART III

## EXPERIMENTAL

---

### Chapter 1

## Experimental procedures

#### 1.1. Scaffolds Morphology Analysis

The morphological micro-architecture of the scaffolds was evaluated by scanning electron microscopy (SEM) performed on specimens mounted onto aluminium stubs using black carbon tapes and sputter coated with gold (Sputter Coater Q150TES, Quorum, Italy). The specimen surface was examined using high resolution SEM (FEI, Quanta 200, UK) at a pressure of 0.1m Torr at an accelerating voltage of 15 kV.

The pore size and pore distribution in the wet scaffolds were evaluated by imaging of thin slices (20  $\mu\text{m}$  thickness) under a bright field with inverted Ti-E fluorescence microscope (Nikon). The slices were obtained by using a cryostat (Histo-line, 5000 MC) to cut scaffolds previously soaked in phosphate buffer saline (PBS, pH 7.4) for 24 h then embedded in OCT and subsequently quenched into liquid nitrogen.

#### 1.2. Measurement of porosity

Percentage of porosity was measured by gravimetric method [1] conferring total porosity of the scaffold, and by water squeezing method [2] resulting in percentage of macropore volume. Total porosity of the scaffold was defined by measuring density of the dry scaffold ( $\rho^*$ ) and relating it to the known density of our polymers, collagen or gelatin ( $\rho_m$ ), following the formula:

$$\text{Porosity (\%)} = \left(1 - \frac{\rho^*}{\rho_m}\right) \times 100 \quad \rho^* = \frac{\text{mass}}{\text{volume}}$$

where, density of the scaffold ( $\rho^*$ ) is the ratio between the mass and the volume of the sample. Porosity measured by water squeezing method was expressed as a ratio between the water

strongly bound by polymer and the water present in entire porous structure of the polymer. Samples were immersed in milli-Q water for a few hours to obtain complete swelling, weighed ( $W_1$ ), next squeezed and weighed again ( $W_2$ ). Percentage of macropore porosity was calculated by the following equation:

$$\text{Macropore porosity (\%)} = \left( \frac{W_1 - W_2}{W_1} \right) \times 100$$

For both tests three cylindrical samples (diameter: 8-9 mm, thickness: 5 mm) of each composition were measured.

### 1.3. Fluid uptake

The swelling properties of the scaffolds were evaluated by monitoring the ability of fluid uptake with time. Cylindrical samples (diameter: 8-9 mm, thickness: 5 mm) were immersed in PBS at pH 7.4 and at 37 °C to mimic the physiological conditions. After designed soaking time the scaffolds were taken, wiped in filter paper and their weight was noted. The percentage of swelling ability was calculated by the following equation:

$$\text{Fluid uptake (\%)} = \left( \frac{W_t - W_o}{W_o} \right) \times 100$$

where  $W_o$  is a dry weight of the sample and  $W_t$  is a weight after swelling. Four samples for each group were analysed at respective soaking times.

### 1.4. Extent of crosslinking

The degree of cross-linking was quantified by 2, 4, 6-Trinitrobenzene sulfonic acid (TNBS) assay according to the method of Balakrishnan et al [3]. Briefly, 5 mg of crosslinked and non-crosslinked scaffolds were immersed in aqueous solution containing 1 ml of 4% (w/v) sodium hydrogen carbonate and freshly prepared 0.5% (v/v) TNBS (Sigma Aldrich, USA). Next, the mixtures were incubated in a water bath at 40 °C for 2 h. The reaction was terminated by addition of 3 ml of 6 M HCl to each reaction mixture and incubated at 60 °C for 1.5 h. The amount of amine groups bound to TNBS in the scaffolds was assessed by measuring the absorbance at 415 nm wavelength using UV-Visible spectrophotometer (7315 Jenway, UK). Percentage of crosslinking degree was then calculated according to the formula:

$$\text{Crosslinking degree (\%)} = 1 - \left( \frac{A_{\text{crosslinked}}}{A_{\text{non-crosslinked}}} \right) \times 100$$

where,  $A_{\text{crosslinked}}$  was the absorbance of crosslinked samples and  $A_{\text{non-crosslinked}}$  was the absorbance of non-crosslinked control. The experiment was performed in triplicate.

## 1.5. Degradation assays

### 1.5.1. Weight loss measurements

The physiological stability and controlled degradability of the scaffolds were assessed by monitoring the degradation rate. Briefly, 5 cylindrical samples (diameter: 8 mm, thickness: 5 mm) for each time point were immersed in PBS, pH.7.4 at 37 °C for 3, 7, 14 and 21 days. At scheduled time points scaffolds were rinsed two times in milli-Q water and dried at 40 °C. The percentage of weight loss was calculated by the following equation:

$$\text{Weight loss (\%)} = \left( \frac{W_o - W_d}{W_o} \right) \times 100$$

where  $W_o$  is an initial dry weight and  $W_d$  is a final weight of the sample after drying.

### 1.5.2. Collagenase digestion test

Stability of ribose-crosslinked collagen scaffolds was evaluated by *in vitro* enzymatic degradation test [4], [5]. Briefly, glycated and non-glycated collagen scaffolds of 10 mg dry weight were incubated in 1 ml 0.1 M Tris-HCl (pH 7.4) containing 22 CDU/mL (collagen digestion unit/mL) of bacterial collagenase (*Clostridium histolyticum*, Type 1, Sigma Aldrich, USA), at 37 °C. After 6 h, scaffold degradation was determined by protein quantification in the solution after digestion using a colorimetric assay (Kit DC Protein Assay, Bio-Rad). Percentage of degradation of the samples was calculated respect to the non-crosslinked collagen considered to be 100 % degraded. Three samples of each composition were measured.

The time of 6 h, needed for complete non-crosslinked collagen digestion was set by preliminary test according to the method of Sandri et al [5]. The degradation kinetics was evaluated reading the absorbance at  $\lambda = 280$  nm, corresponding to the absorbed wave number of the aromatic amino acids, Tyrosine and Tryptophan, released during the enzymatic collagen degradation. At different time points, percentage of digested collagen was calculated by the following equation:

$$\text{Collagen degradation (\%)} = \left( \frac{A_{280}(t)}{A_{280 \text{ max}}} \right) \times 100$$

where  $A_{280}(t)$  is an absorbance at the particular time and  $A_{280}(\text{max})$  is a final absorbance of the sample which remains constant with increasing time.

## 1.6. Fourier Transform Infrared Spectroscopy (FTIR)

The infrared spectra of scaffolds were obtained using Nicolet 380 FT-IR spectrometer (Thermo Fisher Scientific Inc, Waltham, USA). Initially, 2 mg of the scaffold were mixed with 100 mg of anhydrous KBr and then pressed at 8000 psi into 7 mm diameter discs. The spectra were collected in the wavelength ranging from 400 to 4000  $\text{cm}^{-1}$  with 2  $\text{cm}^{-1}$  of resolution.

### **1.7. Thermal characteristics**

The pyrolytic pattern of the scaffolds was determined using Thermo Gravimetric Analyser (TGA) (STA 449/C Jupiter, Netzsch Germany). Briefly, 10 mg samples were placed in aluminium crucible, crushed and press sealed for complete contact with the crucible. The experiment was carried out in the temperature range of 30–600 °C at a heating rate of 10 °C /min in nitrogen atmosphere.

### **1.8. Mechanical analysis**

Both static and dynamic compression test as well as creep test were performed in the compressive mode using DMA Q800 dynamic mechanical analyser (TA instruments, IT). For each test, cylindrical samples of gelatin scaffolds (diameter: 8 mm, thickness: 5 mm) and of collagen scaffolds (diameter: 9 mm, thickness: 7 mm) were pre-hydrated in PBS at 37 °C for 24 h prior to testing. Every test was carried out at 37 °C to mimic the physiological conditions. A small preload force was applied to each sample to provide a complete contact between the scaffold's surface and the compression plates.

#### **1.8.1. Static compression**

For standard mechanical evaluation samples were uniaxial compressed using Controlled-Force DMA test with a force ramp rate of 0.5 N/min up to 2N in case of gelatin scaffolds and 0.1 N/min up to 2 N in case of collagen scaffolds. The compressive modulus (elastic modulus) was calculated from the initial linear part of the obtained stress-strain curve. The test was repeated 5 times.

#### **1.8.2. Dynamic compression**

The viscoelastic spectra of the scaffolds in the compressive mode were performed using Multi-Frequency DMA test with frequency scan from 0.1 until 10 Hz measurements. The experiment was performed under a constant strain amplitude of 75 µm. Storage modulus ( $E'$ ) and loss factor ( $\tan \delta$ ) were plotted on graphs. The test was repeated 5 times.

#### **1.8.3. Creep**

The creep test was carried out at the constant stress 0.002 MPa based on the previous stress-strain curves analysis. The samples, after an isothermal period of 5 min at 37 °C, were subjected at the definite stress for 15 min and then left at rest for 15 min (recovery time). Strain and strain recovery values in the function of time were plotted on graphs. The test was repeated 3 times.

### 1.9. 3D cell culture

Three different cell lines were used for the experiments presented in this work. For expansion, cells from each cell line were cultured in standard medium supplemented with 10% Fetal Bovine Serum (FBS, Gibco) and 1% penicillin/streptomycin ( $100 \text{ U ml}^{-1}/100 \text{ } \mu\text{g ml}^{-1}$ ) and they were incubated at  $37 \text{ }^\circ\text{C}$  with 5%  $\text{CO}_2$  atmosphere. The cells were cultured until 80% confluence and detached by trypsinization and centrifugation, later the cell number and viability was assessed by trypan blue dye exclusion test. The media were changed every two days. All cell handling procedures were performed in a sterile laminar flow hood.

**a) MG-63 Human Osteosarcoma cell line** were supplied by Lonza (ECACC 86051601) and used in preliminary cytotoxicity evaluation. Cells were cultured in Dulbecco Modified Eagle's Medium (DMEM, Gibco) with supplementation as mentioned above. The experimental scaffolds were cut out by puncher with dimensions of 8 mm in diameter and 4 mm in thickness and were sterilized with two washing cycles in 70% ethanol for 10 minutes each, one washing cycle in 1X PBS for 10 minutes and UV exposure of each side of the scaffold for 25 minutes. Prior to experimentation, all scaffolds were pre-incubated with 1 ml of culture media for 1 h and afterwards the samples were placed one per well in a 24-well plate. Scaffolds were seeded by dropping  $20 \text{ } \mu\text{l}$  of  $3.0 \times 10^4$  cells suspension in culture media onto the upper layer of the scaffold for initial cell attachment. After 30 min, 1.5 ml of cell culture media was added and incubated at  $37 \text{ }^\circ\text{C}$ , 5%  $\text{CO}_2$  for 7 days.

**b) Human chondrocytes cell line (CHON-002)** were supplied by ATCC® (CRL -2847™, Italy) and used to investigate the cell-scaffold interaction. The chondrocytes were cultured in DMEM (ATCC-30-2021) supplemented as above. Cylindrical samples of the gelatin scaffolds with 8 mm in diameter and 5 mm in thickness were sterilized by 25-kGy gamma-ray radiation. Prior to experimentation, all scaffolds were pre-washed with 50 ml of the culture media (10 samples/falcon) gently shaking for 24 h at room temperature (RT). Samples were placed one per well in a 24-well plate and a drop of  $20 \text{ } \mu\text{l}$  containing  $5.0 \times 10^4$  cells suspension in culture media was added onto the upper layer of the scaffold. After 30 min, 1.5 ml of cell culture media was added and placed in the cell incubator for 14 and 21 days (for gene expression analysis).

**c) Mouse (C57BL/6) mesenchymal stem cells (mMSCs)** were supplied by GIBCO® (Thermo Fisher scientific) and used to investigate cellular behaviour in 3D culture with collagen scaffolds. For expansion, mMSCs were cultured in standard medium DMEM-F-12/Glutamax (Gibco) supplemented with 10% FBS (Gibco) and 1% penicillin/streptomycin as above. For the experiments mMSCs were cultured in chondrogenic medium High-glucose DMEM (Gibco) supplemented with 10 ng/ml TGF- $\beta$ 1 (Invitrogen), 1% ITS (Insulin-Transferrin-Selenium,



Gibco), 37.5 µg/ml ascorbic acid (Sigma),  $10^{-7}$  M dexamethasone and 1% penicillin/streptomycin (100 U ml<sup>-1</sup>/100 µg ml<sup>-1</sup>). Cylindrical samples of experimental scaffolds with dimensions of 9 mm in diameter and 5 mm in thickness were sterilized by 25-kGy gamma-ray radiation. Prior to experimentation, all scaffolds were pre-washed with 50 ml of the culture media (10 samples/falcon) gently shaking for 24 h at RT. Samples were placed one per well in a 24-well plate and a drop of 50 µl containing  $2.0 \times 10^5$  cells suspension in culture media was added onto the upper layer of the scaffold for initial cell attachment. After 30 min, 1.5 ml of chondrogenic cell culture medium was added and incubated at 37 °C, 5% CO<sub>2</sub> for 28 days.

### **1.10. Cell viability**

Cell viability was assessed by Live&/Dead assay (Invitrogen, USA) which is based on the simultaneous determination of live and dead cells with two probes, Calcein and Ethidium homodimer-1 (EthD-1), that measures the recognized parameters of cell viability: intracellular esterase activity and plasma membrane integrity respectively. Briefly, at specified time points of cell culture, depending on the experiment, cell-seeded constructs were washed in 1X PBS (pH 7.4) for 5 min and stained with Calcein acetoxymethyl (Calcein AM) 2 µM and Ethidium homodimer-1 (EthD-1) 4 µM for 15 min at 37 °C. Later the constructs were again washed in 1X PBS for 5 min and viewed under inverted Ti-E fluorescence microscope (Nikon). In case of collagen scaffolds, the ratio of live/dead cells and the cell number were determined by quantifying the number of cells from the upper surface of the scaffold in three random fields of view per sample at the same magnification, using ImageJ software. Two samples per every type of scaffolds were analysed at each time point.

Additionally, the nuclear morphology integrity, as index of cell viability and cell colonization through the scaffolds were evaluated using nuclear fluorescent dye. At individual time points, cell-scaffold constructs were rinsed in 1X PBS and stained with 4',6-diamidino-2-phenylindole (DAPI) and immediately viewed under inverted Ti-E fluorescence microscopy.

### **1.11. Cell proliferation assay**

At regular time intervals of 1, 3, 7 and/or 14 days of cell culture, depending on the experiment, 10% 3-(4,5-dimethylthiazol-2-yl)-2,5-diphenyltetrazolium bromide (MTT) solution of the total volume of the well was added and incubated for 2 h at 37 °C. In this assay, the metabolically active cells react with the tetrazolium to produce formazan crystal salts. After incubation, the scaffolds were transferred to centrifuge tubes and 1ml of dimethyl sulfoxide (DMSO) was added. The scaffolds were crushed using the pestle and vortexed subsequently to

release the formazan salts of the inter-located cells and incubated at RT for 15 min and centrifuged at 1000 rpm for 1 min. Later, 200 µl of the supernatant was transferred to 96-wells plate and read using a spectrophotometer (Multiskan FC Microplate photometer, Thermo Scientific, USA) at optical density of 570 nm. This absorbance is directly proportional to the number of metabolically active cells. Three cell-seeded scaffolds per time were measured. Acellular blank scaffolds were treated equally during the culture time and the experiment. Three blank samples of each type of scaffold tested were used at the individual time point and their absorbance values were subtracted from the cell-seeded constructs.

## **1.12. Cell morphology**

### **1.12.1. Actin-phalloidin staining**

After 3 and 7 days of cell culture, morphology of the cells grown on the scaffolds was evaluated by phalloidin immunofluorescence staining. Cell-seeded scaffolds were washed with 1X PBS for 5 min, then fixed with 4% (w/v) paraformaldehyde in 1X PBS for 15 minutes and washed again 2 times with PBS for 5 min. Permeabilization of cell membrane was performed with 0.1% (v/v) Triton X-100 (Sigma-Aldrich) in PBS for 5 min. Then, FITC-conjugated phalloidin antibody (1:500; Invitrogen) diluted in PBS was added to the samples and incubated for 20 min at RT in the dark in order to visualize filamentous actin (F-actin) in the cell. After another washing in 1X PBS counterstaining with DAPI (1:200; Invitrogen) diluted in PBS was carried out for 5 min to visualize cell nuclei. Rinsed in PBS samples were mounted on the coverslip and viewed under inverted Ti-E fluorescence microscope (Nikon).

### **1.12.2. SEM analysis**

Scanning electron microscopy (SEM) was used to analyse morphology of the cells grown on the scaffolds. Briefly, after specified time, depending on the experiment, the cell-seeded scaffolds were washed with 0.1 M sodium cacodylate buffer (pH 7.4) and fixed in 2.5% glutaraldehyde in 0.1 M sodium cacodylate buffer (pH 7.4) for 2 h at 4 °C, washed in 0.1 M sodium cacodylate buffer (pH 7.4) and freeze-dried. Later, the specimens were mounted onto the aluminium stubs using black carbon tapes and they were sputter coated with gold particles (Sputter Coater Q150TES, Quorum, Italy). The cells on the scaffold surface and inside the scaffold were then examined using high resolution SEM (FEI, Quanta 200, UK).

## **1.13. Glycosaminoglycans (GAG) assay**

After designed time points, the cell-seeded scaffolds and acellular scaffolds were harvested for sulphated glycosaminoglycan (GAG) assay. The scaffolds were treated at 65 °C for 3 h in

750  $\mu$ l of lysis buffer consisting of Hank's Balanced Salt Solution (HBSS, pH 6.4), 125  $\mu$ g/ml papain, 8 mg/ml sodium acetate, 4 mg/ml EDTA and 0.8 mg/ml L-cysteine-HCl (all Sigma Aldrich, USA). The digestive solution was centrifuged and supernatant was collected and mixed with dimethylmethylene blue (DMMB) reagent (Sigma Aldrich, USA) according to the protocol of Richard W. Farndale et al. [6]. GAG quantification was determined by measuring the absorbance of DMMB bound to GAGs at  $\lambda$  530 nm using a spectrophotometer (Multiskan FC Microplate photometer, Thermo Scientific, USA). Shark chondroitin sulphate (Sigma Aldrich, USA) with concentration gradient from 1 to 30  $\mu$ g/ml was used as a standard and scaffolds without cells were used as blank samples. Three scaffolds were measured per each time point.

#### **1.14. RNA isolation and quantitative real-time polymerase chain reaction (qPCR)**

Total RNA was isolated from the harvested cell constructs at designed time points using TriFast® reagent (EuroClone, USA). In brief, the samples were lysed in 1 ml of TriFast® reagent, crushed and centrifuged at 12,000  $\times$  g for 5 min. The collected supernatant was used for RNA purification based on Direct-Zol™ RNA MiniKit (Zymo Research, USA). The purified RNA was quantified using Qubit® RNA BR assay kit and Qubit® fluorimeter. The integrity of the RNA was analysed using native agarose gel electrophoresis. Reverse transcription was carried out on purified RNA (500 ng) to produce cDNA using high capacity cDNA reverse transcriptase kit with RNase inhibitor, according to manufacturer's instructions (Applied Biosystems, USA). Relative quantification of gene expression, using Taqman assays (Applied Biosystems), for transcription factor (SOX9, HS01001343), aggrecan (ACAN, HS00153936) and glyceraldehyde 3-phosphate dehydrogenase, used as housekeeping gene, (GAPDH, HS99999905) was performed by use of the StepOne Real-Time PCR System (Applied Biosystems). Three technical replicates for each sample were used and data were collected using the OneStep Software (v.2.2.2). Relative quantification of the target gene expression was generated normalizing to GAPDH using the comparative threshold (Ct) method [7].

#### **1.15. Western Blot analysis**

After 7 and 14 days, cell-seeded scaffolds and acellular scaffolds used as a negative control were lysed in a Radioimmunoprecipitation buffer (RIPA buffer) supplemented with a proteinase inhibitor cocktail (Cell Signalling). Protein concentration in each supernatant of cell lysate and acellular scaffold lysate was determined by a colorimetric assay (Kit DC Protein

Assay, Bio-Rad) and the real protein concentration was obtained by subtracting concentration of the acellular scaffold from the cell-seeded scaffold. The final samples of concentration 15 µg/ml were diluted in sample loading buffer (3:1), loaded and separated in a 4–15% Mini-PROTEAN TGX stain-free protein gels (BioRad), using a Mini-PROTEAN electrophoresis cell kit (Bio-Rad). The proteins were then transferred to nitrocellulose membranes by means of a Trans-Blot Turbo™ transfer system (BioRad), with the blots incubated thereafter for 30 min at RT in a blocking solution of 5% non-fat dry milk in PBS. The membranes were incubated overnight at 4 °C with primary mouse antibodies anti-SOX-9 (Thermo Scientific) and primary rabbit antibodies anti-β-actin (Cell Signaling) which served as the internal control. Afterwards, the blots were incubated with a horseradish goat peroxidase-linked secondary antibodies anti-mouse and anti-rabbit (Bio-Rad) for 30 min. An enhanced chemiluminescence kit (ECL, BioRad) was used to visualize the protein bands with ChemiDoc XRS+ (Bio-Rad).

### **1.16. Statistical analysis**

Results were expressed as mean ± standard error (SEM) plotted on graphs. Following statistical tests were used in the studies of this thesis:

- One-way ANOVA followed by Tukey's multiple comparisons test: analysis of cell proliferation and analysis of mechanical moduli within two experimental groups;
- one-way ANOVA, followed by Dunnett's multiple comparisons test: analysis of *in vitro* degradation within many compositions of collagen scaffolds;
- two-way ANOVA, followed by Sidak's multiple comparisons test: analysis of mechanical moduli as a function of time;
- two-way ANOVA, followed by Tukey's multiple comparisons test: analysis of cell viability, cell proliferation, gene expression and glycosaminoglycans content within more than two experimental groups;
- unpaired Student's t-test: percentage of porosity within two experimental groups.

Statistical analysis was performed by the Graph Pad Prism software (version 6.0), with statistical significance set at  $p \leq 0.05$ .

## Chapter 2

# DEVELOPMENT OF 3D POROUS GELATIN SCAFFOLDS BY DIFFERENT CROSSLINKING APPROACHES: COMPARATIVE ANALYSIS

---

### 2.1. Introduction

Scaffolds with biomimetic properties are admittedly desired in the field of tissue engineering (TE) as they provide a template for cell growth, cell differentiation, ECM components production and thereby, promote new tissue formation in injured cartilage or bone [8]. In order to facilitate the healing process of damaged tissue, such 3D scaffolds should be tailored to exhibit suitable porosity, mechanical properties and stability *in vivo*. In addition to the 3D porous architecture, great attention must be paid to the scaffold's composition [9].

The major group of materials, which have been widely applied for the generation of such 3D scaffolds, are natural polymers. Natural polymers as collagen and its denatured form gelatin can be functionally superior to synthetic polymers due the presence of specific receptors as Arg-Gly-Asp motif (RGD) which facilitate cell attachment and cell migration [10], [11]. The natural origin and abundance of collagen, especially type I, in mammals tissues make this protein a promising candidate for the production of scaffolds in the field of tissue engineering. Nevertheless, processing of native collagen required purification from telopeptides and virus inactivation which increase the cost of the procedure [12].

Hence, the alternative option can be a gelatin, which is chemically similar to collagen, but its production is less expensive and the antigenicity is lower compared do collagen. Moreover, numbers of studies have demonstrated high biocompatibility and proper biodegradability of gelatin *in vivo* as well as feasibility in modulating the physicochemical properties [9], [13], [14]. However, there are some limitations in use of gelatin as a scaffold in TE like fast dissolution in aqueous environment, thermal instability and poor mechanical properties [15]. In

order to overcome these problems crosslinking treatment has been applied to stabilize chemically and mechanically the material.

Various crosslinking methods are currently in use for scaffolds fabrication such as physical, chemical and natural crosslinking. The example of physical method taken in consideration for this scientific research is a dehydrothermal crosslinking (DHT) in which by applying the high temperature treatment under the vacuum, the water from the material is removed and the intermolecular bonds can be created within the polymeric molecules through esterification or amide formation [16], [17].

Another common crosslinking method is a chemical crosslinking which includes a range of chemical reactants, for instance, carbodiimide hydrochloride (EDC), glutaraldehyde or 1,4-butanediol diglycidyl ether (BDDGE) [18]. The last one is a bi-functional epoxy compound able to form crosslinks among molecules by reaction between two amine groups or an amine group and carboxyl group of amino acids present in the protein depending from the pH of the reaction environment [19].

Among other crosslinkers capable to interact with gelatin units, genipin is a natural compound derived from *Gardenia jasminoides* fruit which has a great potential to be less cytotoxic than chemical crosslinkers [20], [21]. More information about crosslinking treatment can be found in the part I of this thesis (Introduction, Chapter 4.2).

In this work, 3D gelatin porous scaffold were synthesized and stabilized by three different crosslinking treatments: i) DHT, ii) BDDGE and iii) genipin with the aim to develop reinforced and biocompatible scaffolds for cartilage tissue engineering. A comparative evaluation was performed to determine the effect of the various crosslinking strategies on morphology, fluid uptake, degradability, thermal behaviour and mechanical properties of the 3D scaffold. Then, preliminary *in vitro* cytotoxicity test with MG-63 osteosarcoma cell line was performed to exclude any cytotoxic effect of the scaffolds. Subsequently, more biological tests were carried out using human chondrocytes to assess the cell viability, proliferation and morphology, as well as gene and protein expression for chondrogenic markers.

*This study has been already published and done together with Gopal Kumar Shankar [12].*

## **2.2. Preparation of scaffolds**

Commercial porcine skin gelatin (Type A, Bloom number: 280) was purchased from Italgelatine Spa, Italy. The gelatin was dissolved in milli-Q water at 40 °C to obtain the 5 wt% aqueous solution. Then, 3D gelatin constructs were prepared as follows (Fig. 3.1):

(i) DHT crosslinked scaffolds, henceforth coded as G-DHT: the gelatin solution was filled onto a polystyrene Petri plate and allowed to cool at 4 °C to form a gel. Then the gelatin hydrogel was lyophilized by freezing at - 40 °C and drying at 25 °C (5 Pascal, LIO 3000 PLT, Italy) for 48 h under a constant vacuum of 0.1 mbar to obtain porous 3D matrices. Finally, the scaffolds were heated at 160 °C under vacuum (0.001 mbar) for 48 h or 96 h.

(ii) BDDGE crosslinked scaffolds, henceforth coded as G-BDD: the gelatin solution was added with various concentration of BDDGE (Sigma Aldrich, USA); from 1.5 wt% up to 40 wt% at pH = 8 and then mixed under stirring for 5 min. Later, the resultant mixture was filled onto a polystyrene Petri plate and the crosslinking reaction was carried at 25 ± 2 °C for 48 h.

(iii) Genipin crosslinked scaffolds, henceforth coded as G-GEN: the gelatin solution was added with various concentration of genipin (Wako, Germany); from 0.5 wt% up to 2.5 wt% (pH = 5) and then mixed under stirring for 5 min. Later, the resultant mixture was filled onto a polystyrene Petri plate and the crosslinking reaction was carried at 25 ± 2 °C for 48 h.

G-BDD and G-GEN samples after crosslinking were freeze-dried following the above described procedure.

After freeze-drying, all new synthesized scaffolds exhibited sponge-like structure. G-DHT samples were yellowish, G-BDD white and G-GEN had dark blue color as presented on Fig. 3.1.

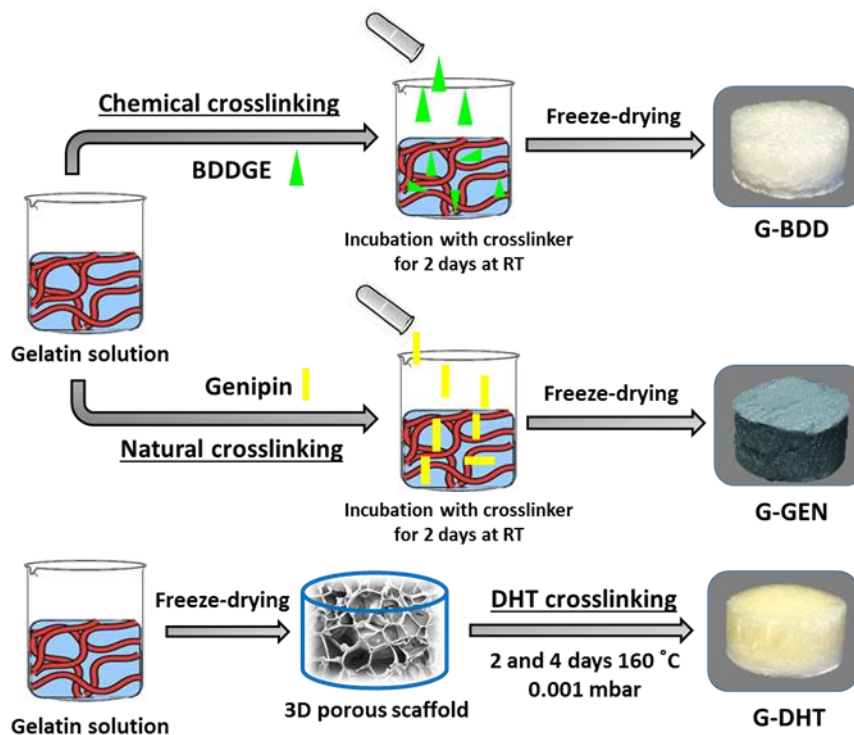


**Fig. 3.1.** Schematic illustration of fabrication gelatin 3D scaffolds with three different crosslinkers.

### 2.3. Physicochemical characterization

In this work a comparative study between the performance of three different crosslinking methods on gelatin using DHT, BDDGE and genipin was carried out. The amount of crosslinkers used in this study is based upon the preliminary screening, previous experience and the literature. Biomimetic scaffolds for TE should be biodegradable however, they should exhibit resistance to degradation at first weeks after *in vivo* implantation to let for a new tissue formation. Taking under consideration the fact that fast dissolution of gelatin scaffolds in aqueous conditions is a main limitation of their use, preliminary stability test in PBS (pH = 7.4) at 37 °C up to 14 days was carried out in order to choose the most stable compositions (Table 3.1.).

Type of crosslinker	concentrations (wt%)	Macroscopic observation with time				
		1d	3d	5d	7d	14d
BDDGE	1.5	+	+/-	+/-	-	-
	5	+	+	+	+/-	-
	10	+	+	+	+	+
	20	+	+	+	+	+
	40	+	+	+	+	+
Genipin	0.5	+	+/-	-	-	-
	1	+	+	+/-	-	-
	1.5	+	+	+	+	+
	2	+	+	+	+	+
	2.5	+	+	+	+	+
DHT	<b>Time of crosslinking</b>					
	48 h	+	+	+	+	+
	96 h	+	+	+	+	+

**Table 3.1.** Preliminary selection of gelatin scaffolds crosslinked with increasing concentrations of BDDGE or Genipin or crosslinked with DHT of two different times of reaction, incubated in PBS at 37 °C up to 14 days. Preliminary assessment has been performed by macroscopic observation where, ‘+’ means stable sample, ‘+/-’ means that sample is losing its structure and ‘-’ refers to complete loss of structure and sample dissolution. Three samples of each group were analysed.

The G-BDD scaffolds of concentration 1.5 wt% and 5 wt% started to losing the structural integrity at day 3 and 7 respectively, and at the end of the test (14 days) these samples were completely dissolved based on the macroscopic observation. Among G-GEN scaffolds, samples crosslinked with 0.5 wt% and 1.0 wt% of genipin were rejected as they exhibited rapid loss of structure in the first days of the test. Only samples of the genipin concentration higher than 1.5 wt% and in case of BDDGE samples with concentration higher than 10 wt% showed stability for 14 days in PBS at 37 °C. Finally, the appropriate crosslinker amount was chosen by taking



into account a minimum concentration of BDDGE (10 wt%) and genipin (1.5 wt%) needed to obtain a 3D scaffold with good physical stability [18], [20]. Higher concentrations than selected ones could manifest cytotoxic effects during cell culture thus, those concentration were excluded from the further experiments (table 3.1) [20], [22]–[24].

Gelatin scaffolds crosslinked with DHT for 48 h or 96 h showed preserved structure for 14 days therefore, further evaluation was needed to select the best time of crosslinking. After careful consideration, BDDGE (10 wt %) named as G-BDD, genipin (1.5 wt %) named as G-GEN and DHT (48 h and 96 h) named as G-DHT '48 h' and G-DHT '96 h' respectively, were selected for physicochemical characterization.

### ***Morphology and porosity***

Architecture of the scaffold, suitable pore size, interconnected pore network and high porosity are crucial parameters for tissue engineering application as they can influence cell growth, transport of nutrients and metabolic waste, deposition of ECM and finally neo tissue formation [25].

All gelatin scaffolds had a highly porous microstructure with interconnected pores and heterogeneous pore size as seen in Fig. 3.2 (A, B, C, D). Observing the longitudinal cross-section of the scaffolds, the pore dimensions, morphology and pore interconnectivity were also well retained within the scaffold walls Fig. 3.2 (E, F, G, H) and no evidence of anisotropic distribution were underlined.

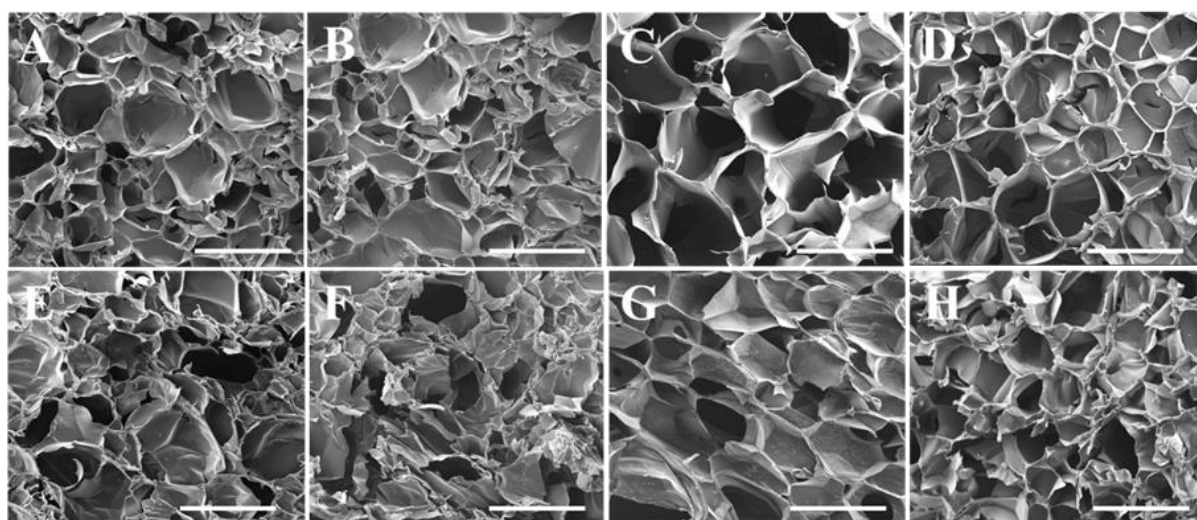


**Fig. 3.2.** Morphology of gelatin scaffolds: (A, E) G-DHT 48h, (B, F) G-DHT 96h, (C, G) G-BDD, (D, H) G-GEN; Upper panel represents transversal cross-sections and lower panel longitudinal cross-sections. Scale bar 500  $\mu\text{m}$ .

The average pore size of the scaffolds was measured from the swollen samples, cut into thin cross-sections as demonstrates the image in Table 3.2. The range of average pore size, was between  $346 \pm 10 \mu\text{m}$  for G-DHT ‘96 h’,  $354 \pm 17 \mu\text{m}$  for G-BDD scaffold,  $368 \pm 10 \mu\text{m}$  for G- GEN and  $390 \pm 14 \mu\text{m}$  for G-DHT ‘48 h’ (Table 3.2).

Adequate porous morphology is considered to be an indispensable element of biomaterials, as this structural feature greatly contributes to extensive cell colonization [1]. Therefore, total porosity (%) measured by gravimetric method and macropores porosity (%) measured by water squeezing method were analysed showing no significant differences among the samples i.e.; about 93-94% of total porosity for all scaffolds, 65-66% of macropore porosity for both G-DHT and G-BDD and  $51.2 \pm 4.3\%$  for G-GEN (Table 3.2). The results obtained from these two methods of porosity measurements cannot be compared due to differences in the principle and in the sensitivity. Summarizing, all scaffolds showed high total porosity and sufficient macropore porosity which is normally lower than total porosity [2], [26].

Although, there were slight differences in the homogeneity or average pore size, all types of scaffolds showed satisfactory porosity and pore size suitable for cell penetration and colonization.

Scaffold type	Average pore size ( $\mu\text{m}$ )	Porosity (%)	
		Gravimetric method	Water squeezing method
<b>G-DHT 48h</b>	$390 \pm 14$	$94.3 \pm 0.6$	$66.0 \pm 3.8$
<b>G-DHT 96h</b>	$346 \pm 10$	$93.2 \pm 0.2$	$65.0 \pm 4.9$
<b>G-BDD</b>	$354 \pm 17$	$94.0 \pm 0.1$	$66.6 \pm 4.8$
<b>G-GEN</b>	$368 \pm 10$	$94.7 \pm 0.3$	$51.2 \pm 4.3$

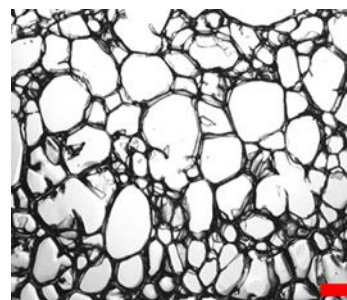


**Table 3.2.** Morphological characteristics of gelatin scaffolds. Average pore size ( $\mu\text{m}$ ) determined by measurement of 50 pores in the scaffolds cross-sections after 24h of swelling in PBS ( $n = 50$ , data are mean  $\pm$  SEM). On the right: representative image of  $50 \mu\text{m}$  cross-section of G-DHT 48h sample, embedded in OCT and cut on the cryostat after immersion. Percentage of porosity measured by gravimetric method (total porosity) and water squeezing method (macropore porosity) ( $n = 3$  data are mean  $\pm$  SEM).

### Fluid Uptake

Fluid binding capacity is an important feature of scaffolds for tissue regeneration, which is function of their surface chemistry and roughness. This knowledge is important from the perspective of materials interacting with physiological fluid and cells because this greatly determines the structural properties and cell-material interaction under *in vivo* conditions [27]. Fig. 3.3 represents the time-dependent swelling behaviour of the gelatin scaffolds showing the

highest fluid uptake value for G-GEN scaffold, i.e.  $644 \pm 16\%$  and  $1111 \pm 1\%$  at 1 and 72 h, respectively. The fluid uptake index at 72 h for other scaffolds was  $609 \pm 6\%$  for G-DHT '48 h',  $458 \pm 15\%$  for G-DHT '96 h' and  $658 \pm 26\%$  for G-BDD.

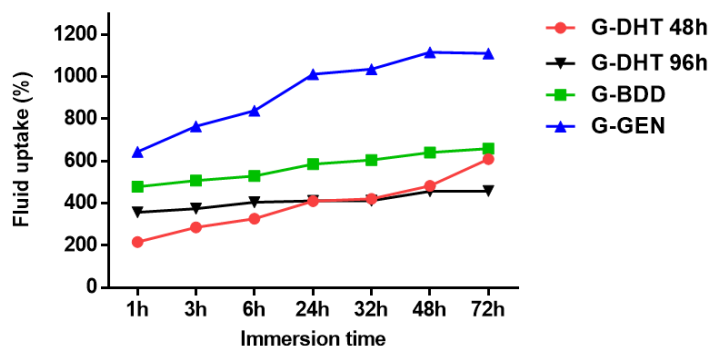


**Fig. 3.3.** Fluid uptake as a function of time of G-DHT (crosslinked for 48h and 96h), G-BDD and G-GEN scaffolds at 37 °C.

Although fluid uptake index for G-DHT '48 h' was the lowest, this scaffold could absorb PBS more rapidly than others, which can be explained by 3-fold increase in fluid-retention ability of the material between 1 h and 72 h of incubation. Whereas, G-DHT '96 h', G-BDD and G-GEN showed only 1.3, 1.8 and 1.7-fold increase respectively (Fig. 3.3). The results of fluid uptake showed that the scaffolds were hydrophilic in nature with capacity to hold equitable water molecules. The ability of the material to interact and hold the water molecule within its network is greater dependent upon the micro-architecture of the scaffolds [28]. Moreover, our results demonstrated that the presence of suitable porosity in all four scaffolds (Table.3.2) might eventually increase the water-retention resulting in good swelling property with maintaining physical stability.

### ***Extent of crosslinking***

The extent of crosslinking of gelatin scaffolds was calculated from the moles of free amino groups per gram of gelatin. The results as illustrated in Fig. 3.4 A showed that BDDGE was sufficient to crosslink 73% of the free amino groups of gelatin whereas, the genipin was able to crosslink only 30%. Among DHT crosslinked scaffolds, the G-DHT '96 h' crosslinked in 41%, exhibited higher crosslinking degree than G-DHT '48 h' sample (31%), which can be correlated to the longer time of crosslinking in the first group (Fig. 3.4 A).

These results manifested that the concentration of coupling agents, time of crosslinking reaction as well as type of crosslinking can be an essential determinant of crosslinking degree. Probably,

the G-BDD scaffolds are crosslinked in a higher extent than G-GEN due to higher amount of crosslinker used in the reaction: 10 wt% of BDDGE and 1.5 wt% of genipin.

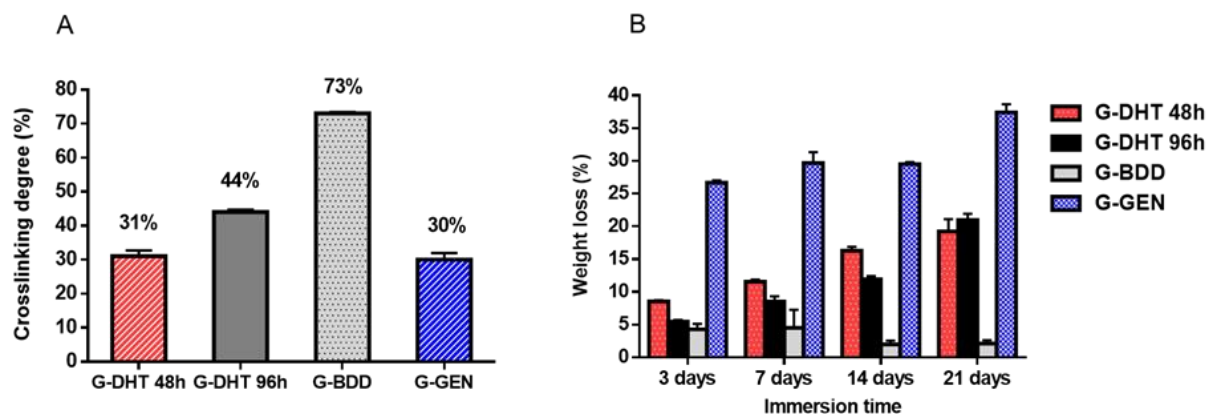


**Fig. 3.4.** (A) Percentage of crosslinking degree expressed as free amine group content per scaffold (B) Degradation assay expressed as change in weight (%) of gelatin scaffolds during 21 day test in PBS at 37 °C. For both tests three samples per condition of each group were measured (n=3 data are mean  $\pm$  SEM).

Furthermore, diverse crosslinking strategies can lead to different extents of crosslinking. High crosslinking degree of G-BDD may be related to the fact that BDDGE contrary to genipin, can react with several functional side groups within the gelatin backbone, which readily undergoes chemical modification. In G-DHT group, the high temperature treatment tends to completely remove the bound water from the material resulting in less surface energy available for crosslinking [16]. Whereas in G-GEN group, increasing the genipin concentration more amino groups would be crosslinked that eventually would lead to higher degree of crosslinking. However, the minimum genipin concentration was used to avoid any cytotoxic response, moreover the crosslinking index observed for G-DHT and G-GEN according to the literature was highly sufficient and suitable for tissue engineering application [29].

### ***Evaluation of degradation rate***

Degradation test was carried out to investigate the stability of the scaffolds and their mass loss with time under physiological conditions. From the macroscopic observation, there was no loss of shape or weakening of structural architecture of the scaffolds when compared to the non-crosslinked gelatin samples which rapidly dissolved within 1 h of incubation in PBS (pH = 7.4) at 37 °C. The highest weight loss was observed for G-GEN, which had a dissolution level of 37  $\pm$  1% at day 21 (Fig. 3.4 B). Among two G-DHT groups there was a slight difference in the weight loss, beneficial towards G-DHT '96 h' at the initial time points whereas, at day 21 the dissolution level of G-DHT '96 h' was higher than G-DHT '48 h', 21  $\pm$  1% and 19  $\pm$  2%

respectively. The overall mass loss of G-BDD was very low, only  $2.0 \pm 0.5\%$  at day 21 which indicates that this scaffold was the most stable under physiological conditions (Fig. 3.4 B). Nevertheless, in the field of TE biodegradability of the materials is extremely important and too slow degradation can disturb a new tissue formation. Additionally, the low dissolution rate of the G-BDD can also be associated with high heterogeneity of the material or with the crosslinking degree data, which showed the highest crosslinking index for G-BDD ( $73.0 \pm 0.44\%$ ) which eventually endowed the lower dissolution rate (Fig. 3.4 A, B). Whereby, it is evident that the effective crosslinking provided the formation of strong covalent bridges through hydroxyl group bonding, which is less accessible to dissolution.

From the presented so far scaffold characterization tests, there were no significant differences in terms of swelling properties, microstructure, porosity and degradation between G-DHT '48 h' and G-DHT '96 h'. Then taking into account, the time consumed for scaffolds fabrication and economical aspects the G-DHT crosslinked for 48 h is more favourable and therefore further analyses are continued only with this scaffold coded from now as G-DHT.

#### ***Fourier Transform Infrared Spectroscopy (FTIR)***

The FTIR spectra of the obtained scaffolds clearly show three characteristic peaks belonging to gelatin (Fig. 3.5) corresponding to Amide I at  $1690\text{ cm}^{-1}$  due to C-O stretching, Amide II at  $1560\text{ cm}^{-1}$  due to N-H deformation and Amide III at  $1250\text{ cm}^{-1}$  due to C-N stretching vibrations [30].

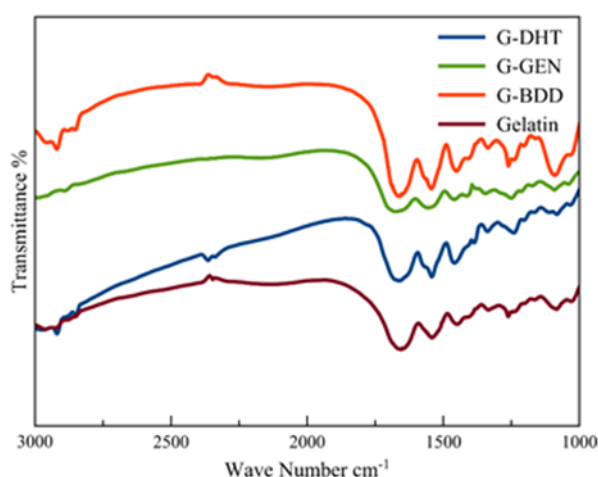


**Fig. 3.5.** FTIR spectra of G-DHT, G-BDD, G-GEN scaffolds and non-crosslinked gelatin.

There were no distinguishable vibrational changes in the spectral peaks of G-DHT and G-BDD scaffolds and their spectra appeared similar to the parent molecule. The G-GEN showed a

spectral peak at  $1650\text{ cm}^{-1}$  which corresponds to the C=N stretching of amine groups in the gelatin molecule to form a secondary amide through carboxymethyl group interaction of genipin. Another vibrational change at  $1100\text{ cm}^{-1}$  indicates the stretching vibration of dihydropyran ring (heterocyclic ring opening) of genipin thus ensuring effective crosslinking of gelatin [31]. In conclusion, the FTIR results confirm that the presence of crosslinkers did modify the chemical properties of the scaffolds to an extent without causing any detrimental effects on the biocompatibility of the scaffolds.

### ***Thermal Characteristics***

The change in weight in relation to temperature was evaluated from the thermal decomposition pattern of the material. The weight loss of all scaffolds was consistent from 100 to 600 °C, after which there was a rapid degradation as seen in the pyrolytic pattern (Fig. 3.6). The initial weight loss was observed between 50-90 °C, mainly due to loss of water molecules. The second weight loss between 250-300 °C is due to destabilization of macromolecule, leading to thermal degradation. All three scaffolds (G-DHT, G-BDD and G-GEN) exhibited a similar pyrolytic pattern with very slight differences in the degradation profile. From the TGA peaks, it can be observed that the presence of crosslinkers did attribute to the increase in thermal durability of the material. The various crosslinking methods have led to increase in length of gelatin molecule thereby ensuring better thermal stability [32].

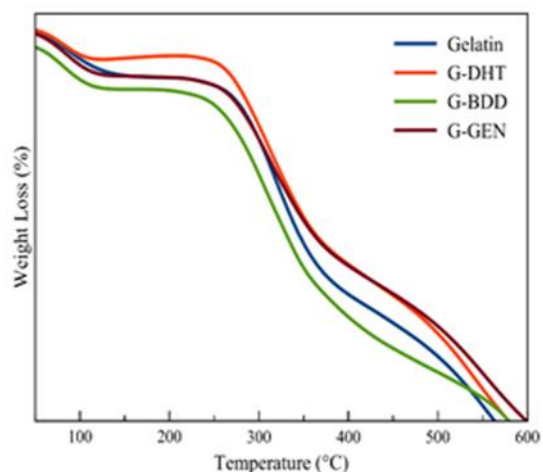


**Fig. 3.6.** TGA curve pattern of G-DHT, G-BDD, G-GEN scaffolds and non-crosslinked gelatin.

## 2.4. Mechanical properties

### *Static mechanical analysis*

Cartilage tissue is constantly subjected to the compressive forces thereby, scaffolds used for cartilage tissue engineering have to be well characterized concerning their mechanical properties. It is also important to underline that materials need to be hydrated prior to testing in order to mimic realistic conditions [33], [34].

Uniaxial compression test as well as dynamic compression test under oscillatory loading were performed to understand mechanical properties of gelatin scaffolds. The distinct material response can be observed in the stress-strain curves pertaining to different crosslinkers as seen in Fig. 3.7 A. G-DHT exhibited the strongest material with mostly elastic region (linear portion of the stress-strain curve) with no failure until the highest force (5 N) was applied. G-BDD also showed elastic behaviour with no visible collapse plateau in the present strain range. G-GEN seems to be the softest materials, which at the maximum force 5 N had already 78% of strain (deformation) while G-DHT and G-BDD reached 62% and 68% of strain respectively. The compressive modulus was the highest for G-DHT ( $54.4 \pm 3.8$  kPa) followed by G-BDD ( $46.0 \pm 2.8$  kPa) and G-GEN ( $16.2 \pm 0.3$  kPa) (Fig. 3.7 B). G-GEN showed significant decrease in compressive modulus respect to G-DHT and G-BDD ( $p \leq 0.0001$ ).

This analysis clearly demonstrated that DHT crosslinking provides sufficient and higher resistance of gelatin scaffold under compression compared to other constructs (Fig. 3.7). Additionally, the compressive moduli of our scaffolds were greatly higher than those found in the literature regarding cartilage tissue application [2], [35].

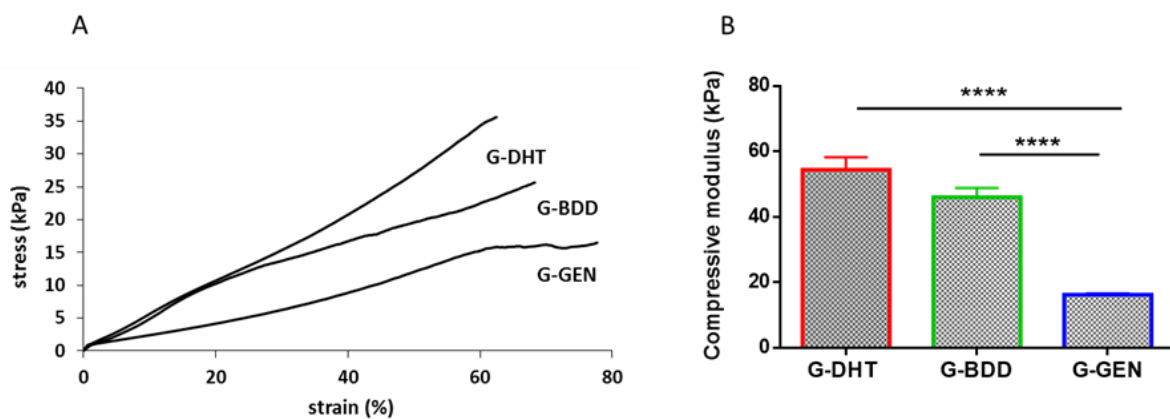


**Fig. 3.7.** Mechanical properties of gelatin scaffolds. (A) Representative stress-strain curves and (B) Compressive moduli of G-DHT, G-BDD and G-GEN scaffolds hydrated in PBS at 37 °C for 24 h; tested at force 0,5 N/min; Data are mean  $\pm$  SEM from 5 samples each type of scaffold. Statistically significant differences between G-DHT and G-GEN (\*\*\*\* $p \leq 0.0001$ ) and between G-BDD and G-GEN (\*\*\*\* $p \leq 0.0001$ ).

### *Dynamic mechanical analysis*

Viscoelastic properties of gelatin scaffolds were evaluated by dynamical mechanical analysis (DMA). DMA test carried out at varying frequencies showed differences in stiffness and viscoelastic behaviour among the compositions (Fig. 3.8). The storage modulus ( $E'$ ) of all the scaffolds increased with increasing frequency (Fig. 3.8 A). G-DHT showed the highest storage modulus that increased from  $41.6 \pm 3.1$  kPa at the frequency 0.1 Hz to  $58.8 \pm 6.0$  kPa at 10 Hz. For G-BDD and G-GEN storage moduli increased at lower rates, giving rise from  $36.4 \pm 1.2$  to  $44.4 \pm 1.2$  kPa for G-BDD and from  $17.9 \pm 0.8$  to  $24.0 \pm 1.4$  kPa in case of G-GEN. These data underlined that G-DHT promoted the stiffness of the scaffolds in a higher extent respect to two other groups. In literature it has been reported that scaffold's stiffness and compressive modulus decrease with increasing pore size [36]. In our study the highest modulus value was observed for G-DHT sample which apparently had the biggest pore size (Table 3.2) however, this effect can be counterbalanced by the hydrostatic interaction of the water molecules within the large pores which prevents material deformation and eventually results in higher  $E'$ [37].

Another important parameter of viscoelasticity is the loss factor ( $\tan \delta$ ), which is the ratio of the amount of energy dissipated, representing the viscous portion to energy stored, representing the elastic portion [28], [37]. The loss factor ( $\tan \delta$ ) of G-DHT and G-BDD increased up to certain frequency (3.4 Hz and 4.5 Hz respectively) and after started to drop until 10 Hz, which indicates that these scaffolds at particular point became more elastic than viscous (Fig. 3.8 B). For G-GEN,  $\tan \delta$  is decreasing from the beginning of test, showing only its elastic response upon increasing frequencies. After frequency of 2.3 Hz, negative values of  $\tan \delta$  were observed and they were not included on the graph. At low frequencies, the loss factor of G-DHT and G-BDD increased, demonstrating their higher damping capabilities than G-GEN. Moreover, G-DHT is able to store more energy maintaining the viscous response at higher frequency when compared to G-BDD. Inversely, the G-GEN scaffold represented mostly elastic behaviour without suitable viscosity and stiffness which is necessary in amortization of compressive loading present in articular cartilage [37], [38].



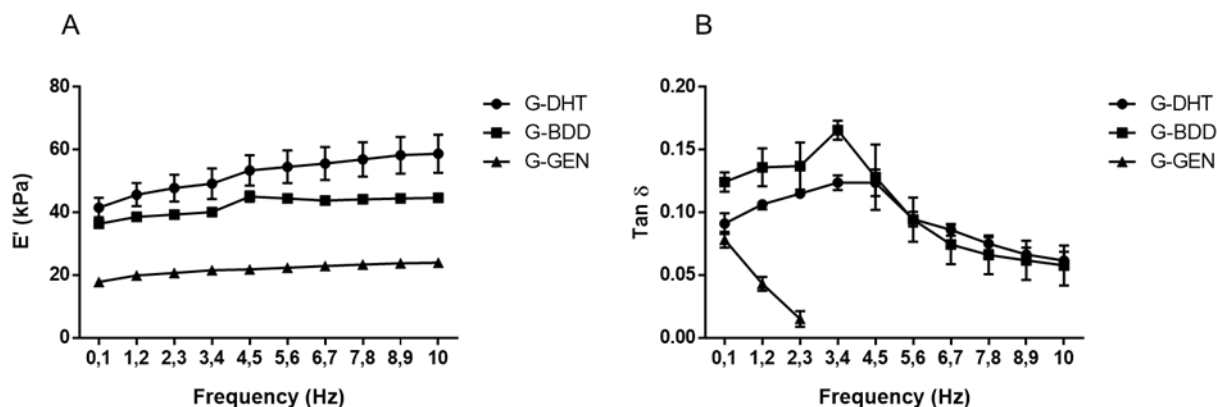


**Fig. 3.8.** Viscoelastic properties of the gelatin scaffolds. (A) Storage modulus ( $E'$ ) and (B) loss factor ( $\tan \delta$ ) of G-DHT, G-BDD and G-GEN scaffolds hydrated in PBS at 37 °C for 24 h; tested at varying frequencies; Data are mean  $\pm$  SEM from 5 samples each type of scaffold.

## 2.5. Biological evaluation

### 2.5.1. Preliminary cytotoxicity assessment

Preliminary *in vitro* studies were performed to investigate safety of the gelatin scaffolds in terms of their potential cytotoxicity. For this purpose, cell viability and cell proliferation assay were carried out using Human Osteosarcoma cell line MG-63, which is a commonly used cell line for the cytotoxicity tests [39]–[41]. Moreover, the impact of scaffold properties on cell morphology was also examined.

#### *Cell viability*

Cell viability of the cells seeded on the G-DHT and G-BDD constructs was visualized by Live&/Dead assay (Fig. 3.9). This test could not be performed on G-GEN scaffold due to the auto-fluorescence of the sample giving a brighter background in TRITC filter (578 nm) which leads to difficulties in visualizing the dead cells. Instead, the nuclear morphology integrity as index of cell viability was evaluated using nuclear fluorescent dye (DAPI staining, Fig. 3.10) [42].

Both G-BDD and G-DHT cell-seeded scaffolds demonstrated high cell viability with hardly detectable dead cells at each time point. The increase of cell density over the experimental time can be observed for both tested groups (Fig. 3.9 A, B).

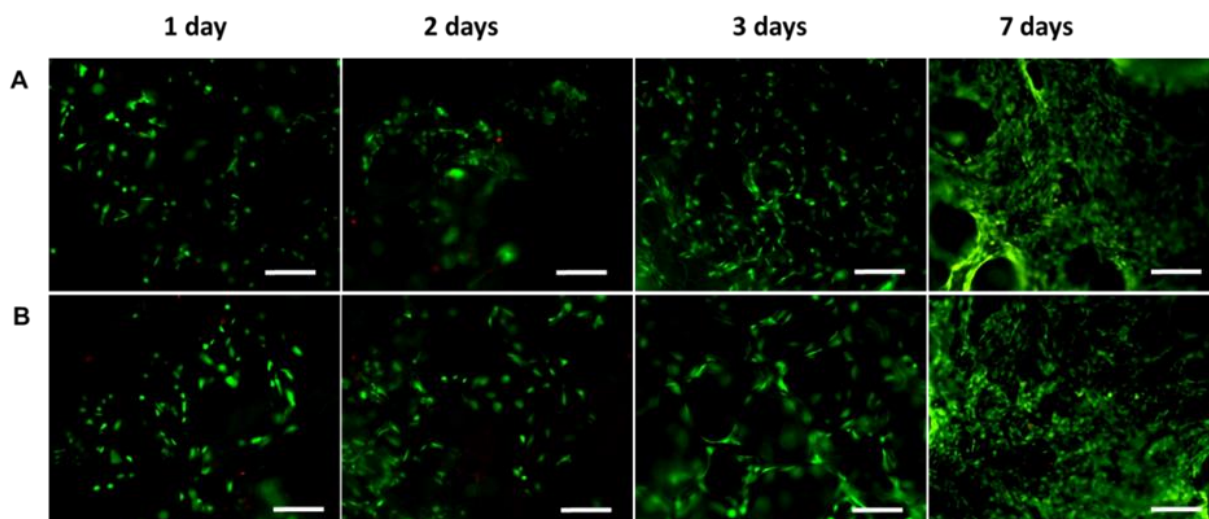


**Fig. 3.9.** Cell viability analysed by the live/dead assay (Calcein stains live cells in green, Ethidium homodimer-1 stains dead cells in red). Panel A presents G-DHT scaffold and panel B, G-BDD scaffold at time points: 1 day, 2 days, 3 days and 7 days. Scale bars: 200  $\mu\text{m}$ .

DAPI staining showed proper round morphology of cell nuclei in all three scaffolds, visualized in blue. Also here, the cell density increased with time as amount of cell nuclei is higher after 7 days compared to 3rd day of culture, emphasizing good cell colonization of the material (Fig. 3.10). Additionally, cells growing on G-GEN are more uniformly distributed than other constructs whereas, in G-BDD, cells are distributed more on the edges of the pores (Fig. 3.10, Fig. 3.9 B). The results from Live&/Dead assay and DAPI staining showed good cytocompatibility of all scaffolds demonstrating that not all the three crosslinkers are cytotoxic in the presented crosslinking conditions.

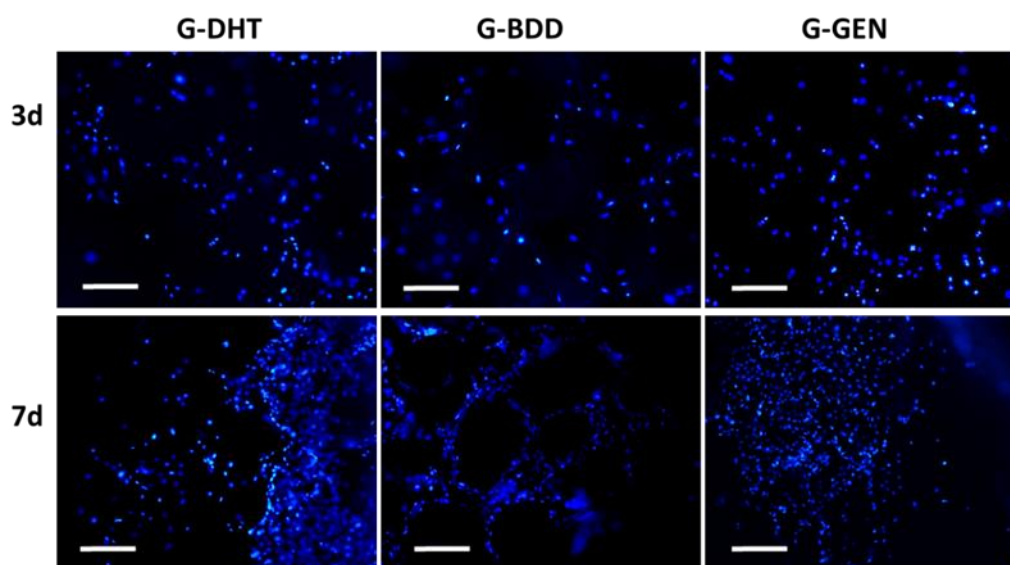


**Fig. 3.10.** Index of cell viability of G-DHT, G-BDD and G-GEN scaffolds analysed by DAPI staining at day 3 and day 7. Images represent upper surface of the scaffolds and cell nuclei are stained in blue. Scale bars: 200  $\mu\text{m}$ .

### Cell proliferation

Cell proliferation was evaluated by the MTT assay showing the increase in cell growth over time for the G-DHT and G-BDD scaffolds (Fig. 3.11). The difficulties with G-GEN scaffolds appeared also in this test and cell proliferation could not be obtained for this composition. The explanation of this event can be a very high absorbance of genipin that disturbs the reading of optical density (OD) during MTT assay. The standard procedure in our laboratory is to incubate acellular blank scaffolds in the same conditions as cell-seeded constructs and in case of MTT test, the real OD of the sample is calculated by subtracting the absorbance of a blank scaffold from the cell-seeded one. Hence, the final absorbance is an absorbance only of the cells however, for G-GEN samples blank scaffolds had higher OD than cell-seeded constructs which can be influenced by genipin properties interfering with colorimetric reaction of MTT [24].

The results from MTT assay of G-DHT and G-BDD scaffolds showed that cells proliferated in a slightly higher extent in the G-DHT group up to 3 days and after 7 days, higher proliferation exhibited G-BDD which was statistically significant compared to G-DHT (\*\* $p \leq 0.01$ ; Fig. 3.11).

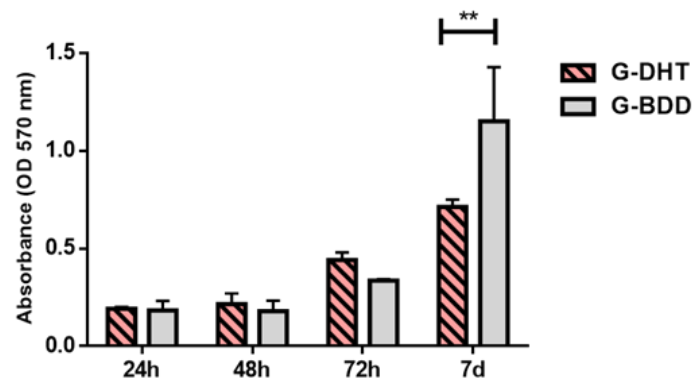


**Fig. 3.11.** Analysis of cell proliferation by the MTT assay after 24 h, 48 h, 72 h and 7 days of cell seeding (MG-63 cell line). Data are mean  $\pm$  SEM; \*\* $p \leq 0.01$ .

Lack of results from the cell proliferation for G-GEN is a limitation of this preliminary study. Nevertheless, DAPI images of G-GEN showed good cell viability and increase of cell density after 7 days, excluding any cytotoxic effects of 1.5 wt% genipin used, and it was the aim of the preliminary cytotoxicity assessment. For further *in vitro* tests, special pre-wash of the scaffolds is recommended to well washout the unbound genipin that can conflicts with OD reading.

### ***Cell morphology***

Preliminary analysis of cell morphology was assessed by actin-phalloidin staining and the representative images of G-GEN scaffold in low and high magnification are presented in Fig. 3.12. The analysis revealed good results in term of cell adhesion and morphology verified after 7 days of cell seeding and no differences were observed for all the scaffolds tested.

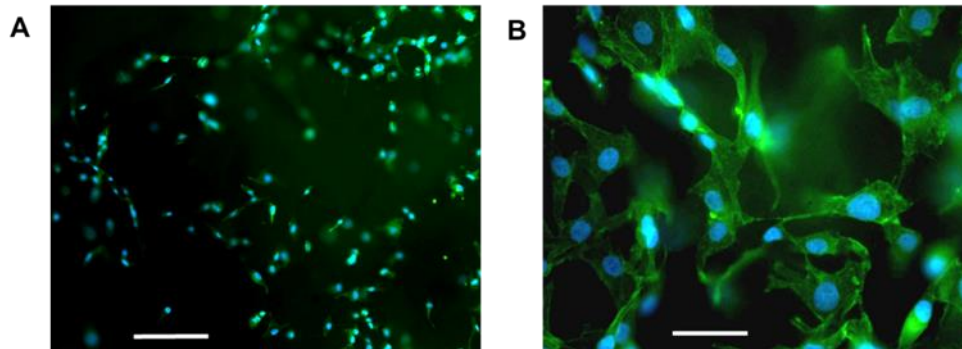


**Fig. 3.12.** Representative images of cell seeded G-GEN scaffolds after phalloidin staining at day 3 (A) and day 7 (B). Actin cytoskeleton stained in green and cell nucleus in blue. (A) magnification 10x, scale bar: 200  $\mu\text{m}$ ; (B) magnification 40x, scale bar: 50  $\mu\text{m}$ .

Cell–surface interaction and cell adhesion are complex processes involving the reorganization of cytoskeleton proteins like actin, and it has an impact on overall material’s biocompatibility [43], [44]. In the presented images, cells attached and spread on the scaffold’s surface with visible in green actin filaments and normal-shaped cell nuclei visualized in blue. Cells possessed fibroblast-like morphology typical for human MG-63 osteoblast-like cells and created cell protrusions to enable for cell-cell contact.

### **2.5.2. *In vitro* tests with human chondrocytes**

Biological evaluation with gelatin scaffolds using human chondrocytes cell line (CHON-002) has been continued. Cell-scaffold interaction was deeply investigated by assessing viability, proliferation and morphology of the cells, as well as glycosaminoglycans content, and gene/protein expression.

### ***Cell viability***

The cell viability of the chondrocytes on the porous gelatin scaffolds was visualized by live/dead assay. The fluorescence of the dead cells were not visible in the G-GEN due to the difficulties described earlier (paragraph 2.5.1). Therefore, the cell viability and colonization on the G-GEN scaffolds were examined through DAPI staining.

As represented in Fig. 3.13, the G-BDD and G-DHT scaffolds demonstrated high cell viability representing good cytocompatibility at each time point. With the increase in culture time there

was increase in cell density especially on day 7 and 14 and the cells appeared to be equally distributed in both the scaffolds surface.

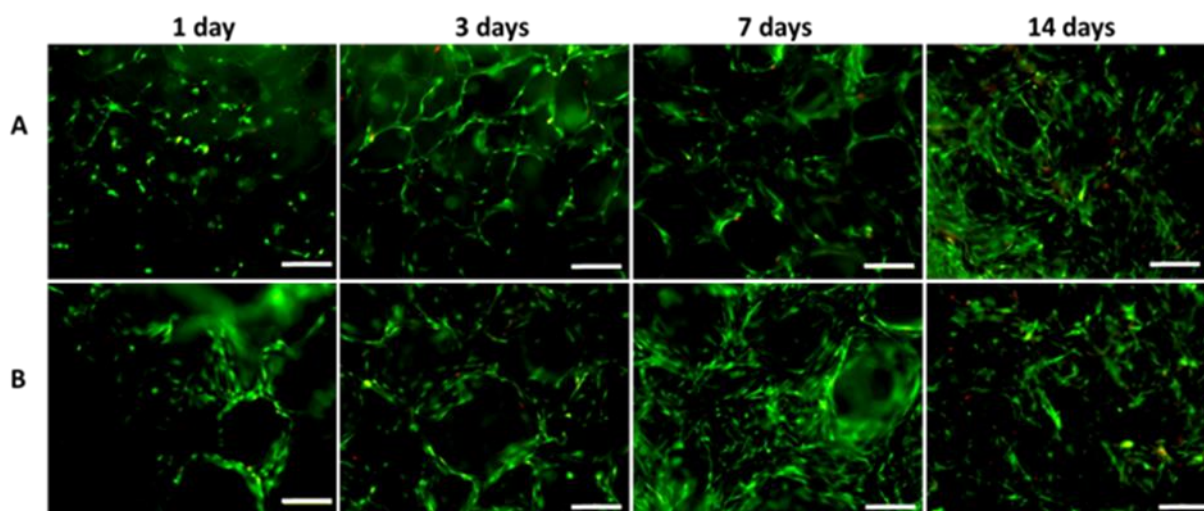


**Fig. 3.13.** Cell viability analysed by the live/dead assay (Calcein stains live cells in green, Ethidium homodimer-1 stains dead cells in red). Panel A. presents G-DHT scaffold and panel B. G-BDD scaffold at time points: 1 day, 3 days, 7 days and 14 days. Scale bars: 200  $\mu\text{m}$ .

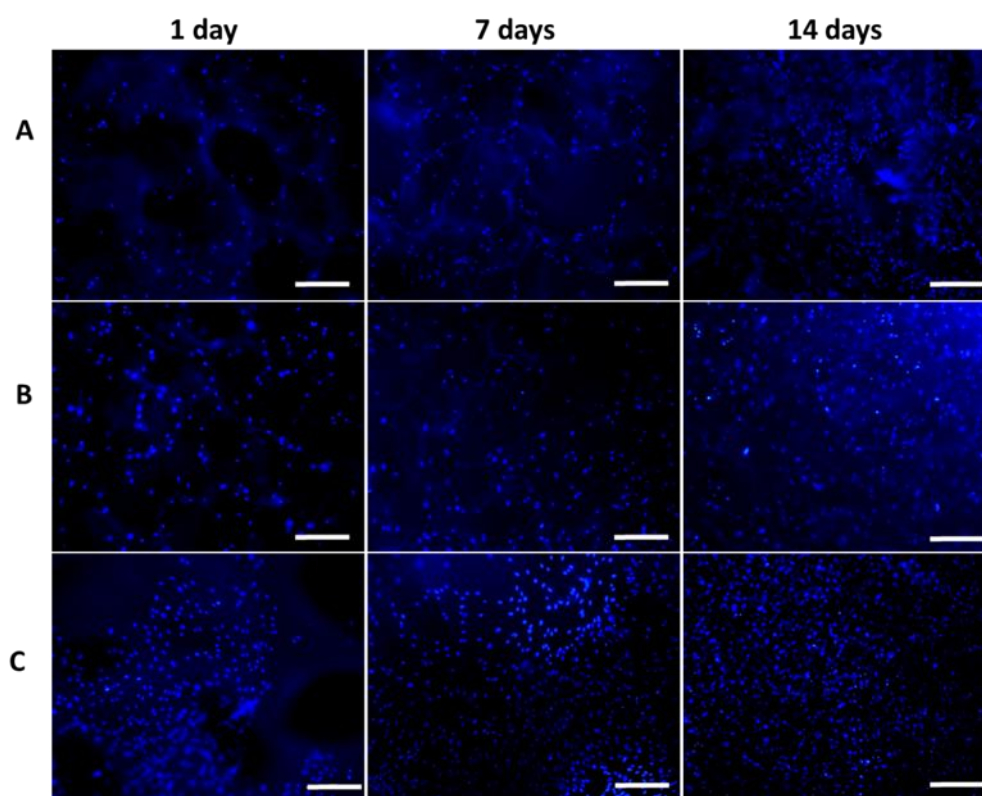


**Fig. 3.14.** Cell colonization of G-DHT (A), G-BDD (B) and G-GEN (C) scaffolds analysed by DAPI staining at day 1, 7 and 14. Cell nucleus stained in blue. Scale bars: 200  $\mu\text{m}$ .

Moreover, DAPI staining of the G-GEN showed proper round cell nuclei morphology visualized in dark blue and along the time, there was increase in cell colonization of the material

(Fig. 3.14 A-C). Both the live/dead and DAPI images shows the gradual increase in cellularity with respect to increase in culture time indicating the absence of cytotoxicity of the studied material. There was no difference in terms of cell viability amongst the scaffolds and the presence of crosslinkers did not impede the chondrocytes expansion and scaffold colonization.

### ***Cell proliferation***

Cell proliferation was evaluated by the MTT assay showing the increase in cell growth with time for all the scaffolds (Fig. 3.15). Comparing to the previous preliminary test on MG-63 osteoblast-like cells, this time all scaffolds were washed properly in cell culture medium for 24 h prior to starting the 3D cell culture and the absorbance of acellular scaffolds, especially G-GEN, was reduced.

The highest cell proliferation was observed for G-DHT which was statistically significant when compared to G-GEN at day 7 and 14 ( $p \leq 0.05$ ;  $p \leq 0.0001$ ) and to G-BDD at day 7 and 14 ( $p \leq 0.05$ ;  $p \leq 0.01$ ). Comparing the G-BDD and G-GEN, the higher cell proliferation rate was observed for G-BDD with statistically significant difference at day 7 and 14 ( $p \leq 0.05$ ;  $p \leq 0.0001$ ). The cell metabolic activity was observed to be in the order: G-DHT > G-BDD > G-GEN as the culture time is prolonged.

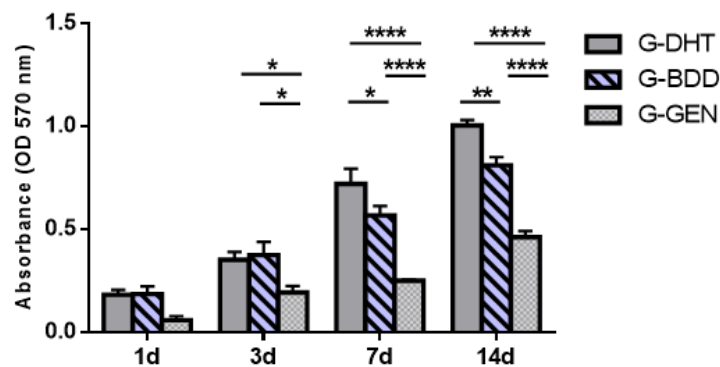


**Fig. 3.15.** Analysis of chondrocytes proliferation by the MTT assay after 1, 3, 7 and 14 days of cell seeding ( $n = 3$ ). Cells seeded on G-DHT and G-BDD scaffolds proliferate in a higher extent compared to cells growing in G-GEN scaffold. \* $p \leq 0.05$ ; \*\* $p \leq 0.01$ ; \*\*\*\* $p \leq 0.0001$ .

The DAPI staining results can be correlated with the MTT assay. The results elucidated a significant increase in number of viable cells in all the scaffold groups as the culture time is prolonged. Nevertheless, when compared to other scaffolds, G-GEN scaffold exhibited slower growth rate and recover in the later stage of culture time. The possible explanation that can contribute to the slower growth rate can be the reaction of genipin with the primary amine groups of arginine residues of gelatin leading to reduction of adhesion promoting RGD-like sequence [16], [45]. Moreover, previously several authors have reported the toxicity of genipin

and they have speculated to be cell and dose dependent [24], [46]. However, the observations of the culture studies also provide the evidence that the crosslinking mechanism assists in providing a more suitable microenvironment for the overall cellular activity, which in turn benefitted their proliferation as well.

### ***Cell morphology and cell attachment***

Spherical shape of primary chondrocytes is a typical morphology present in native cartilage. The human chondrocytes cell line CHON-002 (ATCC (clone number 2847™) used in this study derived from the long bone of an 18-week-old female foetus and was infected by the defective retrovirus containing human telomerase reverse transcriptase gene under G418 selection [47]. The primary cells after immortalization, as in case of CHON-002 cells develop fibroblast-like morphology and can have lacks of some gene expression as has been already reported [47]–[50]. The morphology of our chondrocytes (CHON-002) was firstly observed in 2D and presented in Fig. 3.17 showing indeed spindle-shaped cells with filopodia extensions.

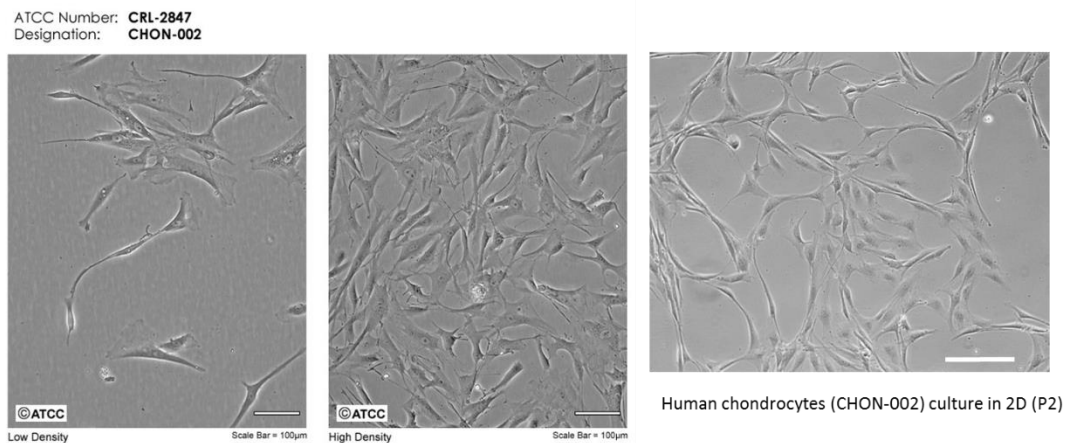


**Fig. 3.16.** Representative images of human chondrocytes (cell line; CHON-002, ATCC) morphology adapted from: [www.lgcstandards-atcc.org](http://www.lgcstandards-atcc.org) (images on the left) and cells culture in 2D in our laboratory on passage 2 (the image on the right; scale bar: 200 µm). The image taken in bright field by optical microscope (Nikon).

The microenvironment quality and the compatibility of scaffolds for cellular infiltration was evaluated using SEM. After 7 days of cell culture, the human chondrocytes were able to adhere, grow and penetrate into the porous material as seen in Fig. 3.17 (A-F). The porous nature of the scaffold enabled easy cell attachment and infiltration. There was no difference in the cell morphology on different scaffolds, all the scaffolds accommodated the chondrocytes to expand and grow with branched spindle shaped morphology. The SEM analysis revealed that chondrocytes were able to attach and spread over all the scaffolds, forming multiple protrusions without any polarization or aggregation (Fig. 3.17). The presence of interconnecting porous

texture characterized by the presence of heterogeneous macro and micro pores could facilitate cell adhesion and penetration [1].

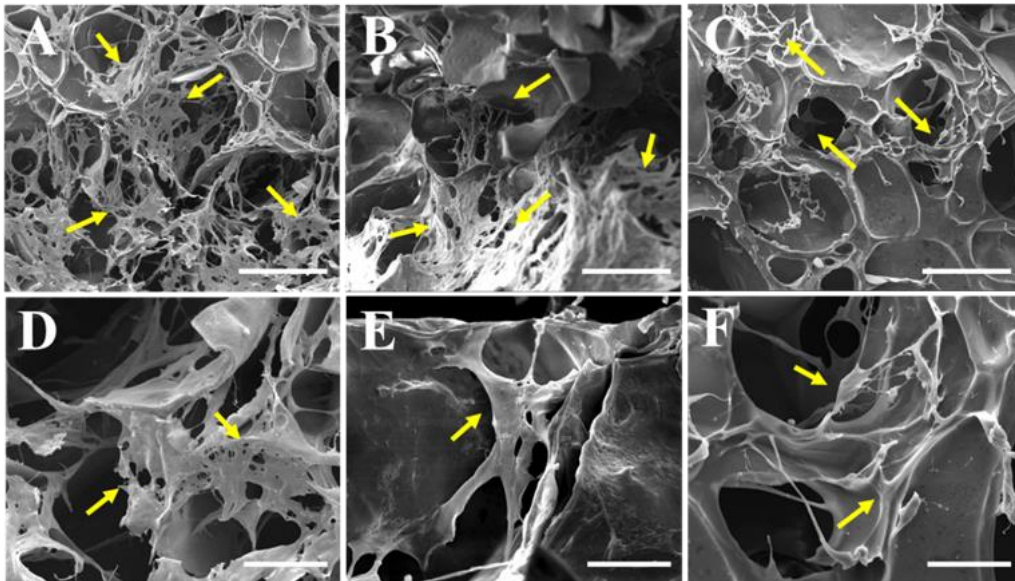


**Fig. 3.17.** SEM images showing cell-scaffold interactions 7 days after seeding. Cell layers (marked with yellow arrows) in direct contact with the biomaterials shows high cytocompatibility of the scaffold itself. (A, D): G-DHT, (B, E): G-BDD and (C, F): G-GEN. Scale bars: (A, B, C) 200  $\mu\text{m}$ ; (D, E, F) 50  $\mu\text{m}$ .

### *Glycosaminoglycans content*

The amount of GAGs produced by the cells in correspondence to the culture time was increased between day 7 and 14 for all the scaffolds without any significant differences (Fig. 3.18). High level of glycosaminoglycans produced by the cells proved the rich deposition of cartilage extra cellular matrix components by the chondrocytes.

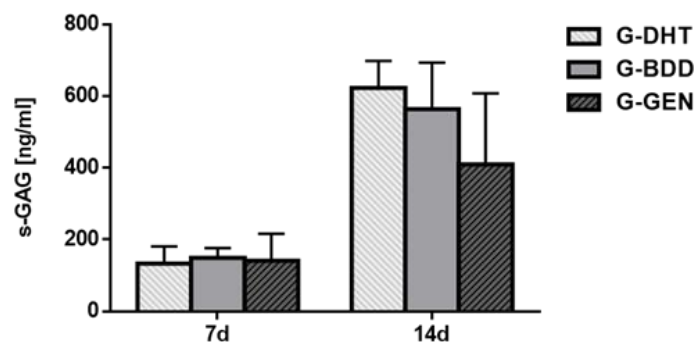


**Fig. 3.18.** GAG deposition by chondrocytes on G-DHT, G-BDD and G-GEN scaffolds after 7 and 14 days of culture. No statistically significant differences among the scaffolds were noticed.

Proteoglycans are considered to be the major ECM component of cartilage synthesized by chondrocytes. Since the proteoglycans are composed of 95% GAGs and 5% protein, it is always



essential to measure the GAG content in order to understand the metabolic activity of the cells [51]. Accordingly, the cells in all the scaffolds were able to secrete more ECM as the culture time prolonged. These results can be coordinated with the scaffold morphology and pore size distribution. The results of GAG quantification suggests that the average pore size of 350  $\mu\text{m}$  helps the chondrocytes to infiltrate and secrete their ECM components through efficient transport of the nutrients or metabolites. Moreover, it has been reported that chondrocytes showed preferential proliferation and ECM production for scaffolds with pore sizes between 250 and 500  $\mu\text{m}$  [22]. Additionally, the good hydration properties of the scaffolds also helped in providing the required microenvironment for cell migration and proliferation. Furthermore, the yield of GAG content was considerable and comparable to results reported in the literature [52].

### ***Analysis of gene expression***

A suitable scaffold for cartilage TE should not only facilitate cell growth, but it should also support chondrogenic phenotype in order to allow functional cartilage matrix to be formed [53]. Following this purpose, the preliminary evaluation of chondrogenic gene expression was performed by qPCR. The chondrogenic markers included transcription factor SOX-9 and the main member of proteoglycans, Aggrecan (ACAN) [38]. At the designed time points RNA isolated from cells, seeded on the gelatin scaffolds underwent reverse-transcription qPCR reaction and the relative gene expression was analysed respect to the housekeeping gene GAPDH (Fig. 3.19) [54].

The mRNA level of SOX-9 increased between day 7 and day 14 of cell culture for all three gelatin scaffolds (Fig. 3.19 A). Then at day 21 there was a slight decrease in the relative gene expression which can be explained by the fact that SOX-9 plays a key role in the early stage of cartilage formation therefore, at the later time of culture its level can be lower [55]. Even if no significant differences were reported at day 14 and day 21, the highest mRNA level of SOX-9 referred to level of GAPDH was observed for G-DHT (Fig. 3.19 A). This transcription factor is highly essential in maintaining the chondrocytes phenotype and also guides the chondrocytes in expressing hyaline cartilage specific genes [56].

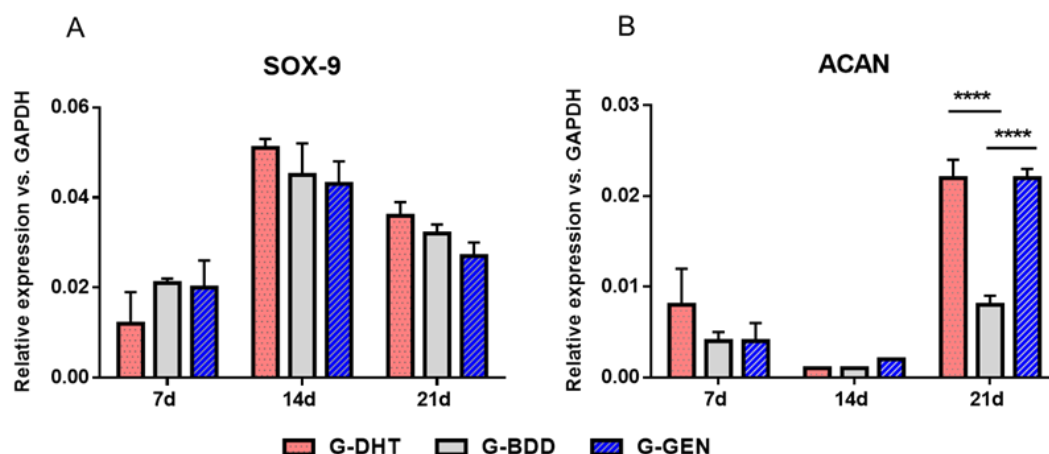


**Fig. 3.19.** Gene expression analysis of SOX-9 and Aggrecan (ACAN) gene. Relative quantification of gene expression after 7, 14 and 21 days of chondrocytes culture on the gelatin scaffolds. Data represent fold changes of target genes relative to the housekeeping gene GAPDH. No statistically significant differences noticed in expression of SOX-9; statistically significant increase of mRNA level of ACAN observed for G-DHT and G-GEN at day 21. (\*\*\*\* $p \leq 0.0001$ ).

The gene expression of aggrecan was also evaluated showing low mRNA level in the initial time points for all gelatin scaffolds and then at day 21 the high increase in the ACAN expression was observed with statistically significant difference for G-DHT and G-GEN compared to G-BDD (\*\*\*\* $p \leq 0.0001$ ; Fig. 3.19 B). Aggrecan plays an important role in structure and function of cartilage and its expression starts at the later time of the cell culture [55], [57]. Surprisingly, very low expression of ACAN gene at day 14 cannot be correlated to the high quantity of GAGs at the same day of culture. These diverse results can be related to post-transcriptional modifications of mRNA and moreover, further experiments of gene expression analysis are highly demanded. Nonetheless, the induction of SOX-9 and ACAN gene observed in cell-seeded gelatin scaffolds could be attributed to the structural suitability of the constructs promoted by the DHT, genipin and BDDGE crosslinkers.

#### ***Analysis of protein (SOX-9) expression***

In order to detect SOX-9 protein in the chondrocytes growing on the gelatin scaffolds after 7 and 14 days of culture western blot analysis was performed using anti-SOX-9 and anti- $\beta$ -actin antibody, which was used as an endogenous control (Fig.3.20). Acellular scaffolds were used as control and their protein concentration was subtracted from the concentration of cellular constructs before loading on the gel in order to eliminate the aspecific signal from the results. Additionally, lysates from the blank scaffolds were also load on the electrophoresis gel and underwent the same immune-detection.

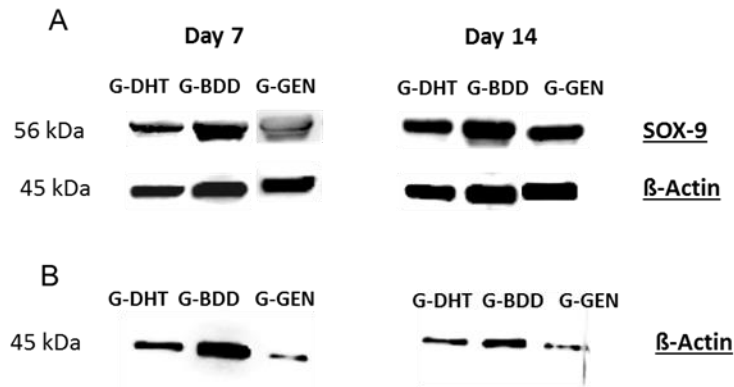


**Fig. 3.20.** Western blot analysis of SOX-9. The image represents protein bands from day 7 and 14 of (A) cell-seeded scaffolds and (B) scaffolds alone.  $\beta$ -actin was used as a control.

As can be seen in Fig. 3.20 A, SOX-9 protein is present in all three gelatin constructs. Accordingly, with the gene expression results, at day 14 the level of SOX-9 protein seems to be higher respect to day 7 (Fig. 3.20 A). In the blot from the blank scaffolds (negative control), the protein band of  $\beta$ -actin due to aspecific signal was observed therefore, quantification of SOX-9 expression which normally should be normalized to the expression of  $\beta$ -actin, was not performed (Fig. 3.20 B). Detection of  $\beta$ -actin in acellular scaffolds can be related to natural origin of our material, insufficiently purified collagen/gelatin or unspecific binding of antibodies. Nevertheless, bands of SOX-9 were noticed only for cell-seeded constructs, which confirms expression of this important for formation and functionalization of cartilage protein, by chondrocytes.

## 2.6. Conclusions

The present study reported a comparative analysis of various crosslinking agents used to reinforced and modified gelatin macromolecule for tissue engineering application. Evaluating the influence of thermal (DHT), chemical (BDDGE) and natural (Genipin) coupling agents on the gelatin reinforcement, we found that the thermal crosslinking process was more appropriate to obtain a 3D scaffold with physicochemical, mechanical and biological features suitable for tissue engineering. We demonstrated that thermal dehydration of the gelatin improves the overall characteristics without affecting the biological properties of the G-DHT scaffold. Moreover, the absence of any chemical residues within the protein network would absolutely avoid the antigenicity in physiological conditions. Similarly, the G-BDD a chemically crosslinked scaffold showed good mechanical behaviour with acceptable chemical composition, topography, hydrophilicity and satisfying biological properties. Whereas, the G-

GEN scaffolds also showed good morphological features however lower cytocompatibility was observed when compared to other two scaffolds but there was slow recovery in the compatibility in the later days of culture due to the cell and dose dependent effect of genipin. Additionally, G-GEN represented lower resistance to compression and lower viscosity respect to other scaffolds.

Taken collectively, our results we can conclude that, the adopted procedures to develop and stabilized a gelatin based 3D porous scaffolds endowed with high, interconnected porosity suitable for cell colonization and tissue regeneration, is worthwhile. The evaluations performed on diverse typologies of samples obtained by the three selected crosslinking mechanisms suggested that the dehydrothermal treatment is the most effective to obtain promising scaffolds for cartilage tissue engineering.

## Chapter 3

# DESIGN AND FABRICATION OF 3D COLLAGEN SCAFFOLDS REINFORCED BY GLYCATION

---

### 3.1. Introduction

Abnormalities in articular cartilage can produce pain and deteriorate quality of life, which finally can lead to development of osteoarthritis (OA). To prevent progression of OA, cartilage defects have to be treated satisfactory and biomaterials play here an important role to support regeneration of the damage tissue. Although, incorporation of many biomaterials into field of cartilage regeneration, appropriate treatment is still hard to achieve [34], [58]. The idea of fabricating innovative scaffolds for tissue engineering is to synthesize materials that can conclusively mimic the native tissue. Following this purpose 3D porous material with suitable microstructure, optimal biodegradation rate and good mechanical properties, especially in cartilage tissue engineering, is necessary to attract the autologous cells and support tissue regeneration [34], [59]. Collagen as it has been already mentioned is one of the natural polymers, widely used in cartilage repair approaches, as can support cell adhesion and cell signalling. Although collagen has been found to be biocompatible and possess low antigenicity, its mechanical properties and fast dissolution in physiological conditions need to be tailored prior to any *in vivo* applications [59], [60]. To improve collagen stability and mechanical strength several components, mostly chemical, have been employed to crosslink collagen-based materials including carbodiimide, glutaraldehyde, 1,4-butanediol diglycidyl ether and more [12], [18], [61], [62]. Many studies confirmed the beneficial role of these crosslinkers; however, their cytotoxicity in certain concentration can be a limitation of their use [60].

In this study we proposed a non-enzymatic crosslinking (glycation) by reducing sugar ribose as an alternative crosslinking strategy for cartilage TE. The fibrous collagen undergoes the non-enzymatic crosslinking basically, by creating intermolecular bridges between amino groups of two adjacent collagen molecule [63]. Before that, Maillard reaction and Amadori rearrangements occur and advanced glycation end products (AGEs) can be formed as was

described in details in part I of this thesis, section 4.2.4 [64]–[66]. AGEs in a high concentration cause stiffening tissues and accelerating protein oxidation as it has been demonstrated particularly in diabetics [67], [68]. Definitely, glycation can influence collagen on many ways, in which improving its strength and resistance to degradation is one of our interests. In our studies we chose ribose as a reducing sugar rather than glucose due to higher crosslinking efficiency of ribose compared to other sugars [66], [69], [70]. A few studies have already presented the positive effect of ribose crosslinking on the viability of human lung fibroblasts *in vitro* and its long-lasting efficiency as a dermal filler has been confirmed in a rabbit model [71], [72]. To our knowledge only one study showed pre- and post-glycation of collagen gel for cartilage tissue engineering approach focusing on measurement of the GAG release and viscoelastic properties [65]. Nonetheless, this study corresponds to non-freeze dried collagen gels and we did not find any other reports that may include broad analysis of non-enzymatic pre- and post-crosslinking on 3D porous scaffolds.

Therefore, ribose as a natural, easily accessible and low-cost crosslinker has been chosen to stabilize collagen fibers in order to produce 3D porous scaffolds that can be potentially used for cartilage repair. Two different crosslinking strategies have been applied as is presented on Fig. 4.1: a) pre-crosslinking (PRE) where, crosslinking reaction occurred before freeze-drying by mixing collagen fibers with the ribose solution and b) post-crosslinking (POST) where, the reaction was carried out after freeze-drying by immersion of 3D collagen scaffolds in the ribose solution. The ribose-collagen compositions were prepared in different weight ratios and various crosslinking reaction times in order to achieve optimal crosslinking conditions.

The aims of this work were: 1) to verify the effectiveness of ribose glycation as an alternative model in order to create stable 3D porous collagen scaffolds for cartilage tissue engineering; 2) to comparatively investigate two different non-enzymatic crosslinking methods, PRE- and POST-crosslinking, in terms of biodegradability, fluid absorption, microstructure, porosity, chemical bonding characteristics and mechanical behaviour. Additionally, *in vitro* biological tests were performed using mouse mesenchymal stem cells cultured in chondrogenic medium to assess the cell viability, proliferation, morphology, and glycosaminoglycans quantification.

### **3.2. Preparation of scaffolds**

Collagen gel in aqueous acetic buffer solution (pH = 3.5), isolated from horse tendon, was purchased from OPOCRIN SpA, Italy. 1 wt% of collagen gel was diluted in milli-Q water, and assembling of collagen fibers was achieved by increasing the pH up to 5.5 (isoelectric point of

collagen) with slow dripping of 0.1 M NaOH in aqueous solution (Sigma-Aldrich, USA). Collagen fibers were washed three times with milli-Q water and separated from the solvent by sieve. Next, two different crosslinking strategies by ribose glycation was performed obtaining 3D collagen-ribose constructs as follow (Fig. 4.1):

**A. Pre-crosslinking (PRE, before freeze-drying):** collagen fibers were mixed with 50 ml of 30 mM D-(-)-ribose (Sigma-Aldrich, USA) in ethanol/PBS (70% v/v) solution in two different weight ratio 1:1 and 1:0.5 (collagen:ribose) [65], [70]. Then, the crosslinking reaction was carried out at 37 °C for 2 or 5 days gently shaking. After 2 and 5 days of glycation solution was removed by using the sieve, collagen fibers were washed three times with milli-Q water, poured into polystyrene 48-well plate and freeze-dried by freezing at -40 °C and drying at 25 °C (5 Pascal, LIO 3000 PLT, Italy) for 48 h under a constant vacuum of 0.1 mbar to obtain porous 3D matrices. The developed samples will be hereafter named PRE 2D ½, PRE 2D 1, PRE 5D ½ and PRE 5D 1.

**B. Post-crosslinking (POST, after freeze-drying):** collagen fibers were firstly poured into polystyrene 48-well plate and freeze-dried as described above to obtain 3D constructs. Secondly, scaffolds were immersed in 50 ml of 30 mM D-(-)-ribose in ethanol/PBS (70% v/v) solution in two different weight ratio 1:1 and 1:0.5 (collagen:ribose) [65], [70]. Then, the crosslinking reaction was carried out at 37 °C for 2 or 5 days gently shaking. Next, scaffolds were washed three times with milli-Q water and freeze-dried as described above. The developed samples will be hereafter named POST 2D ½, POST 2D 1, POST 5D ½ and POST 5D 1. In total eight compositions were prepared, detailed in the Table 4.1.

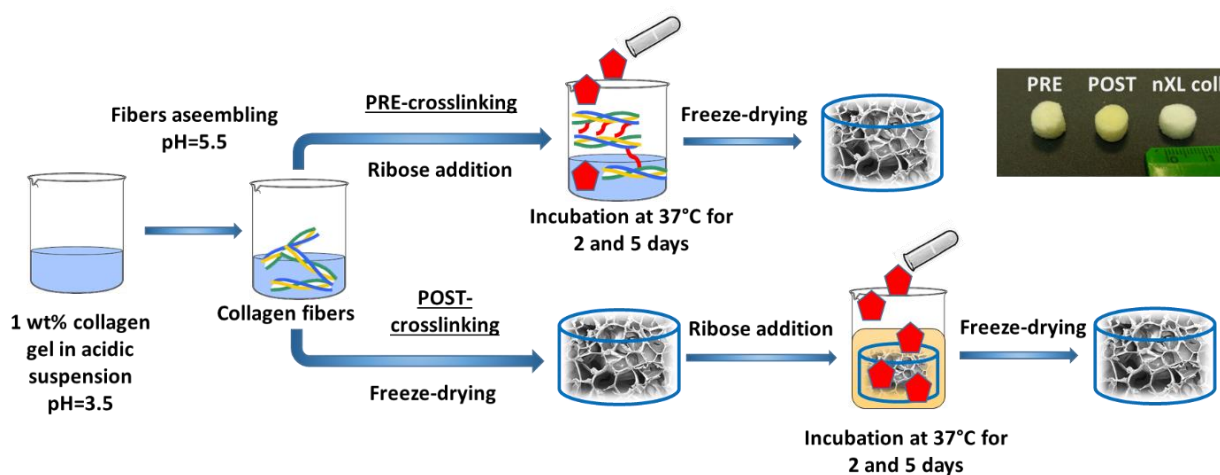


**Fig. 4.1.** Schematic illustration of fabrication ribose-crosslinked collagen scaffolds by two different crosslinking strategies: PRE- and POST-crosslinking. The image on the up right represents PRE and POST constructs as well as non-crosslinked collagen scaffold (nXL coll).

Before the synthesis of designed compositions described above, various amount of ribose in pre- and post-crosslinking method were tested as follow: 2 wt%, 5 wt%, 10 wt%, 25 wt%, 50 wt% and 100 wt% (weight percent respect to collagen weight, i.e. 1:1 collagen:ribose ratio). Crosslinking reaction was carried out for 2 and 5 days in milli-Q water and in the solution of ethanol/PBS (70% v/v) applying different temperature as 37 °C , 4 °C and room temperature. Only compositions with the collagen:ribose weight ratio 1:0.5 and 1:1 crosslinked in ethanol/PBS solution at 37 °C demonstrated stability over 7 days in PBS (pH = 7.4) at 37 °C based on macroscopic observation. Other samples showed to be unstable and start to degrade after one week of test. Therefore, the weight ratio 1:0.5, temperature 37 °C and ethanol/PBS solution have been established as a baseline for the conditions of crosslinking reaction. Proper experiments and comparative analysis have been performed on the compositions described above and summarized in table 4.1.

<b>Crosslinking strategy</b>	<b>Time of crosslinking reaction</b>	<b>Collagen:ribose weight ratio</b>	<b>Abbreviations</b>
Pre-crosslinking	2 days	1:0.5	PRE 2D 1/2
		1:1	PRE 2D 1
	5 days	1:0.5	PRE 5D 1/2
		1:1	PRE 5D 1
Post-crosslinking	2 days	1:0.5	POST 2D 1/2
		1:1	POST 2D 1
	5 days	1:0.5	POST 5D 1/2
		1:1	POST 5D 1
Non-crosslinked collagen			nXL coll

**Table 4.1.** Scaffold compositions and abbreviations.

### **3.3. Scaffolds characterization**

#### **3.3.1. Optimization of crosslinking conditions**

According to lack of previous experience in the ribose crosslinking in our laboratory and little information in literature about optimal crosslinking conditions, several different compositions variable in concentration of ribose and time of reaction were tested (Table 4.1). This section contains characterization of eight various compositions of the collagen scaffolds focusing on their micro-architecture, capability to absorb fluid, biodegradability, extent of crosslinking and mechanical behaviour. Non-crosslinked collagen (nXL) was used as a control in each evaluation.



### Porosity and pore size

Table 4.2 presents characterization of ribose-crosslinked collagen scaffolds based on their average pore size at minimum and maximum diameter and porosity obtained by water squeezing method (percentage of macropores porosity) and gravimetric method (percentage of total porosity). Regarding total porosity PRE samples showed 93% and POST samples 97% of porosity.

Since macropores are essential to provide space for vascularization and tissue ingrowth in *in vivo* condition and to enhance cell proliferation *in vitro*, macropores porosity (%) was measured (Table 4.2) [37]. The percentage of macropore porosity was higher for POST samples compared to PRE without particular differences among POST compositions (84 – 90%). In the PRE group macropore porosity (%) increased corresponding to increasing time of the crosslinking reaction; from  $65 \pm 4,9\%$  for PRE 2D 1 to  $77 \pm 1,4\%$  for PRE 5D 1 (Table 4.2).

Scaffold type	Composition	Porosity (%)		Average pore size ( $\mu\text{m}$ ) min diameter	Average pore size ( $\mu\text{m}$ ) max diameter
		Gravimetric method	Water squeezing method		
PRE-crosslinked	PRE 2D 1/2	$93,3 \pm 0,3$	$67 \pm 0,7$	$118 \pm 5,5$	$204 \pm 11,0$
	PRE 2D 1	$93,2 \pm 0,2$	$65 \pm 4,9$	$138 \pm 7,3$	$244 \pm 14,2$
	PRE 5D 1/2	$93,7 \pm 0,8$	$75 \pm 1,9$	$107 \pm 6,3$	$183 \pm 6,7$
	PRE 5D 1	$95,2 \pm 0,3$	$77 \pm 1,4$	$128 \pm 6,8$	$235 \pm 9,1$
POST-crosslinked	POST 2D 1/2	$96,5 \pm 0,4$	$84 \pm 0,7$	$88 \pm 3,7$	$162 \pm 8,7$
	POST 2D 1	$97,2 \pm 0,0$	$90 \pm 0,3$	$144 \pm 5,3$	$180 \pm 7,9$
	POST 5D 1/2	$97,1 \pm 0,1$	$89 \pm 1,1$	$129 \pm 5,4$	$212 \pm 7,9$
	POST 5D 1	$96,1 \pm 0,4$	$88 \pm 1,0$	$121 \pm 7,3$	$184 \pm 9,7$
Non-crosslinked collagen	nXL coll	$98,0 \pm 0,0$	$75 \pm 3,3$	$120 \pm 4,3$	$194 \pm 8,0$

**Table 4.2.** Morphological characteristics of collagen-ribose scaffolds. Percentage of porosity measured by gravimetric method (total porosity) and water squeezing method (macropore porosity) ( $n = 3$  data are mean  $\pm$  SEM). The pore size ( $\mu\text{m}$ ) determined by analysis of the SEM images; maximum and minimum diameter of at least 20 pores randomly chosen from different images per sample were measured ( $n = 20$ , data are mean  $\pm$  SEM).

Average pore size in minimum and maximum diameter in dry state was measured manually from the SEM images of the scaffolds and it varied from around  $100 \mu\text{m}$  up to approximately  $200 \mu\text{m}$  without significant differences among the samples (Table 4.2).

Morphological analysis of the collagen scaffolds revealed that glycation by ribose did not change significantly porosity and pore size in both PRE and POST group compared to nXL

coll. Furthermore, extent of porosity and average pore size are sufficient for cell migration in all compositions [25], [51].

### ***Fluid uptake***

Good swelling properties of the scaffolds are highly required when designing biomaterials for tissue engineering application. The capacity to absorb fluid from surrounding medium is an important factor because can define retention of cell medium and other physiological fluids *in vivo* which results in cell infiltration and attachment into the scaffolds [73]. As can be seen in Fig. 4.2, all the ribose-crosslinked collagen scaffolds absorb PBS very rapidly, reaching equilibrium after only 1 – 30 min of immersion for PRE compositions or from 2 to 4 h for POST compositions. The swelling test showed that for both PRE and POST scaffolds, crosslinking time of 5 days was more favourable than 2 days. There was no significant difference between the samples concerning the amount of ribose. Additionally, Fig. 2 demonstrated that POST samples have higher fluid index (%) than PRE samples: at 4 h the maximum value of fluid uptake observed for POST 5D ½ was  $2061 \pm 89\%$  whereas, for PRE 5D 1 reached  $1296 \pm 33\%$ . The differences in fluid binding capacity can be correlated to the different total porosity (Table 4.2) and hydrophilicity of the scaffolds [37]. It was noticed that post-crosslinked scaffolds, featured with higher porosity showed higher degree of fluid uptake.

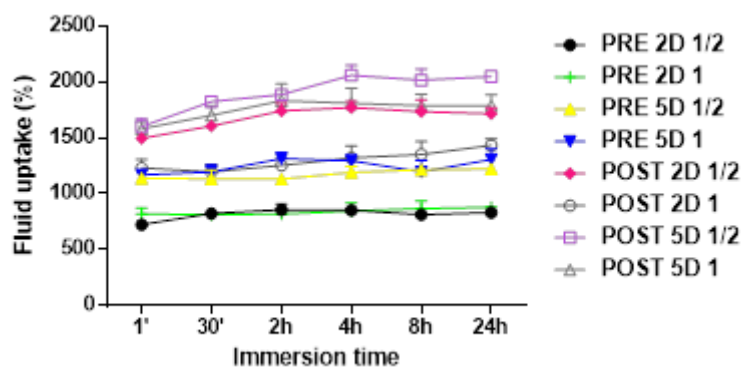


**Fig. 4.2.** Fluid uptake as a function of time of ribose-glycated collagen scaffolds in PBS at 37 °C (n = 3 data are mean ± SEM).

### ***In vitro degradation and extent of crosslinking***

To evaluate biodegradability of ribose-crosslinked collagen scaffolds, enzymatic digestion by collagenase was carried out (Fig. 4.3). Firstly, non-crosslinked collagen samples (nXL coll) were treated with different amount of collagenase and their degradation profiles are presented in Fig. 4.3 A. Higher enzyme activity resulted in higher degradation rate (%) in shorter time; using 38 CDU (collagen digestion unit) nXL coll was completely degraded in 3 h, whereas

using 13 CDU complete degradation was obtained after 26 h. Collagen sample incubated with 22 CDU of collagenase dissolved after 6 h and this time seemed to be optimal, as degradation profile was not too fast or too slow, inversely to samples with other concentrations of enzyme (Fig. 4.3 A). Therefore, ribose-crosslinked collagen scaffolds were treated with 22 CDU and 6 h of incubation demonstrating the greatest resistance to enzymatic degradation for POST samples: 2D 1, 5D ½ and 5D 1 with significance  $p = 0.0001$  when compared to the control nXL coll (Fig. 4.3 B). Among PRE compositions, the biodegradability was around 80% for all compositions except PRE 5D 1 ( $67.7 \pm 2.7\%$ ), which demonstrated statistically significant lower degradation rate compared to nXL coll ( $p = 0.0001$ ).

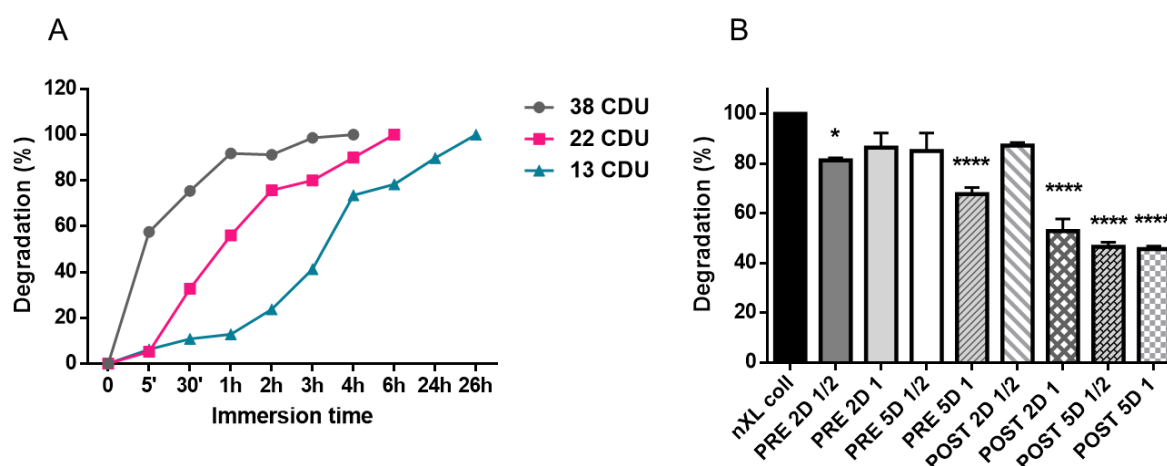


**Fig. 4.3.** (A) Degradation rate (%) of non-crosslinked collagen after treatment with different amount of collagenase expressed as enzyme activity (CDU: collagen digestion unit) per sample. (B) Extent of degradation of ribose-glycated collagen scaffolds after collagenase treatment with 22 CDU of enzyme at 6 h ( $n = 3$ , data are mean  $\pm$  SEM). \*\*\*\* $p \leq 0.0001$ , \* $p \leq 0.05$  statistically significant difference when compared to the control nXL coll.

Extent of crosslinking was calculated as the percentage of primary amine groups' crosslinked by ribose glycation, as illustrated in Fig. 4.4. The crosslinking degree of POST scaffolds ranged from  $13 \pm 1.25\%$  for 2D ½ to  $26 \pm 0.89\%$  for 5D 1 as ribose amount and days of crosslinking increased. The PRE scaffolds were crosslinked in lower extent than POST scaffolds and the differences between days and ribose concentration among PRE samples were negligible. Their values ranged between  $5 \pm 2.00\%$  for 2D ½ and  $9 \pm 0.95\%$  for 5D 1 (Fig. 4.4). Relatively low crosslinking degree in ribose-glycated scaffolds is not surprising considering the data from literature. Not very high values of crosslinking index have been found in studies about non-enzymatic crosslinking by reducing sugars [74]. An explanation of this behaviour can be a different mechanism of crosslinking occurred in glycation process and in crosslinking by chemical components as 1,4-butanediol diglycidyl ether (BDDGE) or 1-ethyl-3-(3-dimethylamino propyl) carbodiimide hydrochloride (EDC) [61], [75]. In non-enzymatic

crosslinking, a reducing sugar can bind the primary amine group of lysine residue of collagen molecule, and this glycated lysine residue can react with arginine residue on another collagen molecule creating the intermolecular bridge [63]. In chemical crosslinking by BDDGE, epoxide group of this component can react with the primary amine group of lysine residues as well as with the secondary amine groups of histidine. Additionally, reactions with the carboxylic acid groups of aspartic and glutamic acid can also occur, thereby increasing the possibility of greater number crosslinked bridges between collagen molecules [75], [76].

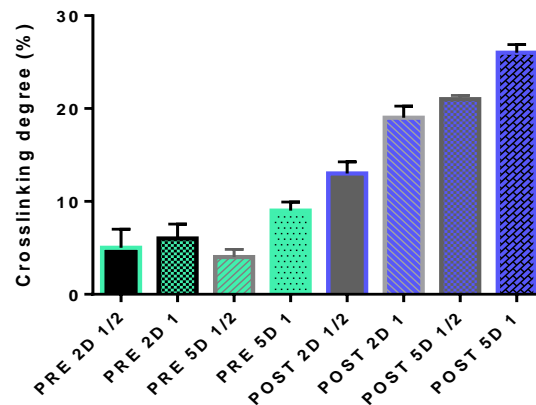


**Fig. 4.4.** Percentage of crosslinking degree express as an amine group content crosslinked per scaffold (n = 3 data are mean  $\pm$  SEM).

The crosslinking index data can be related to the resistance upon enzymatic degradation. High and similar percentage of biodegradability for PRE group, apart from the sample 5D 1, can be explained by similar and small amount of amine groups' crosslinked (Fig. 4.4). The composition PRE 5D 1 had the highest crosslinking degree among PRE scaffolds thus this sample was the most stable. The crosslinking index of POST scaffolds also increased adequately to the rise of their biostability (Fig. 4.3 and Fig. 4.4). In overall, these results indicated that post-crosslinking strategy could be more efficient in terms of amount of crosslinked collagen molecules and material's stability.

#### ***Mechanical properties (elastic modulus)***

It is well-known that cellular activity can be influenced by the stiffness of the material thus, scaffolds in 3D cell culture need to be stiff enough to withstand cell contractile forces [25]. In order to understand the mechanical properties of ribose-glycated collagen scaffolds uniaxial compression test was performed and elastic modulus (Young's modulus, compressive modulus) was calculated for each sample.

Fig. 4.5 A and B showed elastic moduli of PRE and POST group respectively, focusing on relation between days of glycation and amount of ribose. It can be clearly seen that ribose crosslinking reinforced collagen manifesting significant improvement in values of compressive modulus of all compositions compared to nXL coll (Fig. 4.5). In the PRE group, modulus slightly increased between samples 2D ½ and 5D ½ along with increasing concentration or days of crosslinking however without evident differences (Fig. 4.5 A). Then, at the longest time and at the highest concentration of ribose compressive modulus increased up to  $6.7 \pm 0.6$  kPa as showed PRE 5D 1 scaffold (Fig. 4.5 A). Similar trend was observed among POST samples demonstrating compressive moduli of around 4 kPa for POST: 2D ½, 2D 1 and 5D ½ and then great increase of  $11.4 \pm 0.3$  kPa for POST 5D 1 (Fig. 4.5 B). Interestingly, increasing amount of ribose did not significantly influence mechanical behaviour in neither PRE nor POST samples crosslinked for 2 days whereas, double amount of ribose in both PRE and POST constructs crosslinked for 5 days significantly enlarged compressive modulus ( $*p \leq 0.05$ ,  $***p \leq 0.001$ , Fig. 4.5 A, B).

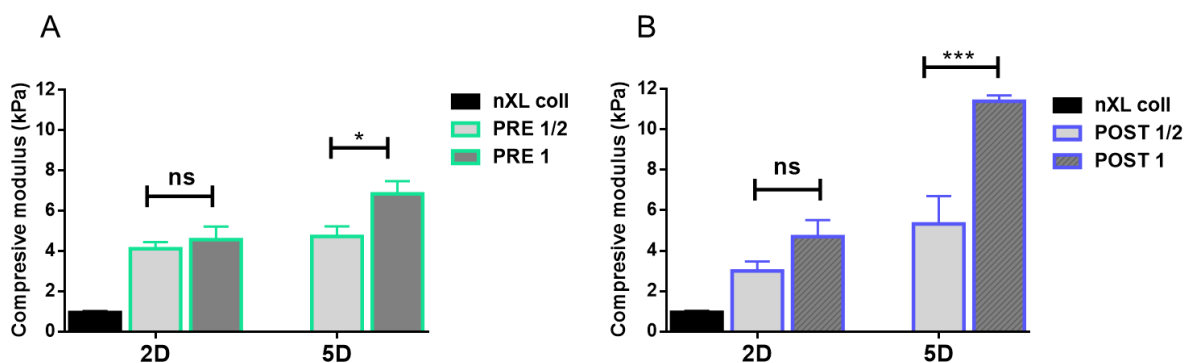


**Fig. 4.5.** Mechanical properties of ribose-crosslinked collagen scaffolds. (A) Compressive moduli of PRE 1 and PRE ½ crosslinked for 2 (2D) and 5 days (5D); (B) Compressive moduli of POST 1 and POST ½ crosslinked for 2 (2D) and 5 days (5D); (A) and (B) statistically significant difference observed between 5D samples in both group:  $*p \leq 0.05$  in PRE,  $***p \leq 0.001$  in POST; No statistically significant differences observed (ns) between samples crosslinked for 2D in both PRE and POST group; nXL collagen used as control.

From these mechanical analysis can be concluded that: i) stiffness of the collagen scaffolds increased upon ribose glycation and ii) that glycation for 5 days in the highest collagen:ribose ratio (1:1) manifested to be the most efficient crosslinking condition to obtain mechanically stable collagen scaffolds for both pre- and post-crosslinking strategy. It is also important to highlight that in all tests the scaffolds were hydrated prior to testing in order to mimic realistic conditions thereby, moduli of materials in a dry state cannot be confront to the moduli in a wet

conditions [77]. Nevertheless, the elastic moduli of fabricated scaffolds were similar or higher than those of other collagen based scaffolds found in the literature [73], [78], [79].

### 3.3.2. Evaluation of final compositions

Taken collectively the results presented so far, POST 5D 1 and PRE 5D 1 showed the best performance on enzymatic degradation and mechanical stability thus those compositions were selected for further more detailed characterization and biological analysis.

#### *Fourier Transform Infrared Spectroscopy (FTIR)*

Fig. 4.6 represents FTIR analysis of PRE 5D 1, POST 5D 1 glycated samples, non-crosslinked collagen and ribose which serve as a control and reference respectively. Characteristic FTIR spectrum of nXL coll with absorption bands of amide I at  $\sim 1650\text{ cm}^{-1}$ , amide II at  $\sim 1560\text{ cm}^{-1}$  and amide III as set of three weaker bands centred at  $\sim 1254\text{ cm}^{-1}$  was observed (Fig. 4.6) [80]. These characteristic peaks of amides were also noticed for both PRE and POST sample, indicating that the conformation of collagen was not significantly altered by ribose attachment. In order to compare spectra of crosslinked samples and crosslinker by itself, FTIR spectrum of D-ribose was analyzed as well, showing intense peaks between 1000 and 1100  $\text{cm}^{-1}$  (Fig. 4). These correspond to C-O, C-C stretching vibrations and C-O-H and C-C-O bending vibrations of ribose [65]. Although, the sharp peak at  $\sim 1030\text{ cm}^{-1}$  correlated to ribose conformation was observed also for nXL coll, the second peak at  $\sim 1080\text{ cm}^{-1}$  seems to be less sharp and shifted compared to PRE 5D 1 and POST 5D 1. Presence in nXL coll spectrum typical peaks of ribose can be associated with immense amount of chemical functional groups of collagen molecule [80].

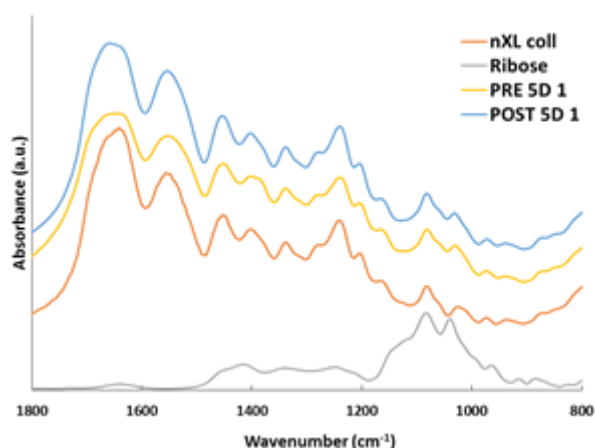


**Fig. 4.6.** FTIR spectra of non-crosslinked collagen (nXL coll), ribose alone and glycated scaffolds (PRE 5D 1 and POST 5D 1).

### ***Morphology and microstructure***

Morphology of the PRE and POST scaffolds as well as nXL coll was analysed by SEM and representative images are exposed in Fig. 4.7. Two different regions of the scaffold are displayed, starting from the top of the scaffold after transversal cut and the inside of the scaffold after longitudinal cut. Morphological observation showed homogeneity throughout the entire scaffold and porous microstructure with interconnected micro- and macropores for all samples (Fig. 4.7). Comparing SEM images of crosslinked samples and non-crosslinked control can be concluded that the glycation reaction did not modify excessively the microscopic structure of the collagen scaffold.

Considering that those scaffold are designed to be used in physiological conditions, we were interested in analysis of mean pore size after swelling therefore, cross-sections of wet PRE 5D1 and POST 5D1 scaffold, embedded in OCT and cut on the cryostat were analyzed with the optical microscope (a typical image was reported in the insert of Fig. 4.8 A). The analyses revealed around 20% and 30% larger pore size after swelling for PRE 5D 1 and POST 5D 1 respectively (calculated respect to data in Table 4.2). Average pore size measured at minimum diameter was  $167 \pm 10.6 \mu\text{m}$  for PRE and  $156 \pm 7.2 \mu\text{m}$  for POST, and average pore size measured at maximum diameter was  $288 \pm 9.3 \mu\text{m}$  and  $279 \pm 12.0 \mu\text{m}$  for PRE and POST respectively.

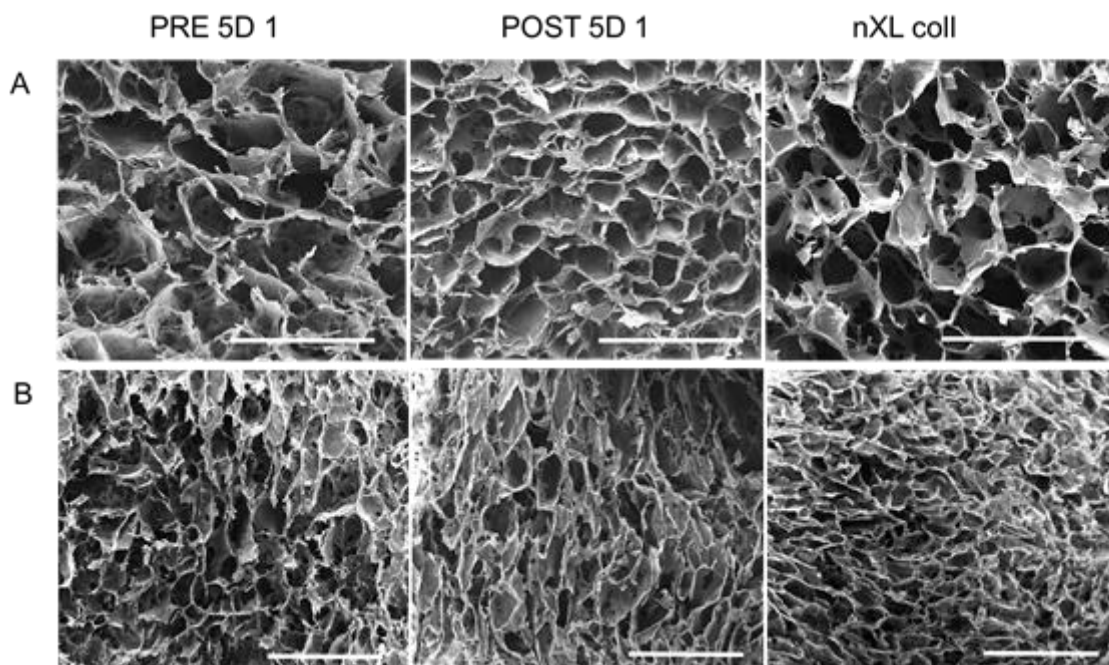


**Fig. 4.7.** Morphology of pre-crosslinked (PRE 5D 1), post-crosslinked (POST 5D 1) collagen scaffolds and non-treated collagen (nXL). (A) transversal cross-sections, (B) longitudinal cross-sections. Scale bars: (A) PRE 5D 1 - 500  $\mu\text{m}$ , POST 5D 1 and nXL coll – 400  $\mu\text{m}$ ; (B) all 1000  $\mu\text{m}$ .

Additionally, pore size distribution in the wet state was also evaluated as presented in Fig. 4.8 A. The analyses demonstrated the wide distribution of pores dimension from 60  $\mu\text{m}$  up to even 380  $\mu\text{m}$  however, the highest number of pores for PRE 5D 1 was found in a range 160-200  $\mu\text{m}$  and for POST 5D 1, the highest amount of pores was noticed between 80 and 120  $\mu\text{m}$ . More frequent presence of small pore size in POST scaffolds can be a result of double freeze-drying process during the synthesis. This notably heterogeneous pore size distribution makes both PRE and POST group versatile for tissue engineering application. It has been demonstrated that mature chondrocytes have high proliferation rate and increased ECM production when seeded on the scaffolds with pore size bigger than 250  $\mu\text{m}$  [51]. Nevertheless, in other studies has been proved that pore size around 100  $\mu\text{m}$  is preferred for chondrogenesis [81] and moreover, pore size between 60 and 200  $\mu\text{m}$  has been shown to enhance cartilage formation in a porcine animal model [14]. Therefore, the pore size range of PRE and POST collagen scaffold can be considered as an optimum for the differentiation and maintaining cell phenotype as well.

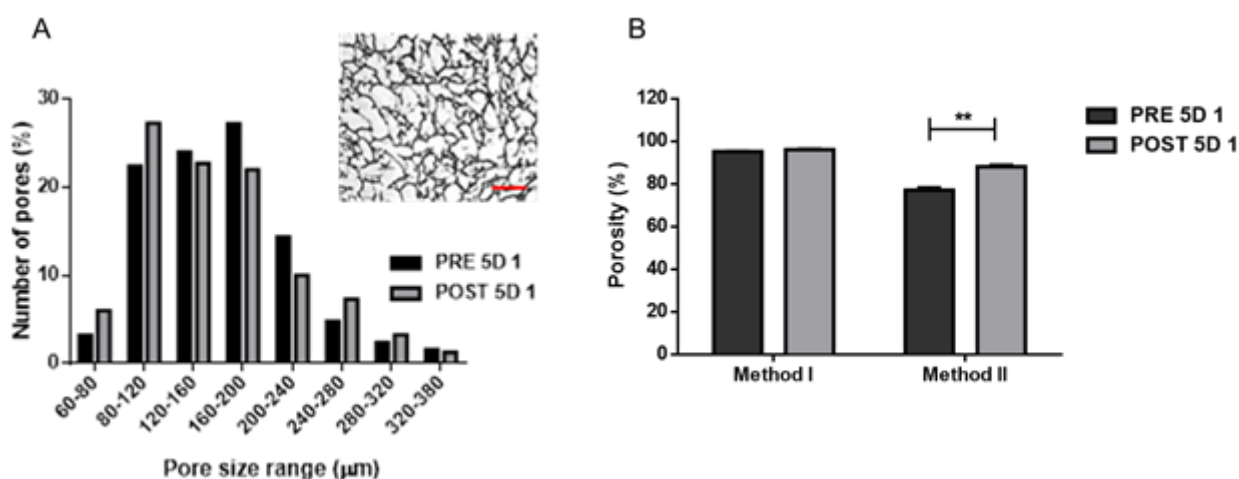


**Fig. 4.8.** (A) Pore size distribution of PRE 5D 1 and POST 5D 1 after 24 h of swelling in PBS and representative image of 20  $\mu\text{m}$  section of ribose-collagen scaffold, embedded in OCT and cut on the cryostat also after the immersion. The graph represents data from 150 pores randomly chosen from 10 images, 5 different sections; (B) Percentage of porosity measured by gravimetric method (Method I) and water squeezing method (Method II) ( $n = 3$  data are mean  $\pm$  SEM); Statistically significant difference in porosity (%) observed between samples measured by method II:  $**p \leq 0.01$ .

Comparing again porosity measured by gravimetric method (Method I) and water squeezing method (Method II) between PRE 5D 1 and POST 5D 1 there is no remarkable difference in the first one, however there is the statistically significant change ( $**p \leq 0.01$ ) in macropore porosity favourable for POST sample (Fig. 4.8 B). Lower porosity in the PRE group can be explained considering that, the pre-crosslinking strategy leads to a lowering of the



collagen hydrophilicity and a consequent decreasing in the gel water content. Because the amount of water before freeze-drying determines the final total porosity and consequently the final scaffold became less porous. This probable minor amount of free hydrophilic groups for PRE scaffolds results in lower fluid binding capacity in contrast to the POST samples as has been shown in the swelling test (Fig. 4.2).

### ***Mechanical properties***

After preliminary static compression test presented in previous section of this chapter more mechanical analyses, only on PRE 5D 1 and POST 5D 1 scaffolds, were performed including static and dynamical mechanical test as well as creep test.

As articular cartilage experiences continuous compression the collagen scaffolds were exposed to compressive loading under wet condition and at temperature 37 °C. All samples were incubated 24 h in PBS for swelling prior to any test.

Fig. 4.9 A shows stress-strain curves of PRE 5D 1, POST 5D 1 and nXL coll obtained from the uniaxial compression test under the controlled force. We can observe typical for soft polymers non-linear strain-stress curves in compressive mode. The curves confirmed distinct material response regarding different crosslinking methods and the control. The final fracture (collapse region) is difficult to notice, rather the samples underwent immediate densification after the linear response [27], [73].

From the linear part of stress-strain curve compressive moduli were calculated showing significant enhancement in their values for crosslinked scaffolds compared to control; 12-fold increase for POST 5D 1 and 7-fold increase for PRE 5D 1 respect to nXL coll (both \*\*\*\* $p \leq 0.0001$ , Fig. 4.9 B). POST scaffold exhibited also better ability to withstand the compressive forces which was proved by almost 2-fold significantly higher modulus compared to PRE 5D 1 (\*\*\*\* $p \leq 0.0001$ , Fig. 4.9 B).

To determine viscoelastic properties of the scaffolds dynamical mechanical test (DMA) at varying frequencies and creep test were performed. Looking at the graph of storage modulus the increase of  $E'$  with increasing frequency was observed for both PRE and POST sample and control (Fig. 4.9 C). Storage modulus cannot be referred to compressive modulus however also here similar trend can be noticed i.e., promotion of  $E'$  by glycated scaffold compared to control. POST sample showed the highest  $E'$  at each frequency thus, this scaffold enhanced stiffness of collagen in a greater extent than PRE.

Creep test is a common analysis used in cartilage TE because it can investigate material's capacity to recover after mechanical deformation as well as can define time needed for that

recovery [82], [83]. In this study, scaffolds were subjected to the constant stress for 15 min (loading) and left without any force applied for another 15 min (deloading). Average DMA creep curves expressed as change of strain (%) in a function of time are displayed on Fig. 4.9 D. After 15 min of loading the related strain values yielded 33 and 45% for POST 5D 1 and PRE 5D 1, respectively and then the load was stopped (Fig. 4.9 D). Strain of both scaffolds decreased immediately and at 30 min reached 5% for PRE 5D 1 and 3% for POST 5D 1. This behaviour can be confirmed by values of strain recovery (%) calculated from the creep curve. Both constructs showed high strain recovery at the end of the test: 95% of strain recovery for PRE and 97% for POST.

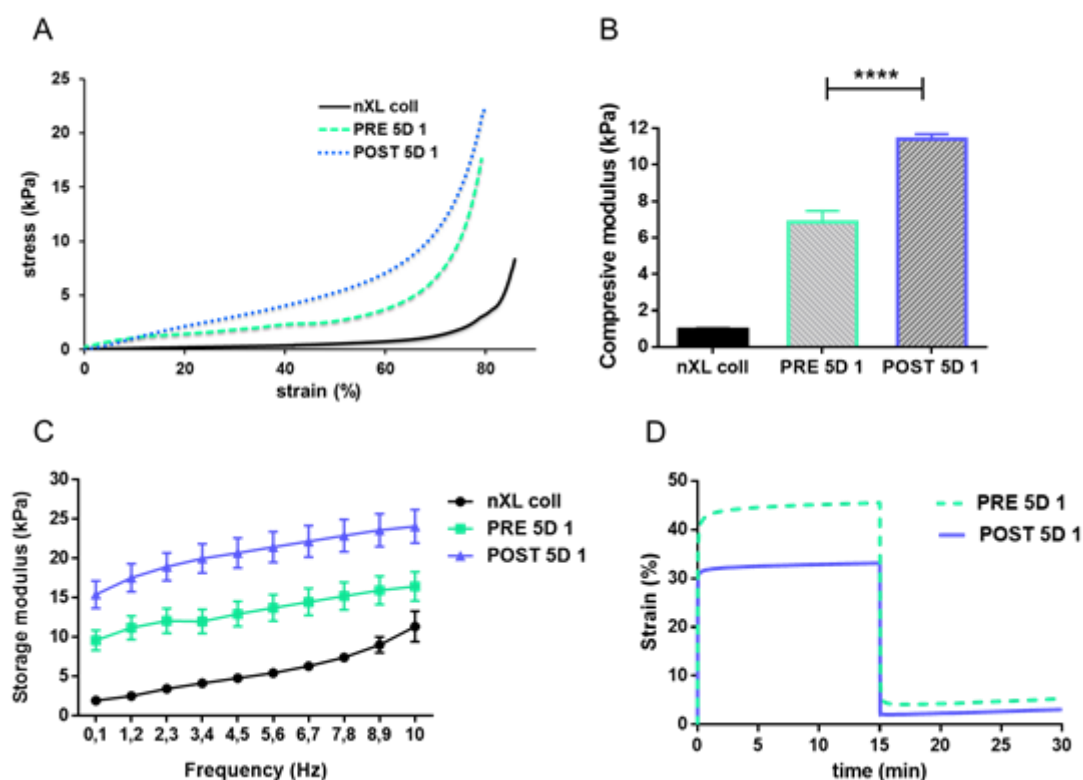


**Fig. 4.9.** Detailed mechanical properties of PRE 5D 1 and POST 5D 1 collagen scaffolds. (A) Mean stress-strain curves of PRE 5D 1, POST 5D 1 and nXL coll; (B) Compressive moduli of crosslinked scaffolds and the control; statistically significant increase of modulus for POST 5D 1 compared to the PRE 5D 1: \*\*\*\* $p \leq 0.0001$  and also for both POST and PRE compared to nXL coll (not shown on the graph): \*\*\*\* $p \leq 0.0001$ ; (C) Storage modulus ( $E'$ ) measured by dynamic compression test; (D) Creep test expressed as strain change (%) during loading and deloading in a function of time. All samples were hydrated in PBS at 37° C for 24h prior to testing (n = 3 for the uniaxial compression, n = 4–5 for the dynamic and creep test, data are mean  $\pm$  SEM).

We can notice that even with higher extent of deformation at the beginning of the test and also after 15 min in PRE respect to POST, at 30 min PRE scaffold restored its initial height in the same rate as POST (Fig. 4.9 D). nXL coll as a control has not been plotted on the graph as by

applying the same stress (0.002 MPa) after 5 min of loading the sample completely collapsed. Concluding, both PRE 5D 1 and POST 5D 1 manifested their elastic behaviour upon compression showing fast recovery and almost complete persistence of the original shape after loading and deloading.

Mostly, dense structure of the material results in good mechanical strength but lower porosity therefore, balance between mechanical properties and porosity of the scaffold can be extremely difficult to accomplish [1], [33]. Remarkable porous microstructure of our scaffolds have not been compromised by enhance of mechanical stiffness in pre- or either post-crosslinking strategy (morphology and microstructure section). Probably higher compressive and storage modulus for POST than PRE can be correlated to abundance in smaller pores and greater amount of amine groups crosslinked as reported by crosslinking degree values in case of POST scaffold (Fig 4.4, Fig. 4.8 A).

### 3.4. Biological assessment

#### *Cell viability and morphology*

To investigate the impact of ribose-crosslinked collagen on cell behaviour, mMSCs were seeded on PRE 5D 1 and POST 5D 1 scaffolds and cultured for 28 days in chondrogenic medium.

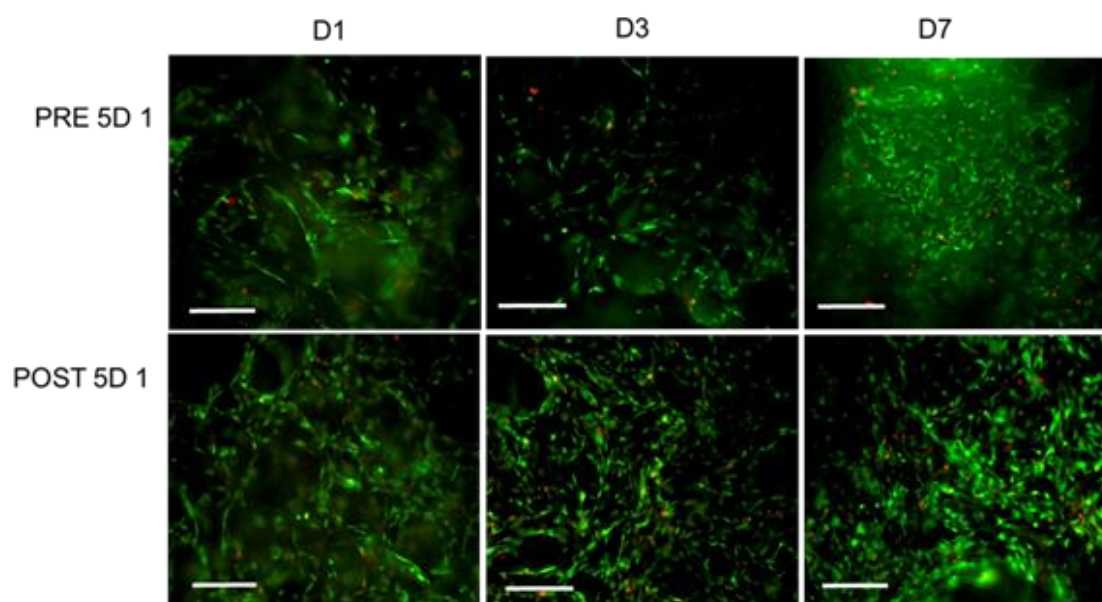


**Fig. 4.10.** Cell viability analyzed by the Live&/Dead assay (Calcein stains live cells in green, Ethidium homodimer-1 stains dead cells in red) on cell seeded PRE 5D 1 and POST 5D 1 scaffolds at day 1, 3 and day 7. Scale bars: 200  $\mu$ m.

Fig. 4.10 represents cell viability assessed by Live&/Dead assay at 1, 3 and 7 days of culture demonstrating overall high cell viability for both POST and PRE samples. The cell density increased over the time of culture and cells appeared to be uniformly distributed in both the scaffolds upper surface (Fig. 4.10).

From the quantitative analysis of cell viability we can observed statistically significant increase of live cells for PRE respect to POST ( $p \leq 0.05$ ) at day 3 of culture and, on the contrary, a statistically significant decrease of live cells for PRE respect to POST ( $p \leq 0.01$ ) at day 7 (Fig. 4.11 A). Moreover, the % of cell viability for PRE was reduced from  $88 \pm 2\%$  to  $71 \pm 2\%$  from day 1 to day 7 whereas, for POST scaffold it remained approximately over 80% at each day (Fig. 4.11 A).

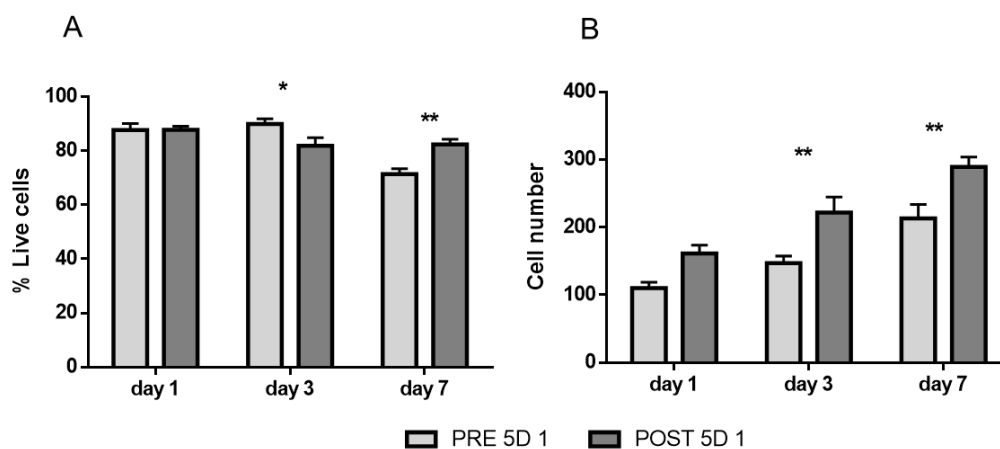


**Fig. 4.11.** Cell viability and proliferation analysed by Live&/Dead assay. (A) Percentage of live cells respect to the total cells counted seeded on PRE 5D 1 and POST 5D 1 scaffolds at day 1, 3 and 7. (B) Number of live cells seeded on PRE 5D 1 and POST 5D 1 scaffolds at day 1, 3 and 7. (A) and (B) represent mean data  $\pm$  SEM from two samples, in total 6 random fields of view ( $n=6$ ) at the same magnification per group. \* $p \leq 0.05$ ; \*\* $p \leq 0.01$ .

Quantification of the cell proliferation was also evaluated showing the augmentation in cell growth over time for all the scaffolds (Fig. 4.11 B). Higher proliferation rate was observed for the POST group respect to PRE group at each time point and this difference was statistically significant at day 3 and day 7 ( $p \leq 0.01$ , Fig. 4.11 B). Taking together these results can be clearly seen that ribose did not hinder the cell growth and the cell viability (Fig. 4.11 A, B). Furthermore, we observed the increasing glycosaminoglycans production until 28 days of culture (discussed in details below) which point us to claim that cells seeded on PRE scaffolds were viable and active even at the late time of the culture.

Cell morphology and cell colonization of the scaffolds were evaluated by SEM images at day 3, as displayed on Fig. 4.12. Cells attachment on the upper (Fig. 4.12 A) and inner surface (Fig. 4.12 A) of the scaffolds was noticed for both PRE 5D 1 and POST 5D 1. These results

proved that suitable pore size and topography of scaffold surface can promote cell colonization and adhesion [25].

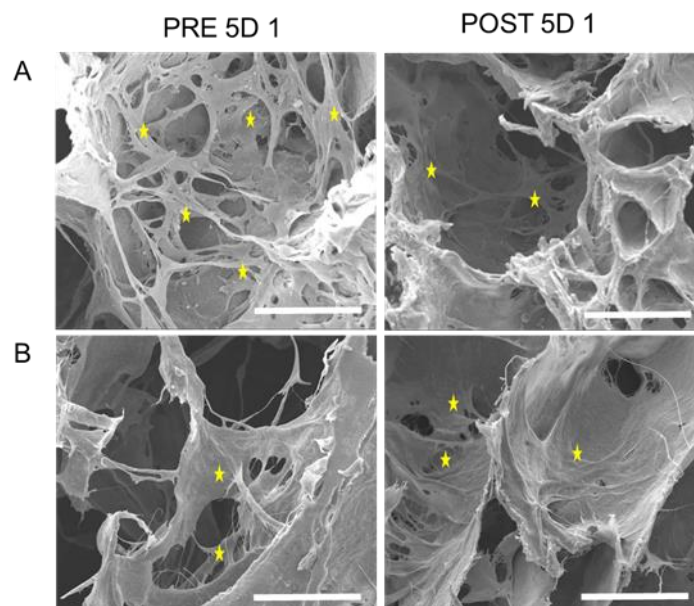


**Fig. 4.12.** Morphology of cell-seeded ribose-glycated collagen scaffolds at day 3. (A) top of the scaffold, (B) inside the scaffold. Scale bars: (A, B) 100  $\mu\text{m}$ . Cells marked by ★

#### ***Glycosaminoglycans content***

Another parameter, which can be monitored *in vitro* regarding cartilage tissue engineering, is the quantification of sulphated glycosaminoglycans (GAGs). The abundance of GAGs contributes to chondrogenic phenotype of the cells and it can also be considered as an index of functionality of differentiated cells [84], [85].

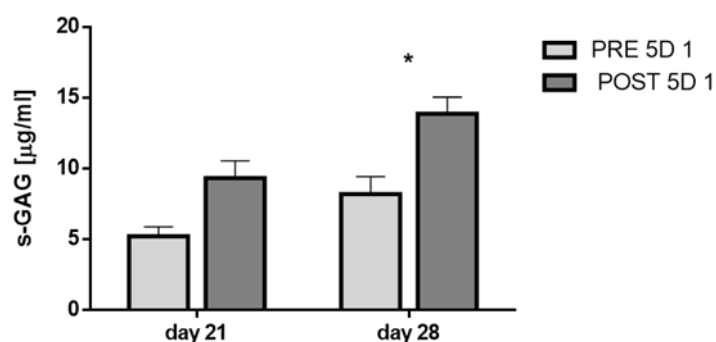


**Fig. 4.13.** GAG deposition by cells on PRE 5D 1 and POST 5D 1 scaffold after 21 and 28 days of culture. Values are reported as mean  $\pm$  SEM (n=3), \* $p \leq 0.05$ .

Thus, after 21 and 28 days of 3D culture in chondrogenic medium, GAG assay was performed on PRE 5D 1 and POST 5D 1 constructs. The amount of GAGs produced by the cells in correspondence to the culturing time was increased from day 21 to day 28 for both PRE and

POST scaffolds (Fig. 4.13). Additionally, POST sample manifested the significantly higher level of GAGs content when compared to PRE at day 28 ( $p \leq 0.05$ ), which can be a good indicator of rich deposition of cartilage ECM components by the cells.

Concluding the biological findings in this study, it was evidently estimated that both pre- and post-crosslinked scaffolds showed cytocompatibility, promotion of cell colonization and secretion of GAGs; however, POST construct turned to be superior to PRE in all these parameters. Better biological performance in POST 5D 1 than in PRE 5D 1 can be correlated with the differences in physical characterization of the scaffolds. It has been postulated that stiffness of the substrate can influence cell motility, morphology, proliferation and stem cell fate [86], [87]. Cells seeded on the stiff matrices proved to be more rigid and well spread in contrast to increased cell motility on flexible substrates [88]. Additionally, it has been demonstrated that different mechanical properties of hydrogels influenced proliferation of fibroblasts in 3D culture [89]. In our study, the greater stiffness expressed as elastic modulus by POST 5D 1 scaffold can be correlated to the higher cell proliferation rate and higher GAG deposition in this construct respect to PRE 5D 1 [86], [87], [90]. In addition, better swelling properties in POST respect to PRE group helped in providing the required microenvironment for cell migration and proliferation [1].

In the scientific community, there are still some doubts regarding cytotoxicity caused by glycation because large amount of the advanced glycation end products released in this process can contribute to the altered ECM and cell death. In fact, collagen matrices post-glycated at the ribose concentration higher than 30 mM have been proved to be toxic for the human lung fibroblasts [71]. In this work, to avoid any cytotoxic effects without compromising material stiffness and resistance to degradation, the final ribose concentration was 30 mM with corresponding to it suitable collagen-ribose weight ratios.


We cannot omit that further biological analyses may help for better understanding the cell-scaffold interactions. Deep investigation of the scaffolds impact on stem cells differentiation by gene and protein expression analyses needs to be performed in future experiments. Moreover, it would be more than interesting to verify mechanical properties of the cell-seeded scaffolds during *in vitro* culture.

### ***Last remarks***

Differences in physical and mechanical characterization as well as in biological performance between PRE and POST scaffolds can be attributed to the different strategies of

scaffolds fabrication, which contribute to distinct ribose distribution in the scaffolds. Hypothetic mechanism of ribose attachment to the collagen matrix has been proposed as depicted in Fig. 4.14. From our point of view in PRE-crosslinking, ribose molecules can react freely with collagen molecules that are later closely packed due to the subsequent freeze-drying process. In this way, ribose units can be entrapped by collagen fibers and they are mainly accumulated inside the collagen matrix and less on its surface (Fig. 4.14 left panel). Instead, in POST-crosslinking, ribose reacts with already formed collagen matrices; it can penetrate the 3D freeze-dried scaffold due to its high porosity and creates crosslinking bonds between collagen fibers on its surface. In consequence, ribose can probably work as a ‘protective coat’ for collagen resulting in smaller biodegradation rate and higher mechanical stability (Fig. 4.14 right panel). Moreover, ribose units which are distributed on the collagen surface in POST constructs can be more accessible for the cells than in PRE, promoting cell attachment and proliferation as ribose is also a natural saccharide which can be attractive for the cells [91], [92].

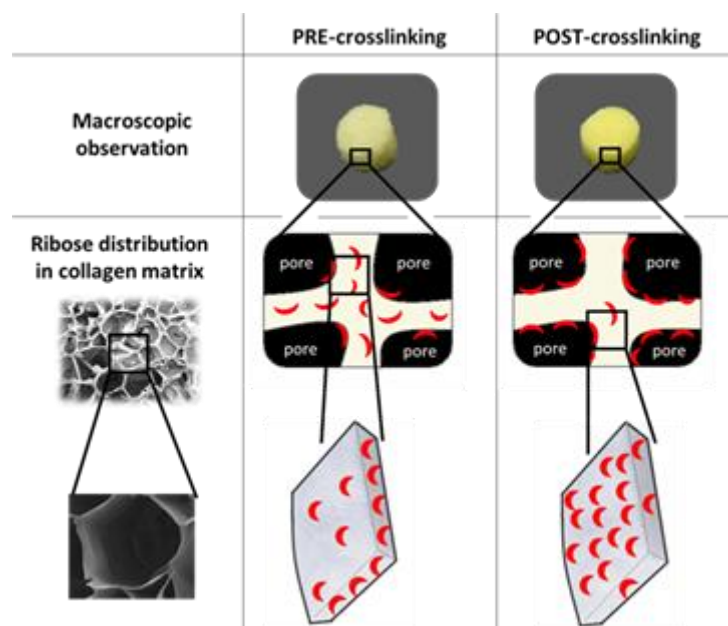


**Fig. 4.14.** Schematic illustration of probable differences in ribose-crosslinking mechanism by PRE- and POST-crosslinking strategy. The illustration presents macroscopic and microscopic point of view. Ribose molecule marked as 

### 3.5. Conclusions

In this study, an unconventional crosslinking method as non-enzymatic glycation by ribose was presented, which showed to be highly efficient in reinforcement of 3D collagen matrices. Ribose-crosslinked collagen scaffolds exhibited significantly higher resistance to enzymatic digestion when compared to non-crosslinked collagen. Good swelling properties and very porous interconnected microstructure revealed to be suitable for cell growth and colonization.

Comparison analysis of two crosslinking strategies: PRE- and POST-crosslinking demonstrated differences in fluid binding capacity, biodegradation, and extent of crosslinking degree between both groups with better performance for POST scaffolds. Both crosslinking methods enhanced mechanical properties of collagen, showing the highest compressive moduli for POST 5D 1 construct. Moreover, it has been proved that glycation by ribose increased the stiffness of the collagen scaffolds without hindering their elasticity. Taken collectively the results from physicochemical characterization, we observed differences among the samples more in a time-dependent manner than a dose-dependent one, favouring 5 days as an optimum time for sufficient crosslinking by ribose.

Preliminary biological assessment demonstrated scaffolds cytocompatibility supported by good cell viability and adhesion onto the surface and inside the scaffold. POST group manifested significantly higher cell viability and glycosaminoglycans production than the PRE.

To conclude, from the comparative study of these two crosslinking strategies, the POST-crosslinking method by ribose glycation results the most effective and promising for the achievement of 3D scaffolds suitable for cartilage tissue engineering.



# PART IV

## FINAL CONCLUSIONS AND FUTURE PERSPECTIVES

---

Poor regenerative potential of cartilage tissue and its anisotropic complex structure makes cartilage restoration extremely challenging and still unsolved issue in medicine today [93]. A variety of barriers exist between new cartilage products and their clinical applications: a ‘gold standard’ treatment is still missing [94]. Nevertheless, plenty of attempts are undertaking to cure cartilage lesions by cartilage TE techniques. A success of such a tissue engineering strategy strongly depends on the choice of an appropriate scaffold and eventually suitable cell source [34]. The main assumption when designing and fabricating the scaffolds is their biomimicry. Such a biomimetic scaffold resembling the native cartilage should be able for a fast and efficient regeneration of a chondral defect [95]. Unfortunately, the reality is still far from the ideal. To provide the biocompatible material with strong physical, chemical and mechanical features is still a huge challenge in the field.

In this PhD work, we wanted to generate biomimetic-like scaffolds focusing on the investigation of different crosslinking strategies. For this purpose, natural polymers, gelatin and collagen were used to synthesize 3D porous scaffolds, as they have great potential in biocompatibility due to their natural origin and they relatively easily undergo physicochemical modifications [96]. However, both gelatin and collagen exhibit fast biodegradation in physiological conditions and weak mechanical properties thus, the use of proper reinforcement (crosslinking) is highly necessary. Among the numerous crosslinkers available on the market it is hard to specify which one is able to not only stabilize physically and mechanically the material but also improve its properties without creating cytotoxic effects [12]. Therefore, in this work two independent projects have been performed; the first, where comparative analysis among three different crosslinking methods, already existing in literature, were applied to the gelatin matrices and the second one where, a new type of crosslinking by glycation was used for fabrication of collagen scaffolds.

In the first study, satisfactory results regarding scaffold's microstructure were obtained for all crosslinking strategies: physical (DHT), chemical (BDDGE) and natural (Genipin). All three groups represented high total porosity (approx. 94%) and relatively big average pore size (over 300  $\mu\text{m}$ ) without significant differences observed. Well-known fast dissolution of gelatin in an aqueous environment was improved in every group with superior results for G-BDD sample which can be correlated to its highest crosslinking degree (73%). Mechanical properties of gelatin were notably enhanced demonstrating the highest stiffness and better viscoelastic behaviour for G-DHT (compressive modulus of 54 kPa). This scaffold was able to store more energy maintaining the viscous response at higher frequency compared to G-BDD and G-GEN. Although, G-GEN manifested the strongest capability to absorb fluid and suitable porosity, this sample showed the highest degradation rate and the weakest mechanical properties. Moreover, in the biological performance, G-GEN had the lowest proliferation rate and chondrogenic markers expression level, putting in doubts cytocompatibility of genipin-crosslinked scaffolds. Cellular response for G-DHT and G-BDD were satisfied with preferable results for DHT-crosslinked constructs.

In the second study, the unconventional non-enzymatic crosslinking (glycation) by reducing sugar – ribose was investigated focusing firstly, on optimization of crosslinking conditions and secondly on comparison between two different reinforcement strategies: PRE- and POST-crosslinking. It has been proved that glycation by ribose can be an alternative model of reinforcement for the collagen scaffold improving its mechanical properties and resistance to enzymatic degradation. To my knowledge, this is the only study using ribose as a crosslinking agent in the synthesis of 3D porous scaffolds. The optimal crosslinking conditions were established as 5 days of reaction at 37 °C using the PBS/ethanol solution with a collagen:ribose weight ratio of 1:1. According to comparative analysis of PRE and POST strategy, POST scaffolds showed better performance on degradation rate, fluid uptake, macropore porosity, mechanical behaviour and cellular response.

One of the major critical point in developing scaffolds for cartilage TE is the conflicting requirement of scaffolds with high porosity and mechanical strength. A highly porous structure is preferred in favour of cell growth and proliferation, but it is generally achieved at the expense of mechanical strength. In our scaffolds the balance between good mechanical properties and efficient porosity was achieved showing high values of elastic moduli, especially for gelatin scaffolds when compared to literature [2], [17], [35], [73]. Moreover, higher cell proliferation and higher GAGs level can be correlated to the scaffolds with superior mechanical results: G-

DHT and POST 5D 1. This can be explained by the fact that cells seeded on the stiff matrices proved to interact better with biomaterial than cells seeded on flexible substrates [88].

Confronting together both studies performed in this thesis, gelatin scaffolds exhibited more porous microstructure and better mechanical properties than collagen scaffolds. Decisively, gelatin can be easier to manipulate and its economic value is more attractive than collagen. Among different crosslinking methods presented in this work, DHT showed the best potential in development of 3D porous scaffolds for cartilage TE. This crosslinking treatment demonstrated the best physicochemical, mechanical and biological performance when compared to other groups of gelatin scaffolds. Besides, DHT reinforcement can be superior to glycation by ribose, BDDGE and genipin crosslinking due to its low-cost, ease and velocity of the procedure that is desired for scale-up production.

I cannot omit that this work has some limitations, mainly in the *in vitro* parts. First of all, more tests about investigation of the scaffolds impact on cartilage formation are necessary. Moreover, use of primary cells is more physiologically significant and the possibility of false positive and negatives is smaller compared with cell lines. Therefore, more analysis of cell differentiation using primary cells and more complex analysis of gene expression would give important inputs into overall assessment of scaffolds functionalization. Finally, repetitions of presented studies is necessary to examine the reproducibility of research.

Concluding the evaluation of different crosslinking strategies used in development of biomimetic scaffolds for cartilage TE, this field will still require precise work to realize an ideal system. Nonetheless, major progress has been made recently in the cartilage repair, which give hope that many remaining challenges will be overcome in the near future.

## References

- [1] Q. L. Loh and C. Choong, "Three-dimensional scaffolds for tissue engineering applications: role of porosity and pore size.," *Tissue Eng. Part B. Rev.*, vol. 19, no. 6, pp. 485–502, 2013.
- [2] A. Arora, A. Kothari, and D. S. Katti, "Pore orientation mediated control of mechanical behavior of scaffolds and its application in cartilage-mimetic scaffold design," *J. Mech. Behav. Biomed. Mater.*, vol. 51, no. December, pp. 169–183, 2015.
- [3] B. Balakrishnan and A. Jayakrishnan, "Self-cross-linking biopolymers as injectable in situ forming biodegradable scaffolds," *Biomaterials*, vol. 26, no. 18, pp. 3941–3951, 2005.
- [4] A. Gaspar, L. Moldovan, D. Constantin, A. M. Stanciuc, P. M. Sarbu Boeti, and I. C. Efrimescu, "Collagen-based scaffolds for skin tissue engineering," *J. Med. Life*, vol. 4, no. 2, pp. 172–177, 2011.
- [5] M. Sandri *et al.*, "A collagen membrane-based engineered heart tissue improves cardiac function in ischemic rat hearts," *Bioinspired, Biomim. Nanobiomaterials*, vol. 2, no. 1, pp. 21–28, 2012.
- [6] R. W. Farndale, D. J. Buttle, and A. J. Barrett, "Improved quantitation and discrimination of sulphated glycosaminoglycans by use of dimethylmethylene blue," *BBA - Gen. Subj.*, vol. 883, no. 2, pp. 173–177, 1986.
- [7] H. S. Verseijden F, Jahr H, Posthumus-van Sluijs SJ, Ten Hagen TL and H. S. Seynhaeve AL, van Neck JW, van Osch GJ, "Angiogenic capacity of human adipose-derived stromal cells during adipogenic differentiation: an in vitro study.," *Tissue Eng Part A*, vol. 15, no. 2, pp. 445–52, 2009.
- [8] A. Tampieri *et al.*, "Design of graded biomimetic osteochondral composite scaffolds," *Biomaterials*, vol. 29, no. 26, pp. 3539–3546, 2008.
- [9] S. Ali Poursamar, J. Hatami, A. N. Lehner, C. L. Da Silva, F. C. Ferreira, and A. P. M. Antunes, "Potential application of gelatin scaffolds prepared through in situ gas foaming in skin tissue engineering," *Int. J. Polym. Mater. Polym. Biomater.*, vol. 65, no. 6, pp. 315–322, 2016.
- [10] A. V. Taubenberger, M. A. Woodruff, H. Bai, D. J. Muller, and D. W. Huttmacher, "The effect of unlocking RGD-motifs in collagen I on pre-osteoblast adhesion and differentiation," *Biomaterials*, vol. 31, no. 10, pp. 2827–2835, 2010.
- [11] S. Moscato *et al.*, "Interaction of human gingival fibroblasts with PVA/gelatine sponges," *Micron*, vol. 39, no. 5, pp. 569–579, 2008.
- [12] K. G. Shankar *et al.*, "Investigation of different cross-linking approaches on 3D gelatin scaffolds for tissue engineering application: A comparative analysis," *Int. J. Biol. Macromol.*, 2016.
- [13] S. B. Lee, Y. H. Kim, M. S. Chong, S. H. Hong, and Y. M. Lee, "Study of gelatin-containing artificial skin V: Fabrication of gelatin scaffolds using a salt-leaching method," *Biomaterials*, vol. 26, no. 14, pp. 1961–1968, 2005.
- [14] W. Xia *et al.*, "Tissue Engineering of Cartilage with the Use of Chitosan-Gelatin Complex Scaffolds," pp. 373–380, 2004.
- [15] M. D. Shoulders and R. T. Raines, "Collagen Structure and Stability," *Annu Rev Biochem*, vol. 78, pp. 929–958, 2010.
- [16] C. S. W. c I. Prasertsung , R. Mongkolnavin, S. Damrongsakkul, "Surface modification of dehydrothermal crosslinked gelatin film using a 50 Hz oxygen glow discharge," *Surf. Coatings Technol.*, vol. 205, no. SUPPL. 2, pp. 133–138, 2011.
- [17] M. G. Haugh, C. M. Murphy, R. C. McKiernan, C. Altenbuchner, and F. J. O'Brien, "Crosslinking and mechanical properties significantly influence cell attachment,

- proliferation, and migration within collagen glycosaminoglycan scaffolds.,” *Tissue Eng. Part A*, vol. 17, no. 9–10, pp. 1201–1208, 2011.
- [18] A. Nicoletti, M. Fiorini, J. Paolillo, L. Dolcini, M. Sandri, and D. Pressato, “Effects of different crosslinking conditions on the chemical-physical properties of a novel bio-inspired composite scaffold stabilised with 1,4-butanediol diglycidyl ether (BDDGE),” *J. Mater. Sci. Mater. Med.*, vol. 24, no. 1, pp. 17–35, 2013.
- [19] V. Maier *et al.*, “Property peculiarities of the atelocollagen-hyaluronan conjugates crosslinked with a short chain di-oxirane compound,” *Mater. Sci. Eng. C*, vol. 42, pp. 243–253, 2014.
- [20] A. Bigi, G. Cojazzi, S. Panzavolta, N. Roveri, and K. Rubini, “Stabilization of gelatin films by crosslinking with genipin,” *Biomaterials*, vol. 23, no. 24, pp. 4827–4832, 2002.
- [21] J. Davies, S. Bosi, and C. Baldock, “The characterisation of a genipin-gelatin gel dosimeter,” *J. Phys. Conf. Ser.*, vol. 250, p. 12008, 2010.
- [22] S. M. Lien, W. Te Li, and T. J. Huang, “Genipin-crosslinked gelatin scaffolds for articular cartilage tissue engineering with a novel crosslinking method,” *Mater. Sci. Eng. C*, vol. 28, no. 1, pp. 36–43, 2008.
- [23] A. La Gatta *et al.*, “Hyaluronan scaffolds via diglycidyl ether crosslinking: Toward improvements in composition and performance,” *Carbohydr. Polym.*, vol. 96, no. 2, pp. 536–544, 2013.
- [24] H. G. Sundararaghavan, G. A. Monteiro, N. A. Lapin, Y. J. Chabal, J. R. Miksan, and D. I. Shreiber, “Genipin-induced changes in collagen gels: Correlation of mechanical properties to fluorescence,” *J. Biomed. Mater. Res. - Part A*, vol. 87, no. 2, pp. 308–320, 2008.
- [25] B. J. Lawrence and S. V. Madhally, “Cell colonization in degradable 3D porous matrices,” no. March, pp. 9–16, 2008.
- [26] T. Dispinar, W. Van Camp, L. J. De Cock, B. G. De Geest, and F. E. Du Prez, “Redox-Responsive Degradable PEG Cryogels as Potential Cell Scaffolds in Tissue Engineering,” *Macromol. Biosci.*, vol. 12, no. 3, pp. 383–394, 2012.
- [27] C. Tonda-turo, P. Gentile, S. Saracino, V. Chiono, V. K. Nandagiri, and G. Muzio, “Comparative analysis of gelatin scaffolds crosslinked by genipin and silane coupling agent,” *Int. J. Biol. Macromol.*, vol. 49, no. 4, pp. 700–706, 2011.
- [28] L. P. Yan *et al.*, “Genipin-cross-linked collagen/chitosan biomimetic scaffolds for articular cartilage tissue engineering applications,” *J. Biomed. Mater. Res. - Part A*, vol. 95 A, no. 2, pp. 465–475, 2010.
- [29] G. Gorczyca, R. Tylingo, P. Szweda, E. Augustin, M. Sadowska, and S. Milewski, “Preparation and characterization of genipin cross-linked porous chitosan-collagen-gelatin scaffolds using chitosan-CO<sub>2</sub> solution,” *Carbohydr. Polym.*, vol. 102, no. 1, pp. 901–911, 2014.
- [30] J. H. Muyonga, C. G. B. Cole, and K. G. Duodu, “Fourier transform infrared (FTIR) spectroscopic study of acid soluble collagen and gelatin from skins and bones of young and adult Nile perch (*Lates niloticus*),” *Food Chem.*, vol. 86, no. 3, pp. 325–332, 2004.
- [31] F. L. Mi, H. W. Sung, and S. S. Shyu, “Synthesis and characterization of a novel chitosan-based network prepared using naturally occurring crosslinker,” *J. Polym. Sci. Part A Polym. Chem.*, vol. 38, no. 15, pp. 2804–2814, 2000.
- [32] H. S. Rathore *et al.*, “Fabrication of biomimetic porous novel sponge from gum kondagogu for wound dressing,” *Mater. Lett.*, vol. 177, pp. 108–111, 2016.
- [33] J. M. Mansour, “Biomechanics of Cartilage,” *Kinesiol. Mech. pathomechanics Hum. Mov.*, pp. 66–79, 2009.
- [34] W. C. Camarero-Espinosa S, Rothen-Rutishauser B, Foster EJ, “Articular cartilage: from formation to tissue engineering,” *Biomater Sci.*, vol. 4, no. 5, pp. 734–767, 2016.

- [35] C. R. Correia *et al.*, “Chitosan scaffolds containing hyaluronic acid for cartilage tissue engineering,” *Tissue Eng. Part C. Methods*, vol. 17, no. 7, pp. 717–730, 2011.
- [36] P. Gentile *et al.*, “Bioactive glass/polymer composite scaffolds mimicking bone tissue,” *J. Biomed. Mater. Res. - Part A*, vol. 100 A, no. 10, pp. 2654–2667, 2012.
- [37] L. P. Yan, J. M. Oliveira, A. L. Oliveira, S. G. Caridade, J. F. Mano, and R. L. Reis, “Macro/microporous silk fibroin scaffolds with potential for articular cartilage and meniscus tissue engineering applications,” *Acta Biomater.*, vol. 8, no. 1, pp. 289–301, 2012.
- [38] A. J. Sophia Fox, A. Bedi, and S. A. Rodeo, “The basic science of articular cartilage: structure, composition, and function,” *Sports Health*, vol. 1, no. 6, pp. 461–8, 2009.
- [39] E. Boanini, P. Torricelli, M. Gazzano, M. Fini, and A. Bigi, “The effect of zoledronate-hydroxyapatite nanocomposites on osteoclasts and osteoblast-like cells in vitro,” *Biomaterials*, vol. 33, no. 2, pp. 722–730, 2012.
- [40] S. Panzavolta *et al.*, “3D interconnected porous biomimetic scaffolds: In vitro cell response,” *J. Biomed. Mater. Res. - Part A*, vol. 101, no. 12, pp. 3560–3570, 2013.
- [41] D. Pasqui, P. Torricelli, M. De Cagna, M. Fini, and R. Barbucci, “Carboxymethyl cellulose - Hydroxyapatite hybrid hydrogel as a composite material for bone tissue engineering applications,” *J. Biomed. Mater. Res. - Part A*, vol. 102, no. 5, pp. 1568–1579, 2014.
- [42] Y. Liu, L. Ma, and C. Gao, “Facile fabrication of the glutaraldehyde cross-linked collagen/chitosan porous scaffold for skin tissue engineering,” *Mater. Sci. Eng. C*, vol. 32, no. 8, pp. 2361–2366, 2012.
- [43] K. Anselme, “Osteoblast adhesion on biomaterials,” *Biomaterials*, vol. 21, no. 7, pp. 667–681, 2000.
- [44] A. Fiorani *et al.*, “Comparative performance of collagen nanofibers electrospun from different solvents and stabilized by different crosslinkers,” *J. Mater. Sci. Mater. Med.*, vol. 25, no. 10, pp. 2313–2321, 2014.
- [45] J.H. Ko, H.Y. Yin, J. An, D.J. Chung, J.H. Kim, S.B. Lee, D.G. Pyun, “Characterization of cross-linked gelatin nanofibers through electrospinning,” *Macromol. Res.*, vol. 18, no. 2, pp. 137–143, 2010.
- [46] C. Wang, T. T. Lau, W. L. Loh, K. Su, and D. A. Wang, “Cytocompatibility study of a natural biomaterial crosslinker-Genipin with therapeutic model cells,” *J. Biomed. Mater. Res. - Part B Appl. Biomater.*, vol. 97 B, no. 1, pp. 58–65, 2011.
- [47] “Human chondrocytes cell line CHON-002 (ATCC® CRL-2847™).” [Online]. Available: <https://www.lgcstandards-atcc.org/Products/All/CRL-2847.aspx#generalinformation>.
- [48] C. C. Cheng *et al.*, “Phytoestrogen bavachin mediates anti-inflammation targeting IκB kinase-IκBα-NF-κB signaling pathway in chondrocytes in vitro,” *Eur. J. Pharmacol.*, vol. 636, no. 1–3, pp. 181–188, 2010.
- [49] J. R. Robbins *et al.*, “Immortalized human adult articular chondrocytes maintain cartilage-specific phenotype and responses to interleukin-1β,” *Arthritis Rheum.*, vol. 43, no. 10, pp. 2189–2201, 2000.
- [50] R. Lyon, X. C. Liu, J. Z. An, J. Schwab, and Y. Shi, “Effects of extracorporeal pulse activation on in-vitro lipopolysaccharides-treated chondrocytes,” pp. 1–7, 2000.
- [51] S. Lien, L. Ko, and T. Huang, “Effect of pore size on ECM secretion and cell growth in gelatin scaffold for articular cartilage tissue engineering,” *Acta Biomater.*, vol. 5, no. 2, pp. 670–679, 2009.
- [52] N. Bhardwaj, Q. T. Nguyen, A. C. Chen, D. L. Kaplan, R. L. Sah, and S. C. Kundu, “Potential of 3-D tissue constructs engineered from bovine chondrocytes/silk fibroin-chitosan for in vitro cartilage tissue engineering,” *Biomaterials*, vol. 32, no. 25, pp.

- 5773–5781, 2011.
- [53] S. Amadori, P. Torricelli, S. Panzavolta, A. Parrilli, M. Fini, and A. Bigi, “Highly Porous Gelatin Reinforced 3D Scaffolds for Articular Cartilage Regeneration,” *Macromol. Biosci.*, vol. 15, no. 7, pp. 941–952, 2015.
- [54] L. C. Groeneveldt, C. Knuth, J. Witte-Bouma, F. J. O’Brien, E. B. Wolvius, and E. Farrell, “Enamel Matrix Derivative has No Effect on the Chondrogenic Differentiation of Mesenchymal Stem Cells.,” *Front. Bioeng. Biotechnol.*, vol. 2, no. September, p. 29, 2014.
- [55] B. C. Heng, T. Cao, and E. H. Lee, “Directing stem cell differentiation into the chondrogenic lineage in vitro.,” *Stem Cells*, vol. 22, no. 7, pp. 1152–1167, 2004.
- [56] S. R. Tew and T. E. Hardingham, “Regulation of SOX9 mRNA in human articular chondrocytes involving p38 MAPK activation and mRNA stabilization,” *J. Biol. Chem.*, vol. 281, no. 51, pp. 39471–39479, 2006.
- [57] C. Kiani, L. Chen, Y. J. Wu, A. J. Yee, and B. B. Yang, “Structure and function of aggrecan,” *Cell Res.*, vol. 12, pp. 19–32, 2002.
- [58] E. Kon, A. Roffi, G. Filardo, G. Tesei, and M. Marcacci, “Scaffold-based cartilage treatments: With or without cells? A systematic review of preclinical and clinical evidence,” *Arthrosc. - J. Arthrosc. Relat. Surg.*, vol. 31, no. 4, pp. 767–775, 2015.
- [59] A. H. Doulabi, K. Mequanint, and H. Mohammadi, “Blends and nanocomposite biomaterials for articular cartilage tissue engineering,” *Materials (Basel)*, vol. 7, no. 7, pp. 5327–5355, 2014.
- [60] L. Ma, C. Gao, Z. Mao, J. Zhou, and J. Shen, “Enhanced biological stability of collagen porous scaffolds by using amino acids as novel cross-linking bridges,” *Biomaterials*, vol. 25, no. 15, pp. 2997–3004, 2004.
- [61] N. Davidenko *et al.*, “Control of crosslinking for tailoring collagen-based scaffolds stability and mechanics,” *Acta Biomater.*, vol. 25, pp. 131–142, 2015.
- [62] H. C. Ma L, Gao C, Mao Z, Shen J, Hu X, “Thermal dehydration treatment and glutaraldehyde cross-linking to increase the biostability of collagen-chitosan porous scaffolds used as dermal equivalent.,” *J Biomater Sci Polym Ed.*, vol. 14, no. 8, pp. 861–874, 2003.
- [63] H. Chiue, T. Yamazoye, and S. Matsumura, “Localization of the dominant non-enzymatic intermolecular cross-linking sites on fibrous collagen,” *Biochem. Biophys. Res. Commun.*, vol. 461, no. 3, pp. 445–449, 2015.
- [64] G. K. Reddy, “Cross-Linking in Collagen by Nonenzymatic Glycation Increases the Matrix Stiffness in Rabbit Achilles Tendon,” *Exp. Diabetes Res.*, vol. 5, no. 2, pp. 143–153, 2004.
- [65] R. Roy, A. Boskey, and L. J. Bonassar, “Processing of type I collagen gels using nonenzymatic glycation,” *J. Biomed. Mater. Res. - Part A*, vol. 93, no. 3, pp. 843–851, 2010.
- [66] S. Tanaka, G. Avigad, E. F. Eikenberry, and B. Brodsky, “Isolation and partial characterization of collagen chains dimerized by sugar-derived cross-links.,” *J. Biol. Chem.*, vol. 263, no. 33, pp. 17650–17657, 1988.
- [67] R. D. Semba, E. J. Nicklett, and L. Ferrucci, “Does accumulation of advanced glycation end products contribute to the aging phenotype?,” *Journals Gerontol. - Ser. A Biol. Sci. Med. Sci.*, vol. 65 A, no. 9, pp. 963–975, 2010.
- [68] B. Boonkaew, K. Tompkins, J. Manokawinchoke, P. Pavasant, and P. Supaphol, “Characterization and cytological effects of a novel glycated gelatine substrate,” *Biomed Mater*, vol. 9, no. 2, p. 25001, 2014.
- [69] T. R. Girton TS, Oegema TR, “Exploiting glycation to stiffen and strengthen tissue equivalents for tissue engineering.,” *J Biomed Mater Res.*, vol. 46, no. 1, pp. 87–92,

- 1999.
- [70] P. Zuzarte, "United States Patent," vol. 1, no. 12, 2004.
- [71] V. Vicens-Zygmunt *et al.*, "Fibroblast viability and phenotypic changes within glycated stiffened three-dimensional collagen matrices," *Respir. Res.*, vol. 16, no. 1, p. 82, 2015.
- [72] S. Pitaru *et al.*, "Long-term efficacy of a novel ribose-cross-linked collagen dermal filler: A histologic and histomorphometric study in an animal model," *Dermatologic Surg.*, vol. 33, no. 9, pp. 1045–1053, 2007.
- [73] C. N. Grover, R. E. Cameron, and S. M. Best, "Investigating the morphological, mechanical and degradation properties of scaffolds comprising collagen, gelatin and elastin for use in soft tissue engineering," *J. Mech. Behav. Biomed. Mater.*, vol. 10, pp. 62–74, 2012.
- [74] M. E. Francis-Sedlak, S. Uriel, J. C. Larson, H. P. Greisler, D. C. Venerus, and E. M. Brey, "Characterization of type I collagen gels modified by glycation," *Biomaterials*, vol. 30, no. 9, pp. 1851–1856, 2009.
- [75] R. Zeeman *et al.*, "Crosslinking and modification of dermal sheep collagen using 1,4-butanediol diglycidyl ether," *J. Biomed. Mater. Res.*, vol. 46, no. 3, pp. 424–433, 1999.
- [76] L. B. Koh *et al.*, "Epoxy cross-linked collagen and collagen-laminin peptide hydrogels as corneal substitutes," *J. Funct. Biomater.*, vol. 4, no. 3, pp. 162–177, 2013.
- [77] V. Singh, A. Misra, R. Parthasarathy, Q. Ye, and P. Spencer, "Viscoelastic properties of collagen – adhesive composites under water-saturated and dry conditions," pp. 646–657, 2014.
- [78] C. M. Murphy, A. Matsiko, M. G. Haugh, J. P. Gleeson, and F. J. O'Brien, "Mesenchymal stem cell fate is regulated by the composition and mechanical properties of collagen-glycosaminoglycan scaffolds," *J. Mech. Behav. Biomed. Mater.*, vol. 11, pp. 53–62, 2012.
- [79] M. G. Haugh, M. J. Jaasma, and F. J. O'Brien, "The effect of dehydrothermal treatment on the mechanical and structural properties of collagen-GAG scaffolds," *J. Biomed. Mater. Res. - Part A*, vol. 89, no. 2, pp. 363–369, 2009.
- [80] B. De Campos Vidal and M. L. S. Mello, "Collagen type I amide I band infrared spectroscopy," *Micron*, vol. 42, no. 3, pp. 283–289, 2011.
- [81] H. Stenhamre, U. Nannmark, A. Lindahl, P. Gatenholm, and M. Brittberg, "Influence of pore size on the redifferentiation potential of human articular chondrocytes in poly ( urethane urea ) scaffolds," no. December 2010, pp. 578–588, 2011.
- [82] a G. Mikos, G. Sarakinos, S. M. Leite, J. P. Vacanti, and R. Langer, "Laminated 3-Dimensional Biodegradable Foams for Use in Tissue Engineering," *Biomaterials*, vol. 14, no. 5, pp. 323–330, 1993.
- [83] S. Korres, L. Sorochynska, and S. Grishchuk, "Swelling , Compression and Tribological Behaviors of Bentonite-Modified Polyacrylate-Type Hydrogels."
- [84] H. A. Awad, M. Q. Wickham, H. A. Leddy, J. M. Gimble, and F. Guilak, "Chondrogenic differentiation of adipose-derived adult stem cells in agarose , alginate , and gelatin scaffolds," vol. 25, pp. 3211–3222, 2004.
- [85] T. D. Bornes, N. M. Jomha, A. Mulet-Sierra, and A. B. Adesida, "Hypoxic culture of bone marrow-derived mesenchymal stromal stem cells differentially enhances in vitro chondrogenesis within cell-seeded collagen and hyaluronic acid porous scaffolds," *Stem Cell Res. Ther.*, vol. 6, no. 1, p. 84, 2015.
- [86] D. E. Discher, "Tissue Cells Feel and Respon to the Stiffness of Their Substrate," *Science (80-. )*, vol. 310, no. 5751, pp. 1139–1143, 2005.
- [87] D. Cigognini *et al.*, "Engineering in vitro microenvironments for cell based therapies and drug discovery," *Drug Discov. Today*, vol. 18, no. 21–22, pp. 1099–1108, 2013.
- [88] Y. U. L. I. W. Ang, "Cell locomotion and focal adhesions are regulated by," *Proc. Natl.*



- Acad. Sci.*, vol. 94, no. December, pp. 13661–13665, 1997.
- [89] K. Bott *et al.*, “The effect of matrix characteristics on fibroblast proliferation in 3D gels,” *Biomaterials*, vol. 31, no. 32, pp. 8454–8464, 2010.
- [90] S. Miot *et al.*, “Effects of scaffold composition and architecture on human nasal chondrocyte redifferentiation and cartilaginous matrix deposition,” vol. 26, pp. 2479–2489, 2005.
- [91] L. Russo *et al.*, “Preliminary Study,” 2014.
- [92] F. G. Meng *et al.*, “Chondrogenesis of MSC in novel HA Collagen Tricalcium phosphate scaffolds for knee repair,” *Eur. Cells Mater.*, vol. 31, pp. 79–94, 2016.
- [93] D. Correa and S. A. Lietman, “Articular cartilage repair: Current needs, methods and research directions,” *Semin. Cell Dev. Biol.*, 2016.
- [94] J. Farr and A. H. Gomoll, “2016 Barriers To Cartilage Restoration,” *J. Clin. Orthop. Trauma*, vol. 7, no. 3, pp. 183–186, 2016.
- [95] F. J. O’Brien, “Biomaterials & scaffolds for tissue engineering,” *Mater. Today*, vol. 14, no. 3, pp. 88–95, 2011.
- [96] S. A. Poursamar, J. Hatami, A. N. Lehner, C. L. Da Silva, F. C. Ferreira, and A. P. M. Antunes, “Gelatin porous scaffolds fabricated using a modified gas foaming technique: Characterisation and cytotoxicity assessment,” *Mater. Sci. Eng. C*, vol. 48, pp. 63–70, 2015.

## List of publications

Gostynska N, Shankar KG, Campodoni E, Panseri S, Montesi M, Sprio S, Kon E, Marcacci M, Tampieri A, Sandri M. *3D porous collagen scaffolds reinforced by glycation with ribose for tissue engineering application*. Biomed. Mater. 2017. Under review.

Shankar KG, Gostynska N, Campodoni E, Dapporto M, Montesi M, Panseri S, Sprio S, Kon E, Marcacci M, Tampieri A, Sandri M. *Ribose mediated crosslinking of collagen-hydroxyapatite hybrid scaffolds for bone tissue regeneration using biomimetic strategies*. Mater Sci Eng C. 2017. In press.

Gostynska N, Shankar KG, Montesi M, Panseri S, Sprio S, Kon E, Marcacci M, Tampieri A, Sandri M. *Investigation of different cross-linking approaches on 3D gelatin scaffolds for tissue engineering application: A comparative analysis*. Int. J Biol. Macromol. 2017. 95: 1199-1209.

Perdisa F, Gostynska N, Roffi A, Filardo G, Marcacci M, Kon E. *Adipose-Derived Mesenchymal Stem Cells for the Treatment of Articular Cartilage: A Systematic Review on Preclinical and Clinical Evidence*. Stem Cells Int. 2015. (2015): Article ID 597652, 13 pages.

Di Matteo B, Perdisa F, Gostynska N, Kon E, Filardo G, Marcacci M. *Meniscal Scaffolds - Preclinical Evidence to Support their Use: A Systematic Review*. Open Orthop J. 2015. 15(9): 143-56.

## Scientific congresses and schools

Gostynska N, Shankar KG, Campodoni E, Panseri S, Montesi M, Sprio S, Kon E, Marcacci M, Tampieri A, Sandri M. *3D porous collagen scaffolds reinforced by glycation for tissue engineering application*. Conference Materials.it, December 2016, Catania, Sicily.

Shankar KG, Gostynska N, Campodoni E, Kon E, Marcacci M, Panseri S, Montesi M, Tampieri A, Sprio S, Sandri M. *A biomimicry strategy for developing collagen-hydroxyapatite scaffolds substituted with magnesium and crosslinked with D-ribose for bone tissue regeneration*. Conference Materials.it, December 2016, Catania, Sicily.

Gostynska N, K.Gopal Shankar, Montesi M, Panseri S, Sprio S, Kon E, Marcacci M, Tampieri A, Sandri M. *Crosslinking strategies of gelatin scaffolds for tissue engineering application*. TERMIS, September 2015, Boston, USA.

T. M. Fernandes Patrício, S. Sprio, M. Sandri, N. Gostynska, M. Montesi, S. Panseri, A. Tampieri. *Hybrid Superparamagnetic Collagen-like Peptide Microparticles Applied On Bone Tissue Regeneration*. TERMIS, September 2015, Boston, USA.

A. Roffi, E. Assirelli, G. Filardo, L. Pulsatelli, V. Canella, E. Mariani, Gostynska N, E. Kon, M. Marcacci, A. Facchini. *In vitro effects of different Platelet-Rich Plasma preparations on human synoviocyte response*. Osteoarthritis Research Society International (OARSI) World Congress, April 2014, Paris, France.

### Workshops:

- Laboratory animal science course, FELASA Category C, May 2016, IBMC Porto, Portugal;

- "Vitro/Vivo Preclinical Models and Imaging in Musculoskeletal Tissue Regeneration"  
TERMIS Winterschool, Radstadt, Austria 2015;